ONE-DIMENSIONAL SHOCK WAVE FORMATION BY AN ACCELERATING PISTON

DISSERTATION

Presented in Partial Fulfillment of the Requirements for the Degree Doctor of Philosophy in the Graduate School of The Ohio State University

By

Michael John Mann, B.A.E., M.S.A.E.

* * * * * *

The Ohio State University
1970

Approved by

R. Edse

Adviser
Department of Aeronautical and Astronautical Engineering

Title: One-Dimensional Shock Wave Formation by an Accelerating Piston, Ph D Thesis, The Ohio State University; Columbus, Ohio, 1970.

Author: Michael J. Mann, Langley Research Center; Hampton, Virginia.

Abstract:

A study was made of the formation of a shock wave by a solid accelerating piston. No weak shock assumption was made. A theoretical solution using the method of characteristics for a perfect gas showed that a complex wave system exists and that the compressed gas can have large gradients in temperature, density and entropy. Experiments were performed with a piston tube where piston speed, shock speed and pressure were measured. The comparison of theory and experiment was good.

ACKNOWLEDGMENTS

I am sincerely grateful to my adviser, Professor Rudolph Edse, for his guidance and encouragement throughout my Ph.D. program.

I am very grateful to Dr. William A. Strauss for his counsel and many helpful suggestions during the experimental phase of this research.

Thanks are due to the National Science Foundation for the support of this research and throughout the full-time studies of my Ph.D. program. Thanks are also due to the U.S. Air Force for support during my part-time studies.

I also want to express my appreciation to the personnel of the Aeronautical and Astronautical Research Laboratory for the construction of the experimental apparatus. In particular I want to thank Willard Ebner and Bryce K. Dean.

I am also very grateful to my wife, Hazel, for her patience and encouragement during these studies.

VITA

[redacted]

1962	B.A.E., University of Florida, Gainesville, Florida
1962-1967	Officer, United States Air Force
1963.....	M.S.A.E., Air Force Institute of Technology, Wright-Patterson AFB, Ohio
1963-1967.....	Aeronautical Engineer, Air Force Flight Dynamics Laboratory, Wright-Patterson AFB, Ohio
1963-1967.....	Part-Time Graduate Student, Department of Aeronautical and Astronautical Engineering, The Ohio State University, Columbus, Ohio
1967-1970	Graduate Student, Department of Aeronautical and Astronautical Engineering, The Ohio State University, Columbus, Ohio

PUBLICATIONS

"Radar Reflection of Transparent Materials" (paper presented at the Eighth Conference on Transparent Materials for Aerospace Enclosures, Dayton, Ohio, 8-10 December 1964). Also Air Force Materials Laboratory TR-65-212, Wright-Patterson AFB, Ohio, September 1965.

"A Rapid Method of Computing Hypersonic Wind Tunnel Test Section Flow Conditions With Application to the AFFDL Two-Foot Electro-Gasdynamic Facility," Air Force Flight Dynamics Laboratory TR-66-185, Wright-Patterson AFB, Ohio, August 1967. (Coauthor: William A. Rockwell).

FIELDS OF STUDY

Major Field: Aeronautical and Astronautical Engineering

Studies in Aerodynamics and Airplane Design. Professor William H. Miller

Studies in High Speed Aerodynamics. Professors Rudolph Edse and Ting Y. Li

Studies in Physics. Professor Wave H. Shaffer

TABLE OF CONTENTS

LIST OF TABLES

LIST OF ILLUSTRATIONS

LIST OF SYMBOLS

Symbol	Definition
A_p	Piston acceleration
$\bar{A}_p$	$= A_p L_o / a_o^2$
A_T	Area of inside of driven tube
a	Speed of sound
$\mathcal{a}$	$= a/a_o$
C	Constant
c_p	Specific heat at constant pressure
d	Tube inside diameter
E	Total energy of gas considered
e	Internal energy per unit mass
F	Force
L_o	Reference length $= a_o t_o$
$M_{W'}$	Shock Mach number $= W'/\mathcal{a}'$
$M_{W''}$	$= W''/\mathcal{a}''$
m	Mass of gas under consideration
n	Exponent for self-similar flow
P	Riemann variable (dimensionless)
$\bar{P}$	Riemann variable $(= Pa_o)$
p	Static pressure
$\mathcal{P}$	$= p/p_o$

Symbol	Definition
Q	Riemann variable (dimensionless)
$\bar{Q}$	Riemann variable ($= Qa_o$)
R	Specific gas constant
r_s	Reflection coefficient for a shock wave
r_e	Reflection coefficient for an entropy discontinuity
S	$= s/\gamma R$
s	Entropy per unit mass
T	Temperature
t	Time
u	Flow or particle velocity relative to the tube
$\mathcal{U}$	$= u/a_o$
v	Specific volume
W	Shock wave speed with respect to local gas divided by a_o
w_p	Piston work
$\mathcal{W}$	Dimensionless shock wave speed relative to the tube $= \mathcal{U}' + W'$
x	Coordinate along tube length
y	Dummy variable $= x-x_F$

Greek

γ	Ratio of specific heats
$\Delta( )$	Finite change in a quantity
ξ	x/L_o
ρ	Density
Σ	Summation

Symbol	Definition
τ	ta_o/L_o
ϕ	Dummy variable = $t-t_F$

Superscripts

( )"	Downstream of shock wave
( )'	Upstream of shock wave

Subscripts

A	Point where piston velocity becomes constant
DN	Driven gas
DR	Driver gas
E	Experimental
F	Focus point
f	Final conditions
i	Initial conditions; incident wave
o	Reference conditions
p	Piston
R,L	Right and left of entropy interface
r	Reflected wave
s	Shock wave
T	Theoretical; Tube
t	Transmitted wave
1,2,3,···	Points defined on wave diagram

CHAPTER I

INTRODUCTION

Background and Objective of This Study

The formation of a shock wave is important in several practical flow problems. Shock waves are formed in shock tubes by breaking a diaphragm or by forming an accelerating flame front which results in a detonation wave. In some situations the shock formation may occur over a significant portion of the total flow time and therefore have a significant effect on the flow. In one type of hypersonic test facility the test gas is created by an accelerating piston. The manner in which the shock is ultimately formed, and deviations from the desired process are very important in creating an acceptable test flow. Hall[1] and Stoddard[2] discuss such a free-piston hypersonic wind tunnel. A third application is the equivalence of unsteady one-dimensional flows to steady two-dimensional flows. This equivalence has a mathematical foundation for hypersonic small-disturbance theory and can be used as an analogy for other flows.

Shock formation over some significant tube length is not as elementary a problem as one might initially suppose. The infinitesimal compression wavelets created by the piston will merge together as they travel down the tube, since the

absolute speed of each succeeding wavelet is greater than that of the wavelets ahead of it (wavelets are distinguished from waves in that a finite wave is imagined to be made up of many infinitesimal wavelets). As the wavelets merge, the gradients of temperature, pressure, and velocity steepen and a shock wave forms. However, a shock wave does not compress the gas to the same state as a series of compression wavelets does prior to merging since the latter is isentropic whereas the shock is not. Thus an expansion wave must move from the merging location in the opposite direction of the shock motion.

A second feature which complicates the flow pattern is the growth of the shock strength. This growth results in shocked gas with an entropy gradient, and therefore temperature and density gradients. The entropy gradient also causes reflected waves when any wave system passes through it.

The objective of this study is to determine the characteristics of the flow field which result when a shock wave forms in front of a continuously accelerating piston (though the acceleration may vary with time). A solid piston is assumed to accelerate from rest along a constant area tube which is initially filled with a uniform nonreacting gas at rest. The study is not restricted to weak shocks; however, the flow downstream of the shock wave is considered frictionless, adiabatic and one-dimensional. The gas is assumed

to be a perfect gas, that is, thermally and calorically perfect.

Both a theoretical and experimental study is made of the shock wave formation problem. The theoretical and experimental methods used will be described after the literature survey has been discussed.

Literature Survey

The first general solution to the shock formation problem, for a weak or "moderate strength" shock wave, was given by Friedrichs.[3,4] The basis of this treatment is the assumption that the entropy and appropriate Riemann variable do not change across the shock, so that the region behind the shock contains a simple wave. The solution gives the shock path and the shock strength in terms of pressure, velocity and speed of sound increase. Pillow[5] gave a similar treatment for a weak shock. Laponsky and Emrich[6] performed experiments which reasonably well verified the weak shock theory of Friedrichs. The shock path and velocity were measured and compared to the theoretical values. Their maximum shock pressure ratio based on measured shock velocities was 1.73.

Friedrichs also treated the case of an instantaneously created shock followed by an expansion wave from the piston which is decelerated to zero velocity. Although this decaying shock problem is not the same as the shock

formation problem, a verification of Friedrichs' treatment by Lighthill[7] gives additional insight into the shock formation problem. By a conservation of energy analysis, Lighthill showed that Friedrichs' theory is sound, but that higher order errors are due to the neglect of waves which are reflected back from the shock wave. This energy approach will be discussed in Chapter II.

Shunk[8] has made the only attempt to study the nature of the formation of a strong shock, that is a shock with an entropy increase so large that it can not be neglected. Shunk made some progress by showing that weak shock theory did not compare favorably with experiment for a strong shock. He also theoretically justified that an expansion wave must be reflected from the shock as the compression waves merge (Shapiro[9] also justified the existence of this expansion wave). However, Shunk's theory involved so many approximations that the results are questionable as to accuracy and completeness. Further clarification is needed of the physical requirements for reflected waves, the entropy gradient effect on these reflected waves and the nature of the resulting flow.

Shunk's experimental verification of his theory is not convincing. It involved just one case where only the density was examined, and was based on the fact that his theory compared more favorably with experiment than an isentropic theory. The present author does not feel that such a

comparison verifies the features of the flow since it is expected that a theory involving a shock wave would always be superior to an isentropic theory.

Moretti[26] also studied shock formation due to an accelerating piston. His emphasis was on the mathematical techniques with minor attention paid to the physics of the problem.

Several piston tube studies have been made where the main objective has been to analyze the performance of a facility and not to analyze shock formation.[10-14] In References 11 and 12 isentropic flow was assumed while in 10 an ingenious method equivalent to hypersonic tangent-wedge theory was developed. In References 13 and 14 the flow resulting from the multiple reflection of a shock between a moving piston and an end wall was studied. Enkenhus[13] used the approximation mentioned for Reference 10 for the primary and first reflected shocks, and Humphrey[14] utilized the method of characteristics. Although Humphrey apparently obtained an accurate solution of the shock formation, there is no analysis of the results. Due to the step by step nature of the method of characteristics, if care is not taken, it is possible to obtain results which give an incorrect physical picture. There is not enough detail in the report or its references to assess whether or not the solution is entirely correct. However, one experimental shock path for a weak shock was compared with theory and

good agreement was obtained (maximum shock pressure ratio in region of comparison was about 1.5).

In summary, a study of the literature shows that although the tools for analyzing shock wave formation have long been available, no rigorous analysis has been made for a strong shock wave.

Theoretical Considerations

Two types of wavelet mergers will be examined. One is a special case where all the wavelets merge at once and is called a focused wave. The other is a more general case where the wavelets merge one after the other and is called a dispersed wave. An example problem is worked out for each of these waves. These example problems are referred to as Cases I and II for the focused wave and the dispersed wave respectively.

When viscosity and heat conduction are neglected, the one-dimensional unsteady flow created by an accelerating piston is governed by the following equations for the conservation of mass, momentum and energy

$$\frac{\partial \rho}{\partial t} + \rho \frac{\partial u}{\partial x} + u \frac{\partial \rho}{\partial x} = 0 \qquad (1)$$

$$\rho \frac{\partial u}{\partial t} + \rho u \frac{\partial u}{\partial x} + \frac{\partial p}{\partial x} = 0 \qquad (2)$$

$$\frac{Ds}{Dt} \equiv \frac{\partial s}{\partial t} + u \frac{\partial s}{\partial x} = 0 \qquad (3)$$

where $s = s(p,\rho)$ is the entropy per unit mass, p, ρ, u are pressure, density and flow or partical velocity, and x,t are distance and time. These equations comprise a set of coupled quasi-linear partial differential equations of the first order.

The boundary conditions used in this study are piston position as a function of time, a uniform stationary gas ahead of the piston at $t = 0$, and an impermeable piston.

For the special case of s = constant and disturbances moving in only one direction, a closed form solution of these equations is possible (an example is the focused wave prior to merging). But for the general case of nonsteady flow in a region where disturbances travel in both directions (dispersed wave), no exact closed form solution exists; although approximate analytical solutions are possible, such as Lighthill's solution.

Two mathematical techniques have been applied by various authors to obtain a general solution of the piston problem. These techniques are self-similar solutions and the method of characteristics. The self-similar approach has been largely developed in the Russian literature (see Hayes and Probstein[15] and Chernyi[16]). When this approach is used to study the continually accelerating piston case, a strong shock must be assumed and certain approximations introduced. But even in this case, the problem is restricted to a power law piston path of the form

$$x = \frac{C}{n+1} t^{n+1} \qquad (4)$$

where C is a constant and n is any constant other than -1.

In order to investigate the usefulness of this power law piston path, several piston paths were calculated by using the method of characteristics with assumed driver and driven tube pressures and piston mass. For each of the resulting paths, an attempt was made to find a value of n which would describe the path; however, it was found that the value of n varied along the path. Due to this difficulty, and the approximate nature of the solution, and the greater flow detail provided by the method of characteristics, the characteristic approach was chosen for the theoretical analysis. Most of the development is based on the techniques described by Rudinger,[17] although Owczarek's method[18] was also used.

Experimental Considerations

An experimental program was undertaken in order to obtain some verification of the theoretical analysis. A piston tube was designed and built. It consisted of 40 feet of stainless steel tubing divided into driver, driven and brake tubes by Mylar diaphragms. The driver section was pressurized with air until the diaphragm broke. Then this high pressure air caused a piston to be accelerated into the

low pressure air of the driven tube. In this tube, measurements were made of the pressure and of the time for the piston to travel between certain stations. The final section of the tube was a high pressure brake tube used to decelerate the piston.

Shock Mach numbers as high as 1.6 were achieved. Experimental measurements of the pressure and the shock path (in the time-distance plane) were compared to the theoretical prediction of these quantities for two cases. These cases are called Cases III and IV. The theoretical solution used in these comparisons was based on an experimentally measured piston path.

CHAPTER II

FOCUSED COMPRESSION WAVE

Although there are various ways in which the infinitesimal wavelets of a compression wave can merge, only the special case when all wavelets merge at one point in the tube will be discussed in this chapter. This focused wave case is the logical starting point in a study of shock formation since it has many of the basic features of the dispersed case, but is much easier to solve. An example is worked out to establish certain features of the shock formation process and to use as an approximate check on the dispersed wave case which will be worked out in the next chapter. Then a closed form solution is found which demonstrates certain features of the flow. This solution is followed by a discussion of shock formation from a conservation of energy viewpoint. Finally, the various conclusions are summarized and examined.

In all cases considered, the initial gas state is motionless with a pressure and speed of sound of p_o, a_o. The tube is constant area. A thermally and calorically perfect gas is assumed.

Possible Compression Wave Patterns

As the piston accelerates from rest, infinitesimal wavelets are sent into the gas ahead. Since these are compression wavelets, each succeeding wavelet travels faster than the preceding one, and thus all of the wavelets will eventually combine into a single thin region or front known as a shock wave. However, the manner in which these wavelets merge depends on the piston path.[4] In the most general case, one or more individual shocks could form between the piston and the front of the wave. Laponsky and Emrich[6] experimentally observed a case where a shock formed in the interior of the wave. A theoretical analysis showed that a second shock also formed at the head of the wave, but it was too weak to be measured. Theoretical predictions of this phenomena are reported in References 3, 5, and 19. Another possibility for a dispersed wave is that the shock forms at the head of the simple compression wave. This dispersed wave is the subject of Chapter III and is shown in Figure 1a.

The third possibility is that none of the wavelets merge until they all merge at once. This is called a focused or centered wave (References 9, 18, and 20) and is particularly easy to analyze because prior to merging there is no shock wave present to cause entropy changes. The process prior to merging involves a simple wave and can be considered isentropic in the same way that a centered

expansion wave can be considered isentropic. A focused wave is shown in Figure 1b.

Solution For Case I

Case I is an example of a focused wave where the piston accelerates to a velocity of $\mathcal{U}_p = 1.578$ and continues thereafter with a constant velocity. The solution for Case I is shown in Figures 2-4. Before the solution for Case I is discussed, however, certain physical features and new viewpoints concerned with the focused wave will be considered.

During the period before the wavelets have merged, velocity, pressure and temperature gradients in a compression wave are usually low enough that, to a good approximation, there is no production of entropy. However, there may be cases when the assumption of $Ds/Dt = 0$ is not good. Consider for example the case of an underground tubular transportion system. Such a device will have a very low acceleration, A_p, and therefore the distance necessary for shock formation, x_F, will be very large (proven in next section). Thus it is not difficult to imagine that a condition could arise where the wavelets could merge close enough to each other to cause steep gradients but not close enough together to form a steady shock wave, and that this condition could exist for a significantly long time. Therefore, a significant portion of the gas would have an

entropy intermediate between that of the earlier isentropically compressed gas and the later shock compressed gas. This intermediate flow is very difficult to analyze because it is both unsteady and viscous and heat conducting. Therefore, neither the isentropic unsteady simple wave equations nor the steady shock wave equations apply. Approaches to this problem are indicated by Liepmann and Roshko,[21] Shapiro,[9] Owczarek,[24,25] and Moretti.[27]

In the above sense a compression wave differs from an expansion wave because the steepest gradients exist in an expansion wave for $A_p = \infty$ (centered wave), and even in this case the wave can be assumed isentropic because the steep gradient lasts such a short time. In this study the view will be taken that previous to wave merging the changes through the wave are isentropic.

Once the waves merge, an initial momentary "discontinuity" exists. The gas on one side of the discontinuity is assumed to have been isentropically compressed and the gas on the other side is in the initial state. However, the conservation equations valid across a gasdynamic discontinuity show that there is an entropy increase. Thus an "arbitrary discontinuity" exists. Zel'dovich and Raizer[20] show that the subsequent flow must consist of shock waves, expansion waves and uniform flow regions. Since a shock wave travels in the same direction as the piston, an expansion will travel in the other direction, as can be

determined from a pressure-velocity or P, U plane analysis (P and U are dimensionless pressure and velocity).

The solution for Case I is obtained by use of the P, U plane shown in Figure 2. This figure shows very clearly that the isentropic compression to a given point, 2, does not satisfy the shock equations. Point 2 is located by knowing the final piston speed. To satisfy the boundary condition across the entropy discontinuity of equal pressure and velocity, a weak expansion will occur along the line 2-3 (the expansion is weak compared to the compression). Figures 3 and 4 show that the shocked gas has a higher speed of sound (therefore higher temperature and higher entropy) and lower density than the isentropically compressed and expanded gas. Thus a discontinuity in density, temperature and entropy persists and travels downstream.

Thus the study of the focused wave made in the literature has demonstrated some important aspects of the shock wave formation problem. First, when isentropic waves merge into a nonisentropic shock, a weak expansion wave is reflected back toward the piston. Secondly, even though the pressure and velocity approach uniform values, gradients in entropy, density and temperature will persist.

Closed Form Solution

Due to the simplicity of the focused shock wave formation, it is possible to obtain closed form expressions for the piston path and the energy equation. In this section the piston path will be obtained and some conclusions drawn from it. Glass and Hall[22] have developed the equation for the piston path in the x,t plane. Since their forms for the piston velocity and acceleration are not convenient ones, new forms are presented here. For the sake of completeness, the derivation of the piston path will be reproduced.

The physical characteristics are the wavelet paths in the x,t plane. In a simple wave the characteristics are straight lines and all flow variables are constant along them. Thus from Figure 1b, the absolute speed of a wavelet can be expressed as

$$u + a = \frac{x_F - x}{t_F - t} \tag{5}$$

where x_F, t_F is the focus point. Also for a right traveling simple wave the $\bar{Q}$ Riemann variable is constant giving

$$\bar{Q} \equiv \frac{2}{\gamma - 1} a - u = \frac{2}{\gamma - 1} a_o \tag{6}$$

where the reference conditions are taken to be the undisturbed flow conditions and γ is the ratio of specific heats. Solving Equations (5) and (6) for u

$$u = \frac{2}{\gamma+1}\left[\frac{x-x_F}{t-t_F} - a_o\right] \tag{7}$$

Equation (7) is valid anywhere in the flow field. To obtain the piston path or particle path, set

$$\frac{dx}{dt} = u = \frac{2}{\gamma+1}\left[\frac{x-x_F}{t-t_F} - a_o\right] \tag{8}$$

This is a linear first order differential equation which can be solved by changing variables to $y = x - x_F$, $\phi = t - t_F$ and using an integrating factor. The solution for the piston is obtained by applying its initial conditions $x_i = t_i = 0$. The result is

$$\frac{x_p}{x_F} = 1 - \frac{2}{\gamma-1}\left[\frac{\gamma+1}{2}\left(1 - \frac{t}{t_F}\right)^{\frac{2}{\gamma+1}} - \left(1 - \frac{t}{t_F}\right)\right] \tag{9}$$

where $x_F = a_o t_F$ was used. The piston velocity and acceleration are given by the first and second derivatives of Equation (9)

$$\frac{u_p}{a_o} = \frac{2}{\gamma-1}\left[\left(1 - \frac{t}{t_F}\right)^{-\frac{\gamma-1}{\gamma+1}} - 1\right] \tag{10}$$

$$\frac{A_p t_F}{a_o} = \frac{2}{\gamma+1}\left(1 - \frac{t}{t_F}\right)^{-\frac{2\gamma}{\gamma+1}} \tag{11}$$

Equation (10) can also be obtained by substituting Equation (9) into (7). Equation (11) gives a value for both x_p and

t_F when the initial piston acceleration, $A_{p,i}$, is specified:

$$A_{p,i} = \frac{2 a_o}{(\gamma+1)\, t_F}$$

so, that

$$x_F = a_o t_F = \frac{2 a_o^2}{(\gamma+1)\, A_{p,i}} \qquad (12)$$

Equations (9), (10) and (11) demonstrate some of the physical features of the flow. First, if the piston continued to accelerate past t_F, obviously the wavelets could not reach x_F at t_F. All equations demonstrate this because they are not valid for $t > t_F$. Also it would be expected that if a wavelet were sent out near t_F, it would have to travel very fast to reach the focus point along with the earlier wavelets. Equations (10) and (11) show this because both piston velocity and acceleration go to infinity as $t \to t_F$ and

$$\lim_{t \to t_F} \frac{x_p}{x_F} = 1$$

Equation (9) is derived by Glass and Hall;[22] however, their forms for piston velocity and acceleration depend on x and t instead of t alone. Hall[1] correctly plots piston velocity and acceleration for $\gamma = 1.4$ but does not give any equations for these quantities.

Equation (12) shows that the shock formation point increases as the undisturbed speed of sound increases. This

is logical since if it is imagined that the individual wavelets are initially separated by some Δx and move toward each other with some Δu, then there will be a Δt before they merge. If the waves move fast, they will travel a long way in this Δt. Also the formation point increases as the initial piston acceleration decreases. This also is logical because it would be expected that the Δx would be larger for smaller $A_{p,i}$. Rudinger[17] has developed Equation (12) for the case of a piston with a constant acceleration.

Energy Analysis

Some authors argue the existence of waves reflected back toward the piston from the shock based on conservation of energy. Although these studies are not of a focused wave it is appropriate to mention the results here.

The conservation of energy provides a somewhat different viewpoint of shock formation than is given by the pressure-velocity plane and the speed of sound-velocity plane analyses. It is clear that a simple compression wave can be created in an initially motionless gas by an accelerating piston. Therefore, in a simple wave, that is prior to the merging of any wavelets, energy conservation shows that the work done by the piston on the gas must equal the energy gained by the gas due to the simple wave. A proof of this energy conservation for a focused wave was obtained in this study and is presented in Appendix A. Thus, it is clear

that there is no requirement for reflected waves prior to wavelet merging. Although the proof has been made for a focused wave, this energy conservation must be true for any type of simple compression wave.

Friedrichs[3] studied an instantaneously created shock followed by a simple expansion wave as the piston was slowed to a stop. The entire flow was assumed isentropic. Lighthill[7] verified Friedrichs' theory by an energy analysis. Lighthill compared the piston work to the energy of the simple wave and found that they differed by a "residual energy". This is the energy in the region behind the simple wave and is proportional to the entropy gain there. In the Friedrichs theory the pressure and speed of sound return to initial values. However, examination of the residual energy showed that the average pressure behind the simple wave is below the initial value and is due to a wave which is a reflection of the original simple wave from the shock.

In his study of the formation of a shock wave, Shunk[8] states that Lighthill showed that the energy in a simple wave is greater than the work done by the piston. Therefore, Shunk concludes, an expansion wave must be formed so that its energy plus the energy of the original wave equals the work done by the piston. Although this statement is correct it should be emphasized that only when the non-isentropic process of a shock is present is a reflected

expansion necessary to balance energy. In Lighthill's case a shock is always present but in the shock formation case there is always a period prior to wavelet coalescence when the piston work equals the increase in energy due to a simple wave. Only after coalescence do the conservation laws of fluid flow require an expansion to be reflected as shown earlier by the P , u plane analysis.

An additional point needs to be made in connection with Lighthill's conclusions. The original simple wave from the piston is an expansion, and Lighthill says that the reflection of this wave from the shock drops the pressure behind the simple wave. Thus the reflected wave is also an expansion. But this is not possible since the shock reflection coefficient (to be discussed in Chapter III) is negative so that the simple expansion wave must be reflected from the shock as a compression. The explanation of the pressure drop behind the simple wave may be as follows. The reflection of the simple expansion wave from the entropy gradient will be an expansion wave. These reflected expansions may overpower the reflected compression waves (see Equation (39) in Chapter III).

Summary of Conclusions

As a piston accelerates into initially motionless gas, the gas next to the piston is compressed isentropically and the gas some distance away is compressed nonisentropically,

as the gradients in velocity, pressure and temperature steepen and a shock wave forms. The fundamental difference between these two compressions is the magnitude of the gradients and the corresponding effect on the entropy.[21] Based on the solutions for the focused wave in this chapter, once the nonisentropic process occurs, readjustments in the isentropic flow occur in the form of a weak expansion wave reflected from the shock back toward the piston. Also, as a result of the two different processes, the compressed flow will not have uniform temperature, density or entropy.

Equation (12) gives the point at which the shock first forms and is valid for dispersed or focused waves, as long as A_p is constant for the former.[17] This equation gives an idea of how large the isentropic region may be. In principle this region always exists; however, for a piston which is instantaneously accelerated to a given speed the isentropic region shrinks to zero. On the other hand, in a transportation tube with a slowly accelerating vehicle this region may be very large.

These same phenomena will occur in the dispersed wave case to be studied in the next chapter. The different compressions which occur in that case will not be isentropic verses nonisentropic, but nonisentropic verses more nonisentropic. The shock becomes more nonisentropic as it continues to grow in strength and the width of the region with an entropy gradient depends on the particular case.

CHAPTER III

DISPERSED COMPRESSION WAVE

As already mentioned, most of the basic physical phenomena which occur in a general dispersed wave case have already been observed in the focused wave problem. The only phenomena not treated there is the effect of an entropy gradient on traversing isentropic waves.

Since a focused wave is experimentally difficult to produce[1,2,23] and the dispersed wave is the one which occurs naturally, it is frequently necessary to analyze a dispersed or natural wave. The subject of this chapter is a dispersed compression wave created by a piston whose acceleration is always positive but decreases with time. A single shock wave forms at the head of the compression wave.

The characteristic equations will be presented and the technique of solution described. An example is worked out and the various results are verified. Before the results are verified, some additional viewpoints to the numerical characteristic method are discussed. These include the P, u plane analysis of the effect of an entropy gradient on a wave and reflection coefficients. After the characteristic results are checked, the nature of the resulting flow is

examined and some ideas for simplifying the characteristic method are suggested.

Method of Characteristic Solution

The set of Equations (1-3) are of the hyperbolic type and the numerical method of characteristics can be used to solve them. As indicated earlier, the characteristic technique was chosen since it is an essentially exact solution of the equations. The only approximations are due to errors in taking finite steps in the numerical procedure and in assuming a perfect gas. Of course the equations themselves contain the assumptions of adiabatic, frictionless, and one-dimensional flow.

The technique used for solving the characteristic equations is described in the excellent book by Rudinger.[17] Except where noted, the equations and methods described in this section are based on Rudinger's technique. Humphrey[14] presents a method of solution which is somewhat different, possibly more appropriate for a computer solution.

The numerical computing method is based on changes in the Riemann variables

$$P \equiv \frac{2}{\gamma - 1} a + u \tag{13}$$

$$Q \equiv \frac{2}{\gamma - 1} a - u \tag{14}$$

along the respective physical characteristics which are defined as curves with slopes

$$\frac{d\xi}{d\tau} = \mathcal{U} + \mathcal{A} \quad \text{for } P \tag{15}$$

$$\frac{d\xi}{d\tau} = \mathcal{U} - \mathcal{A} \quad \text{for } Q \tag{16}$$

Here $\mathcal{A}$ and $\mathcal{U}$ are dimensionless speed of sound and flow velocity and ξ and τ are dimensionless distance and time. Dimensionless quantities are preferable to dimensional quantities in the numerical analysis. Physically, Equations (15) and (16) define the paths of wavelets which move in the positive and negative direction with respect to the local flow. Equation (15) defines the P characteristic and Equation (16) defines the Q characteristic. For the assumptions of this study, the only changes which occur in the Riemann variables along the physical characteristics are due to an entropy gradient. These changes are governed by the compatability or state characteristic equations

$$d P = \mathcal{A}(dS) = d Q \tag{17}$$

where $S = s/\gamma R$ is a dimensionless entropy and R is the specific gas constant. Equation (17) is actually a wave equation since it governs the changes in P and Q along the path of a positively or negatively moving wavelet.

Since the shock grows continually in strength, there will be a gradient in entropy from the piston up to the

instantaneous shock location. This entropy gradient through the shock layer (the compressed gas) is treated by dividing the shock layer up into strips parallel to the particle paths (in the ξ , τ plane). Each strip is assigned a value of the entropy which is an average of the highest and lowest values in the strip. It was found in this study that for a change in entropy, dS, along a P or Q characteristic, Equation (17) could be integrated by assuming $d\mathcal{U} = 0$ in the region where dS occurs. This is justified by arguing that $\mathcal{U}$ is the same on both sides of the entropy discontinuity, which is valid in a numerical approach. Using Equations (13) and (14), integration of Equation (17) gives for either P or Q characteristics

$$\frac{a_R}{a_L} = e^{\frac{\gamma-1}{2}(S_R - S_L)} \tag{18}$$

where the subscripts R and L indicate right and left respectively of the entropy discontinuity or "entropy interface." The changes in P and Q are found from the definition Equations (13) and (14) and Equation (18) to be

$$P_R = P_L + \frac{2}{\gamma-1} a_L \left(e^{\frac{\gamma-1}{2}(S_R - S_L)} - 1 \right) \tag{19}$$

$$Q_L = Q_R + \frac{2}{\gamma-1} a_R \left(e^{\frac{\gamma-1}{2}(S_L - S_R)} - 1 \right) \tag{20}$$

Equation (19) shows that when all conditions are known on

the left of an entropy interface, the value of P on the right side can be computed by knowing only the entropy change across the interface. In this respect Equations (19) and (20) are easier to use than the corresponding equations given by Rudinger. His form of Equation (19) also requires a knowledge of Q_R in order to compute P_R. For

$$\frac{\gamma-1}{4}\left|S_R - S_L\right| << 1$$

Equations (19) and (20) can be approximated by

$$P_R - P_L \approx \rho_L (S_R - S_L) \tag{21}$$

$$Q_L - Q_R \approx \rho_R (S_L - S_R) \tag{22}$$

Average values of ρ occur in these equations if Rudinger's form of Equations (19) and (20) is reduced, which probably gives greater accuracy. That Equations (19) and (20) reduce to a form similar to Equation (17) is some justification of the assumption $u_L = u_R$.

Briefly, the computation technique involves knowing two of the four quantities in Equations (13) and (14) and solving for the other two. On the piston face u and Q are known. In the shock layer P and Q are known. When all four quantities P, Q, ρ, u, are known at a point, the P characteristic is drawn in at a slope of $u + \rho$ and the Q characteristic at a slope of $u - \rho$ (according to Equations (15) and (16)). The characteristics are drawn in the ξ, τ

plane on a large sheet of graph paper. When a characteristic crosses an interface (slope of $\mathcal{U}$) the change in P or Q is found by Equations (19) and (20) or (21) and (22). For all curves the slope drawn between two points was gradually changed between the two known values.

Once the speed of sound and entropy are known at a point in the shock layer, the static pressure can be computed. The equation for the change in entropy is

$$s - s_o = c_p \ln \frac{T}{T_o} - R \ln \frac{p}{p_o}$$

Using the relationship between specific heat at constant pressure, c_p, and γ and R

$$\frac{c_p}{R} = \frac{\gamma}{\gamma - 1}$$

and the speed of sound relation

$$\frac{T}{T_o} = \left(\frac{a}{a_o}\right)^2 = \mathcal{a}^2$$

the entropy equation can be rewritten as

$$p = p_o \mathcal{a}^{\frac{2\gamma}{\gamma-1}} e^{-\gamma S} \qquad (23)$$

where S_o is set equal to zero, since only entropy differences are considered. Note that the undisturbed gas conditions have been taken as the reference conditions p_o, a_o, S_o. Even if various undisturbed gas conditions are used, $S_o = 0$ is still valid because the various conditions just

have a different base for the entropy values.

Now that the general computation scheme for the shock layer has been described, consider what happens when wavelets merge into the shock, that is when P characteristics intersect the shock. The beginning of the shock occurs when the first two P characteristics intersect. The shock strength at any point on its path is determined by the difference between the value of P behind the shock at the given point and P ahead of the shock, divided by a ahead of the shock. Thus when a P characteristic is plotted through the shock layer, the value of P being constant except when an entropy interface is crossed, the characteristic will eventually intersect the shock. The shock strength at this point is computed using the final value of P on this characteristic.

The equation governing shock strength is obtained by taking the difference between the P variable definition ahead of and behind the shock. Using a single prime to indicate conditions ahead of the shock and a double prime behind, the result is

$$\frac{P''-P'}{a'} = \frac{2}{\gamma-1}\left(\frac{a''}{a'}-1\right) + \frac{u''-u'}{a'} \qquad (24)$$

Equation (24) is given by Rudinger. However, a form which contains a more familiar combination of variables was obtained in this study in the following manner. The

absolute shock speed for a P shock (a shock moving in the direction of positive velocity which is to the right) is the sum of the flow velocity and the shock velocity with respect to the local flow. This is written

$$\left(\frac{d\xi}{d\tau}\right)_s \equiv w = u' + W' = u'' + W'' \qquad (25)$$

The continuity equation for the shock wave is

$$\rho' W' = \rho'' W'' \qquad (26)$$

Equations (25) and (26) can be combined to evaluate the last term in (24), giving the final result for shock strength as

$$\frac{P''-P'}{a'} = \frac{2}{\gamma-1}\left(\frac{a''}{a'} - 1\right) + M_{W'}\left(1 - \frac{\rho'}{\rho''}\right) \qquad (27)$$

where $M_{W'}$ is the Mach number of the shock wave

$$M_{W'} \equiv \frac{W'}{a'}$$

All variables on the right hand side of Equation (27) are a function of $M_{W'}$ and a standard normal shock table can be used to evaluate them. Rudinger's book contains tables of $(P''-P')/a'$ as a function of $M_{W'}$, $S'' - S'$ and other flow variables. Since P' and a' are known from the initial gas state and P'' is known from the intersecting characteristic, the shock strength is always readily calculated.

Earlier it was said that in the shock layer Q is known. Now that the shock has been discussed this point can be made clear. Prior to any wavelet merging, a simple wave exists. In characteristic terminology this means that all Q characteristics have the same value of Q and this value is the one in the undisturbed flow. After the shock forms, Q just behind the shock can be computed since "U" and "Q" are known. Then the Q characteristic can be drawn in as described above.

A very important point concerning finding Q at the shock should be mentioned. Since finite steps are taken in a numerical procedure, accuracy is increased if quantities between two points are taken as an average of the two points. The entropy strips were defined by particle paths from adjacent computed shock points. Therefore a correct entropy for a given strip must be an average of the entropy at adjacent shock points. Since the value of Q throughout the shock layer depends on the entropy gradient, the correct initial value of Q must also be an average of the Q values at adjacent shock points. The Q characteristic is drawn by starting at the midpoint of the shock increment. Since interpretation of reflected wave phenomena is based on Q values, not using these averages can result in an erroneous interpretation of reflected waves (using an average entropy but not using an average Q value for example).

The order in which computations were made was to work along a P characteristic all the way from the piston path to the shock. Then all existing Q characteristics and particle paths were extended from the preceding P characteristic up to the one just calculated. The slopes are gradually changed between the two known values by use of a French curve. Similarly the shock is extended from the previous point to the one just computed. Appendix B gives a detailed example to clarify the scheme.

The boundary conditions on the problem are an impermeable piston moving along a given path in the ξ , τ plane and initially undisturbed uniform gas ahead of the piston. The piston path can be prescribed as a path determined from experiment, or can be a computed path. A computed piston path is obtained by a simultaneous characteristic solution of the driver and driven tube gases. The resulting pressures give the force on the piston, which is then substituted into Newton's second law of motion. Integration of Newton's second law gives the piston velocity and position as functions of time.

The undisturbed driven gas conditions were always used as the reference conditions in dimensionless quantities. When graphical procedures are used, it is necessary to use the same reference conditions for both the driver and driven gas and for the piston motion.

As indicated earlier, graphical techniques were employed in the characteristic solution by plotting wavelet or characteristic paths, and piston, particle and shock paths in the ξ, τ plane. This procedure is much faster than numerical calculation of the points of intersection; of course, these points would have to be found numerically if a computer solution were used. Note that the spacing of the P characteristics emanating from the piston path determines the size of the mesh. Decreasing the mesh size was found to have a significant effect on only the shock and only during its period of initial growth. The shock strength at later times and the shock layer flow variable distributions were unaffected within the accuracy of the hand computations. The insensitivity of the flow variables to mesh size is due to the primary dependence of pressure and flow velocity on the piston path and the relative constancy of these quantities along the P characteristics. Once the P characteristic intersects the shock, the new shock strength is then established by the flow velocity on that characteristic (the shock strength is fixed by $(u'' - u')/a'$).

Another great time saver was a graphical method due to Schmidt for obtaining the slope of P and Q characteristics and particle paths.[18] Also, Equations (13) and (14) for the Riemann variables can be used to plot an a, u state plane; however, it takes about the same time to solve Equations (13)

and (14) on the state plane as it does by use of a hand calculator. With a specified piston path, an accurate solution required about 12 man-hours, whereas Shunk's[8] technique required 10 days.

An example problem labeled Case II has been worked out according to this theory. A piston is accelerated from rest to the same final speed and into the same gas as the focused wave example in Chapter II (Case I). The wave is a dispersed wave and the wavelets merge into each other one after the other. A single shock wave forms at the front of the compression wave. The piston path up to $\tau = 0.5$ is one which had been previously calculated for a frictionless piston of 0.4 lb_m, with an initial driver tube pressure of 100 atm and an initial driven tube pressure of 0.01 atm. The driver gas was hydrogen and the driven gas was argon, both initially at room temperature. Both the driver tube and the driven tube inside diameter was 1.5 inches. At $\tau = 0.5$ the acceleration was abruptly brought to zero and maintained there. Tables 1-4 give the results of the calculations, the piston path and the initial gas conditions (only the driven gas is of interest). Figure 5 is the graphical wave diagram solution.

Before the results of the characteristic solution of Case II are examined, some additional viewpoints will be developed. These will be used in verifying and interpreting the characteristic solution. First, the P, u plane is

used to examine the effect of an entropy gradient on a wave, followed by a discussion of the reflection coefficient concept.

P, U Plane Analysis of Entropy Gradient Effect on Waves

Some objectives of this study are to determine just what types of waves are passing through the shock layer, how strong they are, what effect the entropy gradient has on them, how they die out, and so on. As explained previously, the entropy gradient is treated by dividing the shock layer into strips of constant entropy. A tool which can assist in clarifying the nature of the shock layer wave system, and also serve as some check on the characteristic results, is the effect of a single entropy interface on an isentropic simple wave. The question arises, of course, whether results from a simple wave analysis apply in a nonsimple wave region (a region where waves travel in both directions simultaneously). A reasonable justification of such an application is to imagine that the right and left moving wave can each be represented by a series of small waves. These small waves are selected so that the entropy interface is crossed alternately by one from the left and then one from the right. Thus the problem reduces to that of analyzing a simple wave as it crosses the entropy interface. A further justification of this application of simple wave theory is that the conclusions drawn from a simple wave

analysis do agree with the method of characteristics analysis of a nonsimple wave. This will be demonstrated in the section Analysis of Case II Results.

The effect of an entropy interface on a simple wave is determined by use of the P, u plane. Since no reference was found which satisfactorily discussed the P, u plane, a brief analysis is made in Appendix C. For the P, u plane shown in Figure 6 the pressure and velocity are made dimensionless with p_o and a_o determined by the initial conditions. For a wave moving in the direction of positive velocity (to the right, i.e. a P wave), changes occur along the curves with a positive slope. For a Q wave, changes occur along the curves with a negative slope. Unlike the a, u plane, lines of constant P or Q are curved and intersect. Which curve is traversed depends basically on the value of the entropy of the gas (therefore on the temperature or speed of sound since the initial pressure is the same).

The P, u plane is not the only method of analyzing the effect of an entropy discontinuity on a simple wave. Application of the general principles of the method of characteristics, without use of any numbers, very quickly gives the same results. However, use of the P, u plane is something of an independent check on the characteristic solution.

The flow situation to be analyzed is a flowing gas of uniform velocity, pressure and specific heat. The gas is separated into two parts by an entropy or temperature "discontinuity", each part having its own but uniform entropy and temperature. Incident upon this discontinuity is a simple wave. Assume that the discontinuity is moving to the right initially and the wave approaches from the left. Four possible situations exist then: a compression wave moving from low to high entropy or high to low entropy; and the same two possibilities for an expansion wave. As in the solution of the focused wave, the basic boundary condition to be satisfied is that the final pressure and velocity are the same on both sides of the discontinuity. An example of a compression wave moving from a region of low to high entropy is given in Figure 7. When the compression wave hits the entropy discontinuity, a compression wave is transmitted and an expansion wave is reflected.

Note that left moving waves would not be different than the ones considered above because if right moving waves are viewed from the other side of the tube, they will be left moving waves. Likewise, the direction of the initial gas velocity is unimportant as long as the wave crosses the discontinuity.

From the analysis of the above four situations for a simple wave crossing an entropy discontinuity or interface, the following useful rules are concluded:

(i) Regardless of the type of wave (expansion or compression) or direction of entropy change (increase or decrease), the transmitted wave is always of the same type as the incident wave.

(ii) When the incident wave moves from a low to high entropy region, the reflected wave is of the opposite type to the incident wave; the transmitted wave is weaker pressure wise but stronger velocity wise than the incident wave.

(iii) When the incident wave moves from a high to low entropy region, the reflected wave is of the same type as the incident wave; the transmitted wave is stronger pressure wise but weaker velocity wise than the incident wave.

Reflection Coefficient

The treatment of the focused wave in Chapter II indicated that when an isentropic wave overtakes a shock wave, the isentropic wave is partly reflected. The P, u plane analysis of the previous section showed that when an isentropic wave crossed an entropy interface, it is partly reflected. Although both analyses showed what type of wave is reflected, neither analysis gave any general rule for the strength of the reflected wave. The purpose of this section is to present expressions by which the strength of the reflected wave compared to the incident wave can be

calculated. Such an expression is called a reflection coefficient. Reflection coefficients for both an entropy interface and for a shock wave will be discussed.

Knowledge of the strength of reflected waves is very useful. If the reflected wave is much weaker than the incident wave (small reflection coefficient), then the wave system will die out quickly after the piston reaches a constant velocity. Also, if the reflected waves are weak, certain simplifying approximations can be made in the calculations, as will be discussed in the last section of this chapter. The sign of the reflection coefficient indicates what type of wave is reflected. In this sense, the reflection coefficient serves as a check on conclusions from alternate viewpoints.

The entropy reflection coefficient will be derived first. Consider what happens when an isentropic wave suddenly hits an entropy interface. The P, u plane analysis showed that both a transmitted and a reflected wave were required to maintain the boundary conditions of equal pressure and equal velocity on both sides of the interface. The basis of the reflection coefficient approach is to ratio the pressure change of the reflected wave along one characteristic to the pressure change of the incident wave along the opposite characteristic. From Equations (13) and (14) the compatability equations for isentropic flow are

$$o = d\bar{P} = \frac{2}{\gamma-1} da + du \qquad (28)$$

$$o = d\bar{Q} = \frac{2}{\gamma-1} da - du \qquad (29)$$

Since the boundary conditions are in terms of pressure and velocity and the reflection coefficient involves pressure changes, Equations (28) and (29) must be transformed into dp and du. Using the isentropic relation

$$\frac{p}{\rho^{\gamma}} = \text{constant}$$

and the speed of sound relationship

$$a = \sqrt{\frac{\gamma p}{\rho}}$$

it is found that

$$da = \frac{a(\gamma-1)}{2p\gamma} dp$$

Thus Equations (28) and (29) become

$$dp = -\frac{\gamma p}{a} du \quad \text{along} \quad \frac{dx}{dt} = u+a \qquad (30)$$

$$dp = \frac{\gamma p}{a} du \quad \text{along} \quad \frac{dx}{dt} = u-a \qquad (31)$$

Consider the incidence of a P wavelet or characteristic on an entropy interface such as occurs between points 18 and 19 in Figure 5b. The strength of the incident, reflected and

transmitted waves are, by Equations (30) and (31) (the reflected wave is not shown in Figure 5b)

$$dp_i = -\frac{\gamma p_i}{a_i} du_i \tag{32}$$

$$dp_r = \frac{\gamma p_i}{a_i} du_r \tag{33}$$

$$dp_t = -\frac{\gamma p_i}{a_t}\left(du_i + du_r\right) \tag{34}$$

where the pressure and velocity boundary conditions have already been applied. The reflection coefficient is defined as

$$r_e \equiv \frac{dp_r}{dp_i} = -\frac{du_r}{du_i} \tag{35}$$

where Equations (32) and (33) have been substituted. In order to evaluate du_r/du_i the pressure boundary condition is again applied

$$dp_i + dp_r = dp_t$$

Substituting Equations (32), (33) and (34) it is found that

$$\frac{du_r}{du_i} = -\left(\frac{a_i - a_t}{a_i + a_t}\right)$$

Thus the reflection coefficient can be written as

$$\eta_e = \frac{1 - \frac{a_R}{a_L}}{1 + \frac{a_R}{a_L}} = \frac{1 - \sqrt{\frac{T_R}{T_L}}}{1 + \sqrt{\frac{T_R}{T_L}}} \qquad (36)$$

where (i,t) have been replaced by (L,R). Therefore, the reflected wave strength depends on a_R/a_L. If $a_R > a_L$, that is the wave travels from a region of low to high entropy, the reflection coefficient is negative and the wave is reflected in the opposite sense. This agrees with the P, u plane analysis. Other convenient forms for the reflection coefficient can be found. Substituting the speed of sound ratio across the entropy interface from Equation (18) into Equation (36), the reflection coefficient takes the form

$$\eta_e = -\tanh\left[\frac{\gamma-1}{4}\left(S_R - S_L\right)\right] \qquad (37)$$

By use of Equations (18), (19) and (37) and the definition of P_L and Q_R, the reflection coefficient can also be written as

$$\eta_e = -\left(\frac{P_R - P_L}{P_L + Q_R}\right) \qquad (38)$$

Properties of the hyperbolic tangent show that approximate forms of Equation (37) are

$$r_e \approx -\left[\frac{\gamma-1}{4}\left(S_R - S_L\right)\right] \quad \text{when} \quad \left|S_R - S_L\right| \leq \frac{0.4}{\gamma-1} \tag{39}$$

and

$$r_e \approx \mp 1 \quad \text{when} \quad \left(S_R - S_L\right) \begin{cases} > \frac{.12}{\gamma-1} \\ < -\frac{.12}{\gamma-1} \end{cases} \tag{40}$$

Equation (40) gives the condition for almost total reflection of the incident wave. Such a condition could exist for a flow where M_W, varied from 1 to ∞. On the other hand, Equation (37) shows that as γ approaches 1, r_e approaches 0. Note that all the above expressions for the reflection coefficient are valid for P waves only. The reflection coefficient for Q waves is just the negative of that for P waves.

An expression for the shock reflection coefficient is given by Equation (48) of Lighthill. In the present notation it is

$$r_s = \left[\frac{a'' + u'' - W'}{a'' - u'' + W'}\right]\left[\frac{1 - \rho'' a''\left(\frac{du}{dp}\right)_s}{1 + \rho'' a''\left(\frac{du}{dp}\right)_s}\right] \tag{41}$$

Where $(du/dp)_s \equiv (du''/dp'')$ is for the shock wave (this quantity appears in the derivation in place of a transmitted wave effect). Using Equation (25) for the absolute shock speed and $u' = 0$, the first term in Equation (41) can be rewritten as

$$\frac{a'' + u'' - W'}{a'' - u'' + W'} = \frac{1 - M_{w''}}{1 + M_{w''}}$$

Now Equation (41) can be written in a more convenient form

$$\pi_s = \left[\frac{1 - M_{w''}}{1 + M_{w''}}\right]\left[\frac{1 - \frac{\gamma p''}{a''}\left(\frac{du}{dp}\right)_s}{1 + \frac{\gamma p''}{a''}\left(\frac{du}{dp}\right)_s}\right] \qquad (42)$$

When the relation between flow velocity u'' and pressure p'' for a moving shock wave is differentiated, the expression in the second bracket of Equation (42) can be evaluated. The result is (where $u' = 0$ has been used)

$$\frac{\gamma p''}{a''}\left(\frac{du}{dp}\right)_s = \frac{\gamma \frac{p''}{p'}}{\frac{a''}{a'}}\left[\frac{1}{\sqrt{\frac{p''}{p'}\frac{\gamma(\gamma+1)}{2} + \frac{\gamma(\gamma-1)}{2}}}\right. \qquad (43)$$

$$\left. - \frac{\left(\frac{p''}{p'} - 1\right)\frac{\gamma(\gamma+1)}{4}}{\left(\frac{p''}{p'}\frac{\gamma(\gamma+1)}{2} + \frac{\gamma(\gamma-1)}{2}\right)^{3/2}}\right] = \frac{\gamma \frac{p''}{p'}}{\frac{a''}{a'}}\left(\frac{du}{dp}\right)_s$$

Equation (43) is most easily evaluated by approximating $(du/dp)_s$ by use of shock tables such as Table 1 of

Rudinger's book.[17] From Equations (42) and (43) it is seen that r_s is a function of only $M_{w'}$ and γ. Figure 8 shows the variation of r_s with $M_{w'}$ for $\gamma = 1.667$. It is seen that the magnitude of r_s increases as $M_{w'}$ increases and that r_s is always negative. Since r_s is negative, a compression wave will reflect from the shock as an expansion wave, which is the same result that was found for the focused wave.

Some additional insight is provided by the limiting form of r_s for large $M_{w'}$. First, for large $M_{w'}$ (therefore $p''/p' \gg 1$), Equation (43) reduces to

$$\frac{\gamma p''}{a''}\left(\frac{du}{dp}\right)_s = \sqrt{\frac{\gamma}{2(\gamma+1)}\frac{\rho''}{\rho'}}\;\frac{p''}{p'} \gg 1 \qquad (44)$$

For large $M_{w'}$, the normal shock wave equations (written in a coordinate system attached to the shock) yield the following limiting values for the density ratio across the shock and the downstream Mach number

$$\frac{\rho''}{\rho'} = \frac{\gamma+1}{\gamma-1} \qquad M_{w'} \to \infty \qquad (45)$$

$$M_{w''} = \sqrt{\frac{\gamma-1}{2\gamma}} \qquad M_{w'} \to \infty \qquad (46)$$

When Equations (44), (45), and (46) are substituted into Equation (42), the resulting expression for r_s is a simple

function of γ only

$$r_s = \left[\frac{1 - \sqrt{\frac{\gamma-1}{2\gamma}}}{1 + \sqrt{\frac{\gamma-1}{2\gamma}}}\right]\left[\frac{2\sqrt{\frac{\gamma-1}{2\gamma}} - 1}{2\sqrt{\frac{\gamma-1}{2\gamma}} + 1}\right} \quad (47)$$

$$M_{W'} \longrightarrow \infty$$

Table 5 shows the variation of r_s with γ according to Equation (47). It is seen that as γ approaches 1, the value of r_s approaches -1, which is total reflection of the wave at the shock.

Very little previous work on reflection coefficients has been done for one-dimensional unsteady flow. Lighthill has a very limited analysis of Equation (41) and no reference has been found which discusses r_e. Hayes and Probstein (Reference 15, Section 7.2) discuss both coefficients for two-dimensional flow, where analogous results occur.

It is not sufficient to discuss the effects of reflected waves from entropy interfaces and the shock wave separately since in general they occur simultaneously. For the case of an entropy decrease from the piston to the shock (decaying shock), r_e is postive for P waves. Since r_s is always negative, in this case the primary or first reflected waves will tend to cancel. For an entropy increase from the piston to the shock (shock formation), r_e is negative for P waves. Thus, in this case the primary reflected waves will

reinforce each other. This reinforcement is demonstrated by some calculations for Case II. Based on the characteristic results, Table 6 gives an estimated value of $r_s + \sum r_e$ at the piston for the entire initial compression wave. To obtain the total reflected wave strength a single entropy strip next to the piston must be used. The incident wave strength was the pressure change between points 1 and 18 of Figure 5 and the reflected wave strength was estimated by assuming an average P = 6 and using the drop in Q from points 1 to 34 (the result is not sensitive to P). The result is $r_s + \sum r_e = - 0.044$. Alternately, by use of Equations (42) and (43), it is found that $r_s = - 0.0035$ assuming an average $M_{W'} = 2$ of shock point 11. Across the entropy interface between strips 3 and 4, it is found that $r_e = - 0.0167$ by use of Equation (39). Therefore, assuming an average of two to three entropy interfaces (some reflected waves cross one interface and some cross four), the value of $r_s + \sum r_e$ is approximately - 0.045, which agrees with the characteristic estimate.

Analysis of Case II Results

Since the P, u plane and reflection coefficient concepts have now been discussed, these techniques can be used to aid in the analysis of the characteristic solution for Case II. The method of analysis of the Case II wave diagram solution will be to follow one wave for three

traverses of the shock layer. On each traverse the various features of the flow will be discussed.

The distribution of flow variables and wave phenomena are best revealed by viewing the flow in different ways. Four illuminating ways of viewing the flow which have been used in this study are:

(i) along a particle path or entropy strip

(ii) in ξ direction at constant τ

(iii) in τ direction at constant ξ

(iv) along a P characteristic

Method (i) is used in this section to study wave phenomena. Methods (ii) and (iv) are used in the next section to describe the nature of the resulting flow. (Method (iv) has already been used in discussing the effect of variation in mesh size.) Methods (ii) and (iii) are used in Chapter V for the comparison of the theoretical and experimental results. The advantages of the particular method used will become clear at the time of its use.

Figure 5 and Tables 1-4 give the results of the graphical solution for Case II. Figure 5 is called a wave diagram since it shows the paths of sound waves and shock waves in the dimensionless τ, ξ or time-distance plane. It is seen that the piston velocity (slope of the piston path) increases from $\tau = 0$ to 0.5 and is constant from then on. Likewise, the shock wave forms at $\xi = 0.24$ and has a subsequent increase in velocity until the final compression

wavelet created by the piston at $\tau = 0.5$ merges into the shock (a finer characteristic mesh would alter the shock formation point). Small variations in shock strength occur after this final wavelet merges; however, they are too small to be detected on the diagram. Using Equation (12) and an average value of $\bar{A}_p = 4.21$ for the time interval $\tau = 0$ to 0.10, an approximate value of the shock formation point is found to be $\xi = 0.178$. This value is an approximate check on the characteristic value. In Figure 5 the solid lines in the shock layer are characteristics or wavelet paths, and the dashed lines are fluid particle paths which define the entropy interfaces.

Previously, the entire disturbance created by the piston from $\tau = 0$ to 0.5 was called a wave and each individual disturbance such as 2-3 was termed a wavelet. Now, however, since no confusion can arise, and to be in conformity with usual terminology, the individual disturbances will be called waves.

The analysis will be initiated by considering the P waves (or characteristics) 12-16, 18-23 and a portion of their reflection, the average Q wave (or characteristic) 22-34. In the interest of simplicity, reflections from the entropy interfaces will be ignored for the moment. The rules obtained from the P, U plane analysis require that at an entropy interface the transmitted wave always be the same type as the incident wave. Therefore, since the piston

sends out (primary) compression waves as it accelerates, the P waves 12-16 and 18-23 (and others such as 4-6) should be compression waves. Also, according to the focused wave analysis, the merging of compression waves causes an isentropic process to become a nonisentropic process. The readjustments in the isentropic flow are made by an expansion wave reflected back towards the piston from the shock. A similar situation exists in the case of a dispersed wave. The gas particle initially at $\xi_1 = 0.422$ is compressed by the shock at point 6 and is further compressed by the gradual compression wave 8-10. However, the gas particle at $\xi_1 = 0.63$ is subject to the combined effects of these two compressions as a single shock at point 11. Therefore, the latter particle has a greater entropy increase than the former and it would be expected that readjustments in the former particle would occur by a weak reflected expansion wave. Thus the Q wave 22-34 (and others such as 5-12, 10-17) should be an expansion wave. That the shock reflection coefficient, r_s, is negative is also an indication that the compression waves from the piston should be reflected from the shock as expansion waves. Since r_s is small in absolute value, the reflected expansion waves should be weak compared to the primary compression waves.

That the P waves 12-16 and 18-23 are compressions and that the Q wave 22-34 is an expansion can be seen in Figures 9a,b which shows the interaction between right moving

isentropic compression waves and left moving isentropic expansion waves. Since the flow is isentropic, Q is constant on Q characteristics and P is constant on P characteristics. It is seen that in the region of mixed compression and expansion waves the value of P increases and the value of Q decreases along a particle path. From Figure 5 and Table 1 it is likewise seen that for the isentropic flow along a particle path such as along points 5, 13, 19 that P increases and Q decreases (these points are all in the same entropy strip and $DS/D\tau = 0$). Therefore, it is proven that the characteristic analysis has given the correct type of wave system in the region of the shock layer below the P wave 18-23 (the piston stops accelerating at point 18). The fact that the shock strength increases also shows that the P waves 12-16 and 18-23 are compression waves.

Before continuing, consider the reflections of the above P and Q waves at the entropy interfaces. Since the expansion Q waves are much weaker than the compression P waves, reflections of the Q waves will be ignored. The results of the $\mathcal{P}$, $\mathcal{U}$ plane analysis and the entropy reflection coefficient, r_e, show that reflections of the compression P waves will be weaker expansion waves. Hence, the weak expansion Q waves from the shock will be slightly reinforced by weak expansion Q waves from the entropy interfaces. Therefore none of the above conclusions are affected by reflections at the entropy interfaces.

That the total reflected expansion is weak compared to the primary compression was proven in the preceding section where $r_s + \sum r_e$ was determined. The value of this summation is further supported below where Cases I and II are compared.

It should also be mentioned that the terms right and left moving waves mean with respect to the local gas. Waves moving along a Q characteristic can actually obtain a rightward motion with respect to the laboratory frame. Rightward moving Q waves occur when $u > a$ so that $u - a$ is positive (see Equation (16)). Points 25 and 34 are two examples of such a motion.

Next consider the reflection of the expansion Q wave 22-34 as a P wave 34-41. These waves are typical of the region above the P wave 18-23. Again the wave type must not change in a single traverse of the shock layer. Since the Q wave is an expansion, the boundary condition at the piston of constant velocity requires that the reflected P wave also be an expansion. Hence, the region above the P wave 18-23 should contain expansion waves traveling to the left and to the right. Figures 9c and d show the interaction of left and right moving isentropic expansions. It is seen that along a particle path in the nonsimple flow region that both P and Q values drop. Likewise Figure 5 and Table 1 show that along a particle path such as 18, 25, 34, that both P and Q drop. Therefore, it is also proven

that the characteristic solution has given the correct wave system in the region above the P wave 18-23. As the P wave 34-41 intersects the shock, the shock is slightly weakened as seen from Table 2. This weakening of the shock also demonstrates that the wave 34-41 is an expansion wave. (The P wave 25-31 is also an expansion but makes the shock slightly stronger due to small numerical errors and the weak nature of the wave.) Since both reflection coefficients are small in absolute value, reflections of waves such as 22-34 and 34-41 will not alter the foregoing conclusions.

A numerical verification of the characteristic solution can be made by comparing Cases I and II. As mentioned earlier, both cases have the same initial gas state and the same final piston speed. Since the two techniques of solution are quite different, a comparison of them is a good verification of Case II. The two cases are not the same since the entropy gradients are much different; however, since the reflection coefficients are small, the cases should agree fairly well. The comparison is made in Table 6.

The primary compression from the piston is compared at the piston face, and is smaller in Case II due to expansion waves reflected back from the shock and entropy interfaces. The reflections of the primary compressions are compared. For Case I all the reflection occurs at the shock, but for Case II the reflections occur at the entropy interfaces as

well as the shock. Since in both cases the flow is adjusted between approximately the same two end points, isentropically compressed gas and gas downstream of the final shock, the reflections at the entropy interfaces should be included for Case II. The comparison is close. The final shock strength is also compared and is weaker for Case II due to expansion Q waves reflecting back off the piston and weakening the shock. In each of the foregoing comparisons the agreement is close enough to support the numerical results of the characteristic solution.

In conclusion, both the general flow features and the major numerical values of the characteristic solution have been verified. The wave phenomena in the shock layer have been verified by use of focused wave concepts, results of the P,u plane analysis, and reflection coefficients. The magnitude of the pressure and velocity changes caused by various phases of the shock formation process have been supported by the focused wave solution of Case I. Hence, it is concluded that the methods described in this chapter give an accurate and detailed theoretical solution for the formation of a shock wave from a dispersed compression wave. Determination of how well the theoretical model agrees with experimental results will be the objective of the following chapters.

Nature of Resulting Flow

The flow variables for Case II have been presented graphically for two times during the piston acceleration, and for a time long after the piston has reached a constant velocity. Figures 10-14 give the distribution of pressure, temperature, density, velocity and entropy during the piston acceleration at τ of 0.4 and 0.5. In each case the variable is divided by its value just downstream of the shock. If the curves for the distribution of a given variable at different τ had exactly coincided, the flow would be self-similar. Then the flow would be described by a constant value of n in the exponential piston path used by Chernyi[16] (Equation (4) in Chapter I). It is seen from the curves that the flow is only approximately self-similar.

Figures 15 and 16 give distributions of the same quantities as above for a τ long after the piston has reached a constant velocity. The last significant wave is the Q wave 22-34 which reflects from the piston as a P wave and intersects the shock at point 41. To plot the figures it was assumed that the flow variables were constant in the entropy strips after this P wave had crossed. Then the distributions were plotted for $\tau = 1.22$ which intersects the shock between points 31 and 41. The region of the shock layer compressed by the strongly varying shock and the primary compression waves from the piston has the unique feature of a flow in which a shock wave forms or decays. Gas initially

uniform in all properties has been compressed to a uniform pressure and velocity but with strong gradients in temperature, density and entropy. The focused wave was a simple example which demonstrated that such gradients would appear due to the increasing nonisentropicity of the compression process. It is also evident that the wave system did die out quickly once the piston reached a constant velocity. This rapid disappearance of the wave system was predicted on the basis of the fact that both reflection coefficients, r_e and r_s, have an absolute value much less than 1.

A particularly interesting facet of this compression process is that in spite of the eventual development of a strong shock wave, the gas next to the piston has been compressed isentropically. Also, when the reflected waves are weak, the pressure here can be quite accurately calculated from simple wave theory. It will be shown in Chapter V that the theoretical and experimental pressures agree within a few percent in this region.

The region of Figures 15 and 16 where the strong gradients exist is similar to the flow distribution along a P characteristic. This similarity can be understood by noting that if any primary P wave were the last one to be sent out by the piston, only small variations in flow properties would occur after its passage. Along a P characteristic from the accelerating piston of Case II, the pressure drops by about 1% and the flow velocity increases by about 1% due

to reflected expansion waves; however, much larger variations in T, ρ, and S occur. In a simple wave, all flow quantities p, u, T, ρ, and S would be constant along the characteristic.

The gradients in T, ρ and S explain some of the applications of the study of shock wave formation which were mentioned in Chapter I. Gas which is isentropically compressed to a given pressure rather than compressed by a shock wave to the same pressure, has a higher density and would have a lower dissociation if dissociation occurred. Therefore, isentropic compression produces a more realistic test gas for high speed, low altitude aerodynamic simulation.[1,2] In another application, consider the compression of a combustible gas by an accelerating piston. Due to the lower temperature in the isentropically compressed regions, the gas might not burn until the compression waves merged. This would cause combustion to occur far from the face of the piston.[20]

Simplifications in the Characteristic Technique

The method of characteristics gives a very detailed and accurate theoretical solution to the problem of shock wave formation, but it is very time consuming to obtain the final results. A few approximations will be mentioned which would speed up the solution and give approximate answers. The accuracy would depend on the particular flow.

If it is necessary to calculate only the shock strength and shock path, the changes in the Riemann variable P across the entire shock layer can be exactly computed in one step by Equation (19). Then the P characteristics can be approximately drawn in as straight lines. The accuracy of this approximation depends on the degree of variation in the slope of the P characteristics. This slope is $u + a$. As the shock strength increases, the approximation becomes less accurate. The accuracy was investigated for Case III, which will be discussed in Chapter V. There was no error in shock strength during the early stages of growth. The maximum error in pressure rise through the shock at later times was about 1%.

When complete flow detail is desired, two simplifications could be made. One is to assume that Q is constant in each entropy strip which is equivalent to assuming zero shock and entropy reflection coefficients. The two-dimensional steady flow counterpart of this problem is the shock expansion method, but would be more properly termed the "shock compression method" for unsteady one-dimensional shock wave formation. This approximation would be especially accurate in the case of a decaying shock as discussed previously (which would truly be a "shock-expansion method").

The second possible simplification would be to assume self-similar flow. Once enough detail was available to calculate the dimensionless flow variable distributions at

some constant τ, only the shock strength and path would have to be computed from then on. Knowing the shock strength at any subsequent τ, the calculated dimensionless distributions could be used to estimate the distributions of T, ρ, p, u at the subsequent τ.

CHAPTER IV

EXPERIMENTAL EQUIPMENT AND PROCEDURE

The method of characteristics has been utilized to obtain a theoretical solution to the problem of formation of a shock wave from a dispersed compression wave. An experimental program was designed and carried out with the objective of verifying this theoretical solution for a strong shock wave. In the present chapter the experimental equipment and procedure is described, while in the following chapter the experimental results are compared with the theoretical predictions.

Experimental Equipment

The piston tube used in these experiments consisted of sections of constant area circular tubing bolted together to form a 40 foot length. Mylar diaphragms were used to divide this tube into three sections. The first section, called the driver, was filled with air to a very high pressure. When this pressure became great enough to break the diaphragm, a small piston initially placed on the downstream side of the diaphragm was driven into the low pressure air of the second section (called the driven tube). As the piston accelerated into the low pressure air, it formed the

shock wave which was to be studied. A short section called the brake tube was provided at the end of the driven tube in order to decelerate the piston. The only gas used in this study was air.

The description of the piston tube will be divided into three principal parts. The tube design, the instrumentation, and the piston design will each be discussed.

Tube Design

Figure 17 is a diagram of the piston tube and the instrumentation. As mentioned above, the tube was divided by Mylar diaphragms into three sections, driver, driven and brake tubes. With the exception of the brake blind flange bolts, all tubing, flanges, and bolts were made of stainless steel in order to withstand the high gas pressures. High strength chrome-molybdenum bolts with an ultimate tensile strength of 125,000 psi were used on the brake blind flange. All flanges were welded to the tubes (except the brake blind flange which was removeable for cleaning the tube). A circular cross section was used for all tubes since it has the greatest structural strength.

The driven tube was made of five sections 39 1/4 inches long, honed to an inside diameter (ID) of 3.100 + .009 or - .002 inches. The wall thickness was approximately 3/4 inch. The brake tube was made from one section of this size. The driver tube was a single tube 20 feet 4 inches long with

a 3.360 inch ID and a 5/16 inch wall thickness. One end of the driver had a flange for attachment to the driven tube and the other end had a plug welded in it to seal it.

All flanges were 12 inches in diameter with a bolt circle diameter of 9 inches. Bolts with a 1 inch major diameter were used. Each joint had 9 bolts except the diaphragm joints where only 7 bolts were used to allow insertion of the diaphragms. Three C-clamps were used on the brake-driven joint to help strengthen it. With the exception of the blind flange assembly, the flanges were at least 1 3/8 inches thick. The brake blind flange assembly had one 2 1/2 inch thick flange and two 1 3/8 inch thick blind flanges. O-ring seals were used on all joints.

The driven sections were aligned during assembly by use of an expandable piston. The piston was inserted at each joint and expanded against the tube walls while the flange bolts were tightened. The driver and brake tubes were mounted on moveable carts to permit diaphragm insertion and cleaning of the tubes. The brake tube alignment was achieved by two pins inserted through both flanges at the brake-driven joint.

The driven tube was bolted to five stands each of which was in turn bolted to a track in the concrete floor by a single 3/8 inch diameter bolt. One bolt was used to attach the extreme end of the driver tube to the floor. This method of securing the piston tube permitted movement of

about 1 inch of the entire tube during an experiment. Permitting this movement avoided any attempt to rigidly tie down the tube while it was subjected to the extremely large deceleration forces of the piston (over 9000 psi on the brake blind flange).

The purpose of the brake tube was to permit deceleration of the piston without the occurrence of extremely high pressures on the brake blind flange. To illustrate the operation of the brake, the results of an approximate calculation will be given. The calculation determined the peak pressure on the brake blind flange for two tube configurations. In one configuration the brake and driven tubes formed one continuous tube filled to a pressure of 1 atm. In the other configuration, the brake tube was sealed from the driven tube with a diaphragm. The brake tube was filled to a pressure of 50 atm and the driven tube was again at 1 atm.

The calculation assumed that as the shock reflected back and forth between the piston and the blind flange, the regions on both sides of the shock were uniform. A perfect gas was assumed. The peak pressure on the blind flange in the former case was found to be 57,000 psi; but in the latter case the peak pressure was only 12,000 psi. The physical difference between the two cases is that in the case when the brake was at 50 atm, the piston experienced a high pressure much sooner than it did in the other case. As

a result, the piston was slowed down over a longer distance with a lower pressure. Thus, it is seen that from a structural viewpoint it was desirable to employ the brake tube.

Pressures on the order of 9000 psi were repeatedly measured on the blind flange for a piston with about the same acceleration characteristics and maximum velocity as the above mentioned case. The occurrence of these pressures is an approximate verification of the above calculations and therefore indicates that the driver gas leakage past the piston was not excessive (a further verification of the absence of gas leakage is the agreement between theory and experiment discussed in the next chapter).

An additional requirement for the brake tube was discovered when the piston was driven with a moderately high driver pressure of 860 psi in the non-brake configuration (the brake-driven diaphragm was in place but both tubes were at 1 atm). The pressure and temperature of the gas in the brake tube become so great during piston deceleration that hot gas leaked back between the piston and the tube wall and caused the Teflon sleeve of the piston to expand. The expansion caused the piston to become jammed inside the brake tube and the Teflon sleeve was ruined. The calculations of the deceleration process showed that much lower temperatures occurred when the brake tube was used.

An estimate of the boundary layer growth in the shock layer was made by use of the reference temperature method of Eckert.[28] Increasing the inside diameter and the initial pressure of the driven tube reduce both the boundary layer growth and heat transfer to the tube wall (Stoddard[2]). The inside diameter of 3.1 inches and initial pressure of 1 atm were felt to be sufficient. It was also found that if the non-brake configuration had a very low initial driven pressure, the piston came very close to the blind flange.

The brake tube was designed with a safety factor of 3 for a pressure of 12,000 psi. The driven tube was designed for 4500 psi with a safety factor of 6 and the driver tube was designed for 3000 psi with a safety factor of 5. These safety factors may not apply to the flanges of the driver and driven tubes; however, these flanges do satisfy the American Standard criterion for the above pressures. It should be mentioned, however, that these safety factors are based on static loads and may not apply for dynamic loads. The driver tube was filled to pressures up to 2000 psi and the brake tube was filled to one half the driver pressure. The initial driven tube pressure was always atmospheric. The maximum pressure on the brake blind flange was approximately 9500 psi.

The diaphragm material found most useful was 0.005 inch thick Mylar sheet. It was found that approximately one sheet was necessary for every 100 psi of pressure

differential. Multilayered diaphragms with up to 20 layers were used to withstand pressure differentials up to 2000 psi. The clamping technique used was simply to insert the diaphragm between the flanges (both flanges had an O-ring) and uniformly tighten the bolts.

The air supply and control system is shown in Figure 18. The air supply for the driven tube was room temperature and pressure air. The 10,000 psi valve on the brake tube was closed after the tube was filled. Closing this valve prevented the high pressures which occurred during piston deceleration from damaging the tubing and pressure gauges.

Numerious other piston tubes have been built and operated. See for example References 2, 13, 14, 29, 30, and 31.

Instrumentation

The instrumentation used during the motion of the piston consisted of magnetic pickups to measure the piston path and quartz pressure transducers. Data from these devices were recorded on Polaroid film by use of an oscilloscope and camera. In addition, the tube pressures prior to rupture of the driver-driven diaphragm were measured by pressure gauges. Some components of the brake blind flange assembly were monitored for permanent strain by the use of strain gauges. Each of these items is briefly described below.

The piston path in the ξ, Υ plane was determined by use of five type 3055-A subminiature magnetic pickups produced by Electro Products Laboratories. The pickup is 1/4 inch in diameter. When a magnetic material moves near the pole piece at the end of the pickup a voltage output is produced. Hence as the piston passed each pickup a pulse was generated on the oscilloscope trace. Two pickups were placed in the first section of the driven tube because the slope of the piston path changes most rapidly in this region. The other three pickups were spaced at approximately three foot intervals (see Figure 17).

Since voltage output depends, among other factors, on the gap width between the piston and the pole piece, the pickups were inserted flush to the inside diameter of the driven tube (this was accomplished by visual sighting from one end of the driven tube). The voltage output was generally satisfactory with a vertical gain on the oscilloscope of 1 volt per division. Each pickup should have given a pulse for both the front and rear of the piston. Occasionally, however, a pickup would give only one pulse instead of two. The pulse which did appear could always be identified as coming from the front or rear of the piston by comparison of the data with data from an experiment with approximately the same driver pressure. Since the principle of operation of the pickup is electric, the response time should be in the nanoseconds.

Quartz piezoelectric pressure transducers were mounted in the wall of the driven tube and the brake blind flange. This type of pressure detector was chosen because of its very fast response. Three Kistler Model 601 L transducers were mounted in the driven tube (see Figure 17) to measure the shock path and the pressure distribution through the shock layer. They were placed as far downstream as possible in order to measure the shock near its peak strength. However, the last transducer was kept back about 31 inches from the brake-driven joint in order to avoid interference of the reflected shock with the shock layer pressure trace. Furthermore, it was necessary to avoid exposing this transducer to the very high pressures developed in this region due to piston deceleration. These transducers will be referred to as first, second and third transducer since they are arranged in that order, the first one being nearest the driver tube.

Calibration curves for these transducers were obtained from the Kistler Instrument Corporation. These curves were checked by operating the piston tube as a shock tube and measuring the shock wave speed for various driver pressures (driven pressure always at 1 atm). The wave speed was used to calculate the pressure downstream of the shock wave. This calculated pressure was compared to the measured pressure based on the Kistler calibration curves. The agreement

between the calculated and measured pressures was satisfactory.

An attempt was made to use another type of quartz pressure transducer produced by Esprit Enterprises. These were to be used to measure the shock path during the early stages of shock growth. However, their sensitivity was so low that they did not respond to the shock wave.

A single Kistler Model 607 L transducer was installed on the brake blind flange in order to measure the peak pressure there. This measurement not only served as a safety measure but also gave some confidence to the sealing quality of the piston. The face of the transducer was coated with Dow Corning RTV rubber sealant to protect the transducer from the high temperature gas.

A Kistler Model 566 Multi-Range Charge Amplifier was used with each transducer.

The rise time of the transducers was 1.5 to 3 microseconds which was completely adequate since the flow times were on the order of 10 milliseconds (msec).

The output from the magnetic pickups and pressure transducers was recorded on Tektronix, Inc. oscilloscopes and photographed by type C-12 Tektronix oscilloscope cameras. All connections were made with shielded cables. The output of the first and third transducers was recorded on a Type 555 Dual-Beam Oscilloscope and the output of the second transducer and the blind flange transducer was recorded on a

Type 564 Storage Oscilloscope. The 564 oscilloscope was operated in the storage mode and the output was photographed after the experiment. Both of these oscilloscopes are of the single sweep type. The output from the magnetic pickups was recorded on a Type 547 Oscilloscope with a Raster modification. The Raster modification increased the accuracy of the time readings by use of a multiple sweep beam. A sample output is shown in Figure 19a. The beam sweep began in the lower left corner of the screen. Samples of the output of the other oscilloscopes are given in Figures 19b-d. For all the traces of Figure 19, time is measured horizontally and voltage is measured vertically. The beam sweep is initiated at the left of the grid. For Figures 19b-d the vertical voltage deflection is proportional to pressure.

Operation of the storage oscilloscope in the storage mode was unsatisfactory for the magnetic pickups. The two pulses from each probe were blurred into one pulse.

The accuracy with which the pressure trace times could be read was $\pm$ 0.03 msec and the accuracy for the piston path trace was $\pm$ 0.01 msec. The oscilloscopes did not introduce significant error into the sweep times since their rise times are in the nanoseconds. The voltage deflection on the oscilloscopes was calibrated by use of the voltage calibrator on each oscilloscope. The sweep rate of each oscilloscope was calibrated by use of a Tektronix Type 180A Time-Mark Generator. Photographs of the calibration traces were

made in order to include corrections for the parallax of the cameras.

The oscilloscopes were triggered simultaneously by the electrical circuit shown in Figure 20. A slight delay in trigger sometimes occurred on the order of 0.1 msec. This delay was caused by looseness in the triggering wire attached to the piston. The delay was determined by matching the output from the first magnetic pickup with the theoretical solution for the piston path. Before this trigger system was developed the oscilloscopes were triggered by the first magnetic pickup. However, the first complete comparison between the theoretical analysis and the experimental results brought to light significant uncertainties in the time at which the piston motion began. Hence, the trigger system of Figure 20 was developed. Figure 19d is the only data reported where the oscilloscope was not triggered by the circuit of Figure 20.

Pressure gauges were used on each of the three tubes to measure pressure prior to each run. All of these gauges were calibrated. The driven tube gauge read absolute pressure to an accuracy of $\pm$ 0.01 psi. The driver and brake tube gauges read gauge pressure (above atmospheric) to an accuracy of $\pm$ 10 psi. The readings of these gauges and all other pressure instrumentation have been converted to absolute pressure. The driven tube temperature was room air

temperature and was determined by use of a mercury thermometer.

SR-4 type strain gauges were attached to several locations on the brake blind flange. The resistance of each of these gauges was measured after each experiment to see if any permanent deformation in the tube had occurred. No permanent change in the resistance was ever detected.

The instrumentation used in this experiment was similar to that used on many piston tube facilities. However, some experimenters have employed alternate techniques. For example, Belcher[32] developed a microwave resonance technique which gave an almost continuous determination of piston path. Optical methods were used by Laponsky and Emrich[6] to measure both piston path and shock path. They used Lucite tubing to transmit the light beams.

The use of transparent material for instrumentation purposes demonstrates one of the design problems of a piston tube. Transparent sections in a piston tube are not practical when high pressures and large deceleration forces occur as in the present facility. However, in order to study a strong shock wave, high piston velocities and accelerations are necessary. These high velocities and accelerations require a structurally strong piston which makes the piston mass increase. Then the deceleration pressures become large, requiring a very high strength tube. Hence, the key to greater flexibility in the use of a piston tube

is ingenuity in both piston design and the development of piston deceleration techniques. The piston design effort of this study is discussed in the next section. The deceleration method used has already been discussed; however, some additional approaches to decelerating the piston are discussed under the Conclusions in Chapter VI.

Piston Design

The piston design was based on a design used by Humphrey.[14] Figures 21 to 23 show the various parts of the piston. The body was made of high strength aluminum with holes drilled in it to lighten the piston but still maintain structural strength. Keeping the piston light is important since this gives higher accelerations (which in turn creates a stronger shock) without increasing the peak pressure on the brake blind flange. The peak pressure in the brake is the limiting factor in this facility. (Figure 19d shows a typical pressure trace for this flange.)

A Teflon sleeve was used to lower friction and help seal the driver gas behind the piston. The Teflon was force fitted over the body and between the end plates to aid sealing between the various parts of the piston. One sleeve was used on 18 high speed experiments (driver pressure on the order of 1700 psi) and showed some tearing but was still usable. The lower speed experiments did not cause much sleeve wear. The majority of the wear may have been caused

by passage of the piston through the brake-driven diaphragm. This diaphragm was burst in the middle due to gas pressure and then "punched out" by the piston. In most cases, the piston had to pass over small flaps which were not punched out. The higher piston speeds also caused the sleeve to expand somewhat, apparently due to the higher gas temperatures.

The face plate was originally made from steel in order to trigger the magnetic pickups. However, it was found that both the front and rear of the piston gave an output pulse (Figure 19a); hence, the steel face plate was replaced with an aluminum face plate which lightened the piston by about 2 1/2 ounces. For an initial driver pressure of 1720 psi, the effect of this change in mass was to increase the final piston velocity by about 100 fps and lower the peak blind flange pressure by 1300 psi.

The original piston was 2.851 inches long and weighed 1 lb_m 7.3 oz. The length was chosen approximately equal to the diameter because it was felt that this would be a stable configuration. After this piston had been tested over a wide range of speeds, the body was shortened by almost an inch to the present configuration. The present configuration weighs 14.73 oz. At an initial driver pressure of about 1800 psi, the original piston had a shock pressure ratio of 2.0 at the third transducer. For the same driver pressure, the present piston had a shock pressure ratio of

2.8 at the third transducer. Comparing these pistons for an initial driver pressure of about 1700 psi, the lighter piston had a peak deceleration pressure which was 1200 psi lower than the heavier piston. Hence, decreasing the piston mass by approximately 8 1/2 ounces had a very significant effect on increasing shock strength and at the same time lowering the peak deceleration pressure.

In its present configuration, the piston may be as short as possible to maintain stability in this driven tube. The tube sections "bell" outward somewhat at their ends. One additional feature utilized on one piston of this study was a small boss on the inside of the face plate. The boss fit tightly inside the center hole of the body and kept the face plate precisely concentric with the body. Precise concentricity cannot be maintained by machine screws. Such a feature would probably be important if a still shorter piston were used in a tube with a more uniform inside diameter. It may also be possible to lighten the present configuration even more by removing more metal from the interior. The effect on piston speed of a given mass change is very easily determined by a theoretical solution for the piston path. Alternate piston designs are discussed by Stoddard[2] and Knoos.[30]

Experimental Procedure

Preparation for an experiment required inserting the diaphragms and the piston, bolting the flanges together, closing the pressure release valves, and preparing the instrumentation. After the tube had been fired, the pressure was released, data recorded, a safety inspection made, and the tube was cleaned.

Due to the high pressures and high piston speeds involved (piston speeds reached 1400 fps), safety measures had to be continually adhered to. It became evident early in the experimental program that memory alone could not be relied upon to perform the many steps necessary for completing a safe and successful experiment. Thus a check list was developed and used for every experiment. When the facility was under high pressure, the author, who acted as the sole operator, stood behind a sturdy wood barrier eight feet tall.

The step-by-step procedure for conducting an experiment will now be given. Prior to each day of operation, an inspection was made to see if all safety checks had been made and the tube cleaned since the last run. A check was also made to see if the air supply tanks were at the necessary pressure. Then the oscilloscopes and charge amplifiers were turned on so that they had at least a thirty minute warm-up period.

Next, the diaphragm was inserted into the brake-driven joint and this joint and the blind flange joint were bolted shut. The brake tube air-inlet valve was closed. Closing this valve prevented an accidental filling of the brake.

A check was made to see if the driver release valve was open (see Figure 18) and if all control panel valves were closed. The piston was inserted into the driven tube one inch from the flange outer face and was immediately blocked with the driver tube. The one inch insertion distance prevented movement of the piston due to bulging of the diaphragm as the driver tube was pressurized. The trigger circuit was tied to one of the machine screws of the piston. Then the driver-driven diaphragm was inserted and this joint bolted shut. The driven tube release valve was shut. The driver tube was bolted to the floor and the floor bolts on the driven tube stands were tightened.

Next the instrumentation was made ready. A check was made to see if all the magnetic pickups and pressure transducers were connected to the oscilloscopes. The oscilloscopes and charge amplifiers were readied for operation. The driver release valve was closed. The brake tube was filled and given a two minute leak check. The brake air-inlet valve was then closed again. Then the driver tube was pressurized until the diaphragm ruptured.

Following the rupture of the diaphragm, the pressure was released and each tube was checked for atmospheric

pressure. The data were recorded and a safety check of the facility was made. The safety check included checking the strain gauges, inspecting the blind flange weld for cracks, and examining the piston. Finally, the interior of all tubes was cleaned with a rag soaked with methanol.

The complete turn-around time on the facility was two or more hours depending upon the particular problems involved.

This completes the description of the experimental equipment and procedure. In the following chapter the results obtained from this facility are compared with the theoretical analysis.

CHAPTER V

COMPARISON OF EXPERIMENTAL RESULTS WITH THEORETICAL PREDICTIONS

The piston tube was operated for 61 experiments using the piston and 60 experiments as a shock tube. All of these experiments were used to establish the operating characteristics of the facility, check out the instrumentation, develop operating procedures, and obtain useful data.

Of the experiments in which the piston was used, two experiments were selected for comparison with the theory. The theory is the method of characteristics which was described in Chapter III. These comparisons have been labeled Cases III and IV. Figures 24 through 29 are for Case III and Figures 30 through 35 are for Case IV. These figures are discussed below. The initial driver pressures for Cases III and IV are 1555 psi and 1875 psi respectively. The remaining initial conditions and the reference conditions are given on the wave diagram solutions in Figures 25 and 31.

The data for each of the two cases were obtained on a single experiment with the exception of the second wall transducer. An earlier experiment with approximately the same driver pressure was used to provide data for the second transducer. Using data from an earlier experiment was

necessary because on the later experiments the second transducer was not available. Some of the oscilloscope traces for Cases III and IV are shown in Figure 19.

It was generally possible to duplicate a given driver pressure by only $\pm$ 30 psi due to the method of diaphragm rupture. In spite of this variation in driver pressure, it was possible to obtain excellent data repeatability from one experiment to the next. This repeatability lends confidence to the accuracy of the measurements. The time intervals between magnetic pickup pulses agreed within the accuracy with which they could be read. Likewise, the difference between the shock layer pressures from one experiment to the next was less than 5%. The time interval on the pressure traces between the passage of the shock and the passage of the piston had less than 3% variation. Time intervals obtained with the storage mode of the storage oscilloscope showed a somewhat greater difference due to the blurring of the trace.

Since the objective of this study is to understand the formation of a strong shock wave in front of a constantly accelerating piston, the piston tube was operated to as high a driver pressure as possible. As mentioned earlier, the limiting factor in this facility was the peak pressure on the brake blind flange. It was felt that 9000 psi was a reasonable limit which would permit both safe operation and accomplishment of the objective of the study.

A strong shock wave is distinguished from a weak shock wave in that an accurate prediction of flow properties behind a strong shock wave must account for the entropy increase across the wave. The strongest shock wave experimentally measured in this study had a pressure ratio of 2.8. A weak shock calculation (assuming an isentropic compression), with the same velocity change as this strong shock, gives a pressure ratio which is a little over 1% higher. Thus it must be said that the experimental shocks developed in this study were only moderately strong. However, the theoretical analysis of this study made no weak shock assumptions; furthermore, the experimental program achieved pressure ratios larger than Laponsky and Emrich[6] or Humphrey.[14] An additional advancement over previous studies has been the comparison of measured pressures with theoretical pressures.

In the following sections a comparison is made between the experimental and theoretical results for Cases III and IV. First, the method of establishing the experimental piston path is described. This path serves as one of the boundary conditions for the method of characteristics solution. Then the method of finding the experimental shock path and its comparison with the theoretical path are discussed. Next, the experimental and theoretical shock layer pressure distributions are compared. Finally, the sources

of discrepancy between the theoretical and experimental results are identified.

Piston Path

The theoretical and experimental piston paths are shown in Figures 24 and 30. The output from the five magnetic pickups is shown. The time delay between the beginning of the piston motion and the triggering of the oscilloscope was determined by requiring that the output from the first pickup fall on the theoretical path.

The theoretical path was determined by integrating Newton's second law of motion. The driver pressure on the piston was found by the pressure-velocity relation for a simple wave, Equation (58). It was assumed that the piston was frictionless, the driven pressure was zero, the driver speed of sound was a_o = 1130 fps, and the driven and driver tube inside diameters were equal. The assumptions of a simple wave, frictionless piston and zero driven pressure are very good in the early portions of piston motion where the driver pressure is high. The assumption of $a_{DR,i}$ = 1130 fps, which is the room temperature speed of sound of air, is felt to be a good approximation when the driver tube is filled to a pressure near the air supply tank pressure. Assuming equal driver and driven tube inside diameters is an approximation consistent with the other approximations. This approximation is equivalent to neglecting the

chamberage correction given by Enkenhus and Parazzoli.[13]

The initial conditions for the front of the piston (side toward driven gas) are $\xi_p = 0.016$ and $u_p = 0$ at $\tau = 0$. The origin of the ξ axes is always one inch inside the driven tube end flange (outer face) since this was the initial position of the rear of the piston.

The equations governing the piston motion were solved by an iteration technique which involved assuming constant driver pressure for $\Delta\tau$ increments of 0.2. The effect of cutting $\Delta\tau$ to 0.1 was negligible. Stephenson[33] presents a closed form solution to the piston path for the same assumptions used in this study. It would probably be faster to use his results than to use an iterative technique.

The final experimental piston path, an impermeable piston, and the undisturbed driven gas conditions were the boundary conditions for the method of characteristics solution of the shock layer flow.

Shock Path

The experimental shock path in the ξ, τ plane was determined from the three side wall pressure transducers. Figures 19b, c show the shock layer pressure traces for Case III. The undeflected beam sweeps in from the left and the first sudden jump (vertically) is due to the shock wave. The beam deflection in the vertical direction continues to increase as the pressure increases through the shock layer

until a second sudden deflection occurs. This second sudden deflection is due to the passage of the piston (the deflection at the rear of the piston was used since it was due to the driver gas and was easily identified). Figure 19c also shows the trace of the driver gas pressure which has a gradual decrease due to the expansion waves from the rear of the accelerating piston. The magnitude of the driver gas pressure checks approximately with the values computed during the theoretical piston path calculation.

The time interval between the passage of the shock and the passage of the piston was used in conjunction with the experimental piston path to give the experimental shock path. Using this procedure, rather than using absolute times from the pressure traces, eliminated small errors in determining trace origin and errors due to non-simultaneous triggering of the oscilloscopes.

The comparisons of the theoretical and experimental shock paths are given in Figures 25 and 31. The agreement is seen to be fairly good with the maximum discrepancy occurring at the first transducer. Case III shows a crossing of the two paths. A similar "crossing" of the theoretical and experimental pressures also occurred, as will be discussed in the next section. The wave diagram solutions shown in these figures are reductions of the original graphical solutions which were done on large sheets of graph paper.

It is interesting to note that for both cases the theory indicates a growth in shock layer "thickness." This growth occurs in both the ξ direction at constant τ and in the τ direction at constant ξ. Experimentally, Case III shows an increase in the shock layer thickness in the ξ direction but a constant thickness in the τ direction.

Shock Layer Pressure Distributions

The variation of pressure at each side wall transducer is shown in Figures 26-28 for Case III and Figures 32-34 for Case IV. These curves give the pressure distribution along a line of constant ξ in the ξ, τ plane. The solid lines are theory and the dashed lines are experiment. For each curve, the far left is the pressure just downstream of the shock wave and the far right is the pressure at the front of the piston. The percent difference between the theoretical and experimental pressures at the shock and at the piston are given on each figure. For Case III, a similar effect to the crossing of the theoretical and experimental shock paths is seen in these figures. The experimental pressure curve lies above the theoretical curve in Figure 26. Then as the shock progresses on down the tube in Figures 27 and 28, the experimental curve drops down on and then below the theoretical curve.

Figures 29 and 35 give dimensionless shock layer pressure distributions at constant τ. It will be recalled that

the flow is self-similar when distributions of this type coincide. The flow seems to have a closer approximation to a self-similar nature experimentally than it does theoretically.

The discrepancy between theory and experiment for the shock path and shock layer pressures can be accounted for. A major source of error for the theoretical solution is the determination of the piston path. This path was determined by drawing a curve between the magnetic pickup data points. On one occasion, the piston path was drawn on two different sheets of graph paper for the same set of data. The slope of the path gave the piston velocity at any desired point. It was found that differences in the piston velocity between the two curves gave differences in calculated pressures of up to 3%. Additional small errors occur in the theory due to mesh size and P characteristics drawn at the wrong slope (recall discussions on these topics in Chapter III). These sources of error, coupled with experimental measurement errors, are felt to account for the discrepancies between theory and experiment. The only exception to this statement is the shock location and shock pressure at the first transducer. These rather large errors are felt to be caused by uncertainties in the initial portion of the piston path. How the piston path is shaped here depends on such factors as how the diaphragm breaks, initial dynamic instabilities of the piston and so on. Laponsky and Emrich[6] came to a

similar conclusion. They found that uncertainties in the initial portion of the piston motion caused deviations in only the early stages of shock growth.

CHAPTER VI

CONCLUSIONS

The numerical method of characteristics for one-dimensional unsteady flow has been shown to predict the experimental shock path and shock layer pressures. The prediction is within a few percent in the downstream flow regions.

Some of the results of the method of characteristics have also been verified by alternate theoretical techniques. The shock layer wave phenomena predicted by the characteristic solution has been verified by the focused wave solution, a P,u plane analysis and reflection coefficient concepts. The pressure and velocity changes were approximately verified by a focused wave solution.

It was found that the compression process changed from an isentropic one to a nonisentropic one. The result of this change is a shock layer with strong gradients in temperature, density and entropy and a very complex wave system. These gradients persist even when the piston velocity becomes constant and pressure and velocity approach uniform values in the shock layer. The wave system consists not only of the primary or initial compression waves from the piston, but also includes expansion waves reflected from the

entropy interfaces and from the shock wave. These expansion waves then reflect from the piston, the entropy interfaces and the shock wave. For most problems, the reflected waves are weak compared to the primary waves and the reflections quickly vanish. In cases where either the Mach number is very large or the ratio of specific heats approaches one, the reflected waves can become very strong. The complex nature of this unsteady one-dimensional flow is analogous to many steady two-dimensional or axially symmetric flows.

Simplifications in the method of characteristics are sometimes possible. The simplifications include straight P characteristics, neglecting reflected waves, and assuming self-similar flow. The assumption of straight P characteristics becomes less accurate as the shock strength increases. The assumption of neglecting reflected waves was mentioned above. The accuracy of the self-similar assumption depends on how well the piston path agrees with an exponential path. Pressure measurements indicated that the flows of this study were approximately self-similar.

The characteristic mesh size was found to be critical only for the shock during its period of initial growth.

In the operation of a piston tube facility, it was found that a high pressure section at the end of the driven tube was very useful. Such a section reduces peak temperatures and pressures during piston deceleration.

As a result of the work carried out during this period, additional studies in the following four principal areas are suggested:

(1) Since the theoretical model has been verified experimentally, the theory can be used for analyzing various flows. These analyses would best be performed by means of a computer program. Areas which should be studied include:

(a) The sensitivity of the resultant flow to the piston path for an identical final piston velocity

(b) Whether a piston path with an acceleration which increases with time causes shocks to form within the compression wave (References 6 and 19)

(c) Under what conditions the simplifying assumptions for the characteristic solution are accurate

(d) The effect of specific heat ratio

In making such investigations, areas for the practical application of the results should be sought.

(2) Another useful extension would be the study of stronger shock waves. With a properly designed facility it would be interesting to see how well the theory of this study compared with experimental results for strong shock waves. If a monatomic gas were used instead of a diatomic gas, the effects of chemical reactions could be delayed to

higher Mach numbers. Argon is preferable to helium because the speed of sound of helium is so large that the driven tube lengths required to form a shock wave (see Equation (12)) are unreasonable. In addition, the theory could be extended to the study of shock formation when chemically reacting gases are involved so that the effects of non-equilibrium in the gas can be studied.

(3) A piston tube facility may be useful in studying intermolecular forces in the high pressure gas created during piston deceleration. Enkenhus and Parazzoli[13] have taken intermolecular forces into account in computing the conditions of their test gas.

The piston tube may also offer advantages in studying shock-ignited detonations since the piston acceleration can be selected whereas the acceleration of the flame front is inherent in the system. The piston face is a plane surface at all times, which cannot be said for the flame. The piston also maintains an excellent isolation of the driver and driven gases. For example, even though expansion waves exist on the rear of the piston, the front of the piston will continue to send out compression waves as long as the piston accelerates. On the other hand, in a shock tube, the expansion waves can catch up with the shock wave.

(4) Additional studies should be performed to determine means for decelerating the piston without the occurrence of very high pressures and temperatures. Possible

approaches include an open-ended driven tube which would permit deceleration of the piston by means of an external device. It might be possible to use a heavy cart filled with a foam such that both the foam and movement of the cart would absorb the kinetic energy of the piston. The foam would also prevent damage to the piston. Another approach might be use of expendable pistons which were decelerated in such a device. In this case an inexpensive piston made of paper or plastic could be used.

REFERENCES

1. Hall, J. G. et al., "Research on Advanced Gasdynamic Facilities," ARL Report 65-204, Aerospace Research Laboratories, Wright-Patterson Air Force Base, Ohio, October 1965.

2. Stoddard, F. J., "Theoretical and Experimental Studies of Piston-Compressor Techniques for Producing Hypervelocity Test Flows," AIAA Preprint 69-334 (April 28-30, 1969).

3. Friedrichs, K. O., "Formation and Decay of Shock Waves," Communications on Applied Mathematics, 1 (1948), pp. 211-245.

4. Courant, R. and Friedrichs, K. O., Supersonic Flow and Shock Waves, Interscience Publishers, Inc., New York, 1948, Sec. 48, 49, 72-74, 76, 77.

5. Pillow, A. F., "The Formation and Growth of Shock Waves in the One-Dimensional Motion of a Gas," Proc. Camb. Phil. Soc., 45 (1949), pp. 558.

6. Laponsky, A. B. and Emrich, R. J., "Observation of Shock Formation and Growth," J. Appl. Phys., 24 (1953), pp. 1383.

7. Lighthill, M. J., "The Energy Distribution Behind Decaying Shocks. I. Plane Waves," Phil. Mag., 41 (1950), pp. 1101-1128.

8. Shunk, R. A., "Shock Formation From Strong Compression Waves," Lehigh University TR-11, 1956.

9. Shapiro, A. H., The Dynamics and Thermodynamics of Compressible Fluid Flow, Vol. II, The Ronald Press Co., New York, 1954, pp. 1025-1026, pp. 972-979.

10. Winter, D. F. T., "Multiple Shock Compression Using a Piston of Finite Weight," J. of Fluid Mechanics, 8 (June 1960), pp. 264.

11. Raffe, G. A., "The Free-Piston Shock Tube Driver: A Preliminary Theoretical Study," JPL-TR-32-560, December 1963.

12. Peng, T. C. and Elbert, T. F., "On the Piston Motion of a Free-Piston Shock Tube," Aeronautical Quarterly, 16 (November 1965), pp. 369.

13. Enkenhus, K. R. and Parazzoli, C., "Evaluation of Dense Gas Phenomena in a Free-Piston Hypersonic Wind Tunnel," AIAA Preprint 69-169 (January 20-22, 1969).

14. Humphrey, B. G., et al., "A Theoretical and Experimental Investigation of the Free Piston Cycle," Air Force Flight Dynamics Laboratory TR-66-204, Wright-Patterson Air Force Base, Ohio, February 1967.

15. Hayes, W. D. and Probstein, R. F., Hypersonic Flow Theory, Academic Press, New York, 1966, Sec. 2.6.

16. Chernyi, G. G., Introduction to Hypersonic Flow, Academic Press, New York, 1961, pp. 69-94.

17. Rudinger, G., Nonsteady Duct Flow: Wave Diagram Analysis, Dover Publications, Inc., New York, 1969.

18. Owczarek, J. A., Fundamentals of Gasdynamics, International Textbook Co., Scranton, Penn., 1964, Chp. 7, 8.

19. Laderman, A. J. et al., "On the Generation of a Shock Wave by Flame in an Explosive Gas," In Ninth Symposium (International) on Combustion, Academic Press, New York, 1963, pp. 265.

20. Zel'dovich, Ya. B. and Raizer, Yu. P., Physics of Shock Waves and High-Temperature Hydrodynamic Phenomena, Vol. I, Academic Press, New York, 1966, pp. 84-92.

21. Liepmann, H. W. and Roshko, A., Elements of Gasdynamics, John Wiley and Sons, Inc., New York, 1957, pp. 76-77.

22. Glass, I. I. and Hall, J. G., Handbook of Supersonic Aerodynamics, Sec. 18, Shock Tubes, NAVORD Report 1488 (Vol. 6), December 1959, pp. 23-25.

23. Stoddard, F. J., et al., "The Isentropic Compression Tube: A New Approach to Generating Hypervelocity Test Flows With Low Dissociation," ARL Report 67-0133, Wright-Patterson Air Force Base, Ohio, June 1967.

24. Owczarek, J. A., "Theoretical Investigation of the Influence of Viscous Friction on a Plane Wave of Finite Amplitude in a Compressible Fluid," Quart. J. of Mech. and Applied Math., 9, Part 2 (1956), pp. 143-163.

25. Owczarek, J. A., "Measurements of Attenuation of Compression Waves of Finite Amplitude in Air and Evaluation of the Coefficient of Friction," Quart. J. of Mech. and Applied Math., 9, Part 2 (1956), pp. 164-184.

26. Moretti, G., "A Critical Analysis of Numerical Techniques: The Piston-Driven Inviscid Flow," PIBAL Report 69-25, Polytechnic Institute of Brooklyn, July 1969.

27. Moretti, G. and Salas, M. D., "Numerical Analysis of Viscous One-Dimensional Flows," PIBAL Report 69-27, Polytechnic Institute of Brooklyn, July 1969.

28. Eckert, E. R. G. and Drake, R. M., Heat and Mass Transfer, McGraw-Hill Book Co., Inc., New York, 1959, pp. 144, 270.

29. Richards, B. E. and Enkenhus, K. R., "Hypersonic Testing in the V.K.I. Longshot Free-Piston Tunnel," AIAA Paper 69-333 (April 28-30, 1969).

30. Knoos, S., "Bypass Piston Tube, a New Device for Generating High Temperatures and Pressures in Gases," AIAA Journal, 6, (April 1968), pp. 632.

31. Stalker, R. J., "A Study of the Free-Piston Shock Tunnel," AIAA Journal, 5 (December 1967), pp. 2160.

32. Belcher, B. J., "Measurements of the Effects of Piston Mass and Bursting Pressure on the Motion of a Piston in a Hypersonic Gun Tunnel," Nature, 184 (17 October 1959) pp. 1207.

33. Stephenson, W. B., "Theoretical Light-Gas Gun Performance," AEDC-TR-61-1, May 1961.

APPENDIXES

APPENDIX A

FOCUSED WAVE CONSERVATION OF ENERGY

By use of the closed form solution for the focused wave piston path it is also possible to obtain a closed form expression for the conservation of energy. The piston work done on the gas from t = o to t = t_F, focus time, is

$$W_p = \int_0^{t_F} F_p \, dx = \int_0^{t_F} (A_T p_p) \left(\frac{dx}{dt}\right)_p dt$$

The piston will in general accelerate from t = 0 to t = t_A and maintain a constant velocity u_f from then on (see Figure 1b). Since a simple wave is assumed, the pressure on the piston is constant after t_A at the value p_f. Thus, the work per unit cross sectional area of the tube, A_T, is

$$\frac{W_p}{A_T} = \int_0^{t_A} p_p u_p \, dt + p_f u_f (t_F - t_A) \qquad (48)$$

where

$$\left(\frac{dx}{dt}\right)_p = u_p(t)$$

$$p_p = p_p(u_p)$$

so that the above integrand is an easily determined function of time. The velocity $u_p(t)$ for a focused wave is given by

Equation (10), and the pressure on the piston face is just the pressure behind the isentropic simple compression wave and is therefore a function of the velocity

$$p_p(u_p) = p_o \left[1 + \frac{\gamma-1}{2} \frac{u_p}{a_o}\right]^{\frac{2\gamma}{\gamma-1}} \qquad (49)$$

where the sign in front of the velocity is positive because the wave moves in the direction of positive velocities (to the right). The initial gas state is p_o, ρ_o and $u_o = 0$. Substituting Equation (10) into Equation (49), the pressure on the piston face becomes

$$p_p(t) = \frac{p_o}{\left(1 - \frac{t}{t_F}\right)^{\frac{2\gamma}{\gamma+1}}} \qquad (50)$$

Substituting Equations (10) and (50) into (48) results in two integrals which are evaluated by the use of standard integral tables. The final result for the piston work is, after rearrangement and use of Equation (12)

$$\frac{W_p}{A_T} = p_o x_F \frac{\gamma+1}{(\gamma-1)^2} \left[\frac{1 - 2\left(1 - \frac{t_A}{t_F}\right)^{\frac{\gamma-1}{\gamma+1}}}{\left(1 - \frac{t_A}{t_F}\right)^{\frac{2(\gamma-1)}{\gamma+1}}} + 1 \right]$$

$$+ p_f \frac{u_f}{a_o} x_F \left(1 - \frac{t_A}{t_F}\right) \qquad (51)$$

This is the piston work per unit of flow cross sectional area, done on the gas from t = o to t = t_F. The piston accelerates from t = o to t = t_A up to velocity u_f, and moves at

constant velocity from $t = t_A$ to $t = t_F$. The work can be computed by selecting the gas and its initial state, initial piston acceleration $A_{p,i}$ and final piston velocity u_f. The acceleration $A_{p,i}$ determines x_F and t_F from Equation (12), and the velocity u_f determines t_A by Equation (10) and p_f by Equation (49). The condition $t_A < t_F$ must be satisfied or a new $A_{p,i}$ or u_f must be selected.

The next step in the energy analysis is to compute the change in energy of the gas between $x = 0$ and $x = x_F$ at t_F. The total energy of the gas is the sum of its internal energy and the ordered kinetic energy of motion

$$E = \left(e + \frac{u^2}{2}\right) m$$

where m is the mass of the gas. For a perfect gas the internal energy per unit mass is

$$e = \frac{1}{\gamma - 1} \frac{p}{\rho}$$

and the equation for the speed of sound gives

$$\frac{p}{\rho} = \frac{a^2}{\gamma} \tag{52}$$

Thus, the change in total energy between states u_o, p_o, ρ_o and u, p, ρ is:

$$\frac{\Delta E}{m} = \frac{a_o^2}{\gamma(\gamma-1)} \left(\frac{p/p_o}{\rho/\rho_o} - 1\right) + \frac{u^2}{2}$$

For a simple wave the density distribution is given by

$$\frac{\rho}{\rho_o} = \left(1 + \frac{\gamma-1}{2}\frac{u}{a_o}\right)^{\frac{2}{\gamma-1}} = \left(\frac{p}{p_o}\right)^{\frac{1}{\gamma}} \tag{53}$$

So the total energy increase becomes

$$\frac{\Delta E}{m} = \frac{a_o}{\gamma} u + \left(\frac{3\gamma-1}{4\gamma}\right) u^2 \tag{54}$$

The mass of gas under consideration is conveniently found from its initial state

$$m = \rho_o A_T x_F \tag{55}$$

So by use of Equations (55) and (52), Equation (54) gives the total energy change in the focused wave as

$$\frac{\Delta E_F}{A_T} = p_o x_F \frac{u_f}{a_o}\left[1 + \left(\frac{3\gamma-1}{4}\right)\frac{u_f}{a_o}\right] \tag{56}$$

The final step is to equate the piston work, Equation (51), and the energy change in the gas, Equation (56). Note that both equations have the same dimensions. When these equations are equated and p_f/p_o is replaced by its function of u_f/a_o from Equation (49), the result becomes

$$\frac{\gamma+1}{(\gamma-1)^2}\left[\frac{1 - 2\left(1 - \frac{t_A}{t_F}\right)^{\frac{\gamma-1}{\gamma+1}}}{\left(1 - \frac{t_A}{t_F}\right)^{\frac{2(\gamma-1)}{\gamma+1}}} + 1\right]$$

$$+ \left(1 + \frac{\gamma-1}{2}\frac{u_f}{a_o}\right)^{\frac{2\gamma}{\gamma-1}}\left(\frac{u_f}{a_o}\right)\left(1 - \frac{t_A}{t_F}\right) = \frac{u_f}{a_o}\left[1 + \left(\frac{3\gamma-1}{4}\right)\frac{u_f}{a_o}\right] \tag{57}$$

The result is a relation between t_A/t_F and u_f/a_o. Equation (10) is a known correct relation between these same quantities. If Equation (10) is used to eliminate t_A/t_F from the left side of Equation (57), then the left side becomes identical to the right side. This completes the proof that the piston work done on the gas between $t = 0$ and $t = t_F$ equals the energy increase in the gas caused by a simple wave only in the same time (the only gas affected lies between $x = 0$ and $x = x_F$).

APPENDIX B

EXAMPLE CHARACTERISTIC COMPUTATION

Some detailed notes for constructing a typical P characteristic are given in this appendix. The characteristic 18-23 of Figure 5 will be discussed.

First, point 18 is computed. The piston velocity is known. Q is found by interpolating between points 12 and 17 where the Q at 17 must be found first from known conditions at 13.

Second, to aid in the interpolation of Q values, an estimate of the entire P characteristic is sketched in. Estimated particle paths are also sketched in from the preceding P characteristic up to the present one. After all calculations are complete for the P characteristic, these sketches are replaced by accurate lines.

Next find P at 19 by crossing the entropy interface from 18. Q can be estimated by noting the drop in Q in other entropy strips: $Q \approx Q_{13} - .01$. This value can be checked later in the calculations. The best accuracy seems to be obtained by basing all Q values on the average Q values. Thus it is better here to interpolate for Q rather than take Q_{11} and cross the entropy interface.

Find P at 20 by coming along the P characteristic from 19. Get Q at 20 by coming along the Q characteristic from 15. In both cases an entropy interface is crossed.

Compute point 21 similarly to point 19.

Points 22 and 23 are computed simultaneously by iteration. First, estimate P_{22}. Then compute the shock strength at 23. Then average the entropy at 23 and 16 to get the entropy for the strip between these two shock points. Then compute P_{22} by crossing the entropy interface from 21. If the computed value of P_{22} is not close enough to the estimated value, try a new value of P_{22}. Next, as explained in the text, compute an average Q. The average Q can be computed by either of two methods, which agree $\pm$ 0.008 in the value of Q. One method is to average the Q values at 16 and 23. The other method is to use the average entropy computed for the strip and use the shock tables. Then, point 22 can be completed since both P and Q (the average Q) are known. Point 23 is completed once the shock strength is determined.

Note that as the particle paths and Q characteristics are extended from the previous P characteristic to the one just computed, more interpolation is necessary. Take for example the particle path which crosses the P characteristic between points 19 and 20. The slope of the particle path at this intersection is an average of the velocities at these two points.

After the piston has come to a steady velocity at $\tau = 0.5$, no more strong P compression waves come from the piston. Thus at a point such as 24 where only Q is known, a can be estimated by assuming the value for point 19. If it is desired to know only the effect of a characteristic from the piston on the shock, without computing all the intermediate points, the change in P across the whole shock layer can be computed in one step. Then draw the P characteristic in as a straight line with the slope it has at the piston. This approximate slope is even good in the strong compression region, however it is not good there for a Q characteristic. The change in Q can similarly be computed across the whole shock layer. Such a computation also serves as a good verification of the step-by-step calculations. These verifications were made for Case II.

APPENDIX C

ISENTROPIC $\mathcal{P},\mathcal{U}$ PLANE

For isentropic compression or expansion between states p, u and p_1, u_1 the simple wave analysis gives

$$\mathcal{P} = \mathcal{P}_1 \left[1 \mp \frac{\gamma - 1}{2} \left(\frac{\mathcal{U} - \mathcal{U}_1}{\mathcal{A}_1} \right) \right]^{\frac{2\gamma}{\gamma - 1}} \tag{58}$$

where $\mathcal{P} \equiv p/p_o$. The slope of the $\mathcal{P},\mathcal{U}$ curve is given by the derivative of the above equation

$$\frac{d\mathcal{P}}{d\mathcal{U}} = \mp \frac{\gamma \mathcal{P}_1}{\mathcal{A}_1} \left[1 \mp \frac{\gamma - 1}{2} \left(\frac{\mathcal{U} - \mathcal{U}_1}{\mathcal{A}_1} \right) \right]^{\frac{\gamma + 1}{\gamma - 1}} \tag{59}$$

In both of the above equations, the plus sign is for P waves (right moving, i.e. in direction of positive velocity) and the minus sign is for Q waves (left moving). The P and Q waves may be either compression or expansion waves. Expansion into a vacuum, $\mathcal{P} = 0$, gives the extreme values on the velocity. From Equation (58) these are

$$\mathcal{U}_{\substack{\max \\ \min}} = \pm \frac{2}{\gamma - 1} \mathcal{A}_1 + \mathcal{U}_1 \quad \begin{cases} + \text{ Q wave} \\ - \text{ P wave} \end{cases} \tag{60}$$

Consideration of the bracket in Equation (59) (and making use of Equation (60) for the case of an expansion) shows that the bracket is always positive. Thus the slope in the $\mathcal{P}, \mathcal{U}$ plane is always positive for P waves and negative for Q waves. Also, for higher initial temperatures and the same initial pressure (therefore higher entropy), the absolute value of the slope decreases.

For isentropic simple waves, one Riemann variable is always constant throughout the whole flow. For P waves, Q is constant and for Q waves, P is constant. The constancy of a Riemann variable can be verified by plotting Equation (58) for a given $S-S_o$. Fixing $S-S_o$ and $\mathcal{P}_1$ determines $\mathcal{A}_1$ by Equation (23) (with $S-S_o$ in place of S). Then $\mathcal{A}$ can be computed at each point on the curve of Equation (58) by isentropic relations and then Q or P found from the definition of Q and P, Equations (13) and (14). Figure 6 gives the results of a sample calculation.

The effect of initial conditions, $\mathcal{P}_1, \mathcal{U}_1$, on the curves can be eliminated by always choosing the reference conditions, p_o, a_o, to be equal to the initial p and u (i.e. $\mathcal{P}_1 = \mathcal{U}_1 = 1$). Then a given $S-S_o$ will always plot the same curve. Thus choosing $\mathcal{P}_1 = \mathcal{U}_1 = 1$ has no fundamental effect on the $\mathcal{P}, \mathcal{U}$ plane and it can be made universal in nature similar to the $\mathcal{A}, \mathcal{U}$ plane. However, the $\mathcal{A}, \mathcal{U}$ plane does differ in that P and Q are defined functions of $\mathcal{A}$ and $\mathcal{U}$ so that any a_o can be chosen. When both a $\mathcal{P}, \mathcal{U}$

and $\mathcal{Q}, \mathcal{U}$ plane are being used simultaneously, care must be exercised with respect to the reference conditions.

In a given flow problem, p_1, u_1, and a_1 are known. If $\mathcal{P}_1 = \mathcal{U}_1 = 1$ are chosen, then p_o and a_o are fixed. Since $\mathcal{Q}_1$ is then fixed, $S-S_o$ is fixed by Equation (23).

The effect of entropy on the curves enters as an entropy difference between that for the particular curve and the reference value, S_o. In working a particular problem, the value of $S-S_o$ for each region of gas must be known. The value $S_o = 0$ can be used only if entropy tables have been prepared with a base of $S_o = 0$ at the p_o, a_o chosen. If an analysis were made of the gas in the shock layer and p_o, a_o were chosen as the local p, u, then p_o, a_o would not equal the values in the undisturbed gas ahead of the shock. Therefore $S_o \neq 0$ since $S_o = 0$ is true only in the undisturbed gas according to the procedure used in this study ($S_o = 0$ in the undisturbed gas is convenient because shock tables such as in Reference 17 give the entropy increase across the shock). Thus, it would be easiest to keep $\mathcal{P}_1 = \mathcal{U}_1 = 1$ (and therefore use a universal set of $\mathcal{P}, \mathcal{U}$ plane curves) and compute $S-S_o$ by Equation (23) as discussed above.

If new initial conditions are chosen, such as $\mathcal{P}_1 = 1.5$, $\mathcal{U}_1 = 2.5$, the same Q and $S-S_o$ or P and $S-S_o$ will not occur together on the same curve as for $\mathcal{P}_1 = \mathcal{U}_1 = 1$. Also, irregardless of whether Q (or P) or $S-S_o$ is maintained constant, if new initial conditions are chosen and $\mathcal{Q}_1$

changes, then the shape of the curves will change. See Figure 6. However, if only u_1 changes, the curves will simply translate to a new location.

TABLE 1

Method of Characteristic Solution of Shock Layer for Case II[a]

Point[b]	P	Q	$\mathcal{U}$	$\mathcal{Q}$	(1) $\mathcal{Q}^5$	(2) $e^{-\gamma S}$	p=(1)(2)(14.7) psi
1	3.000	3.000	0	1.000	1.000	1.000	14.7
2	3.842	3.000	0.42	1.140	1.926	1.000	28.3
4	4.583	3.000	0.791	1.264	3.22	1.000	47.3
5	4.635	3.045	0.797	1.280	3.44	0.9355	47.4
7	5.225	3.000	1.113	1.371	4.85	1.000	71.2
8	5.282	3.039	1.122	1.388	5.15	0.9355	71.0
9	4.904	2.991	.956	1.317	3.96	1.000	58.1
10	5.381	3.132	1.123	1.419	5.75	0.8322	70.4
12	5.753	2.991	1.379	1.458	6.60	1.000	97.0
13	5.812	3.033	1.390	1.475	7.00	0.9355	96.5
14	5.917	3.124	1.395	1.508	7.80	0.8322	95.5
15	6.056	3.253	1.401	1.552	9.00	0.7165	94.9
17	5.943	2.972	1.486	1.486	7.26	1.000	106.9
18	6.126	2.975	1.578	1.517	8.01	1.000	117.9
19	6.187	3.02	1.583	1.534	8.48	0.9355	116.8
20	6.296	3.115	1.590	1.568	9.49	0.8322	116.1
21	6.439	3.245	1.598	1.614	10.95	0.7165	115.5
22	6.581	3.382	1.600	1.661	12.62	0.619	115.0
24		3.006					
25	6.102	2.945	1.578	1.508	7.80	1.000	114.6
26	6.163	2.970	1.600	1.523	8.20	0.9355	113.0
27	6.271	3.102	1.582	1.562	9.30	0.8322	114.0
28	6.415	3.238	1.588	1.609	10.8	0.7165	114.0
29	6.557	3.377	1.590	1.655	12.4	0.619	112.9
30	6.629	3.446	1.591	1.679	13.3	0.580	113.2
32	6.43	3.241					
33		2.994					

Table 1 (Continued)

Point[b]	P	Q	$\mathcal{U}$	$\mathcal{a}$	(1) $\mathcal{a}^5$	(2) $e^{-\gamma S}$	p=(1)(2)(14.7) psi
34	6.091	2.933	1.578	1.504	7.68	1.000	112.9
35	6.152	2.991	1.581	1.524	8.20	0.9355	113.0
36	6.260	3.098	1.582	1.559	9.20	0.8322	112.5
37	6.403	3.234	1.582	1.607	10.7	0.7165	112.8
38	6.545	3.374	1.587	1.653	12.4	0.619	112.8
39	6.617	3.445	1.588	1.677	13.2	0.58	112.6
40	6.624	3.451	1.587	1.680			
45		2.918	1.578				
46	5.649	3.124	1.262	1.462	6.70	0.8322	82.0
47	5.85	3.028	1.410	1.480	7.10	0.9355	97.7
48	5.282	3.039	1.122	1.387	5.14	0.9355	70.6

a) Table computed with the following gas:

Argon, $\gamma = 1.667$

Initial Conditions: $T_1 = 534.7^{\circ}R$, $a_o = a_1 = 1052$ ft/sec

$p_1 = 14.7$ psi, $u_1 = 0$, $S_o = S_1 = 0$

Therefore $\mathcal{a}_1 = 1$, $\mathcal{U}_1 = 0$, $P_1 = Q_1 = 3$

b) Points and strips in Tables 1-3 are located on the wave diagram in Figure 5.

TABLE 2

Method of Characteristic Solution of Shock Wave for Case II[a]

Point	P"	$\frac{P"-P'}{\mathcal{Q}'}=P"-3$	$M_W=\mathcal{W}=(\frac{d\xi}{d\tau})_s$	$\frac{\mathcal{U}"-\mathcal{U}'}{\mathcal{Q}'}=\mathcal{U}"$	$\frac{\mathcal{Q}"}{\mathcal{Q}'}=\mathcal{Q}"$	$\frac{p"}{p'}$ (1)	p"=(1)(14.7) psi	S"-S'=S"	Q"
3	3.842	0.842	1.314	0.414	1.143	1.91	28.1	0.013	3.015
6	4.635	1.635	1.645	0.778	1.286	3.14	46.1	0.0675	3.080
11	5.381	2.381	1.969	1.096	1.428	4.60	67.5	0.153	3.188
16	6.056	3.056	2.265	1.367	1.562	6.16	90.5	0.248	3.323
23	6.581	3.581	2.494	1.570	1.670	7.53	110.8	0.327	3.440
31	6.629	3.629	2.516	1.589	1.680	7.66	112.8	0.335	3.451
41	6.624	3.624	2.513	1.587	1.679	7.64	112.1	0.3345	3.450

a) Conditions ahead of shock are Initial Gas Conditions: $P' = Q' = 3$, $\mathcal{U}' = 0$, $\mathcal{Q}' = 1$, $S' = S_o = 0$, $p' = 14.7$ psi, $\gamma = 1.667$

TABLE 3

Entropy Strip Results for Case II

Strip	S	$S_R - S_L$	(R-L)
1	0.006	0.034	(2-1)
2	0.040	0.0703	(3-2)
3	0.1103	0.0902	(4-3)
4	0.2005	0.087	(5-4)
5	0.2880	0.043	(6-5)
6	0.3310	0.004	(7-6)
7	0.3350		
8	0.3345		

TABLE 4

Piston Path in Time-Distance Plane, Including Velocity and Acceleration, for Case II[a]

τ	ξ	u_p	$\bar{A}_p$
0	0	0	
0.05	0.00526	0.210	4.21
0.10	0.021	0.420	
0.15	0.0466	0.605	3.71
0.20	0.0815	0.791	
0.25	0.1251	0.952	3.22
0.30	0.1767	1.113	
0.35	0.2359	1.246	2.66
0.40	0.3016	1.379	
0.45	0.373	1.478	1.985
0.50	0.450	1.578	

a) $u_p = 1.578$ for $\tau \geq 0.50$
$\bar{A}_p = 0$ for $\tau \geq 0.50$

TABLE 5

Shock Reflection Coefficient for $M_{w'} = \infty$

γ	1.667	1.4	1.3	1.2	1.1	1.05	1
r_s	-0.0213	-0.0628	-0.0938	-0.148	-0.261	-0.388	-1.0

TABLE 6

Comparison of Cases I and II[a]

	Primary Compression Strength[b]		Expansion due to Reflection of Primary Compression From Shock (and Entropy Interfaces for Case II)		Final Shock Strength[b]	
	$\frac{p}{p_1}$, $\frac{p}{p_i}$	$\mathcal{U}$	$\frac{\Delta p_{Reflected}}{\Delta p_{Initial\ Compression}}$	$\frac{\mathcal{U}_f - \mathcal{U}_i}{\mathcal{U}_i}$	$\frac{p}{p_1}$, $\frac{p}{p_i}$	$\mathcal{U}$
Case I	8.30 (2)	1.578 (2)	r_s = - 0.0549 (2-3)	2.85% (2-3)	7.90 (4)	1.623 (4)
Case II	8.01 (18)	1.578 (18)	$r_s + \Sigma r_e$ = - 0.044 (Incident: 1-18) (Reflected: 2-34, P_{avg} = 6)	2.20% (2-34)	7.53 (23)	1.570 (23)

a) Points on wave diagrams are in parenthesis

b) For Primary Compressions and Final Shocks: $\mathcal{U}_i = 0$; p/p_1 is for Case I; p/p_i is for Case II

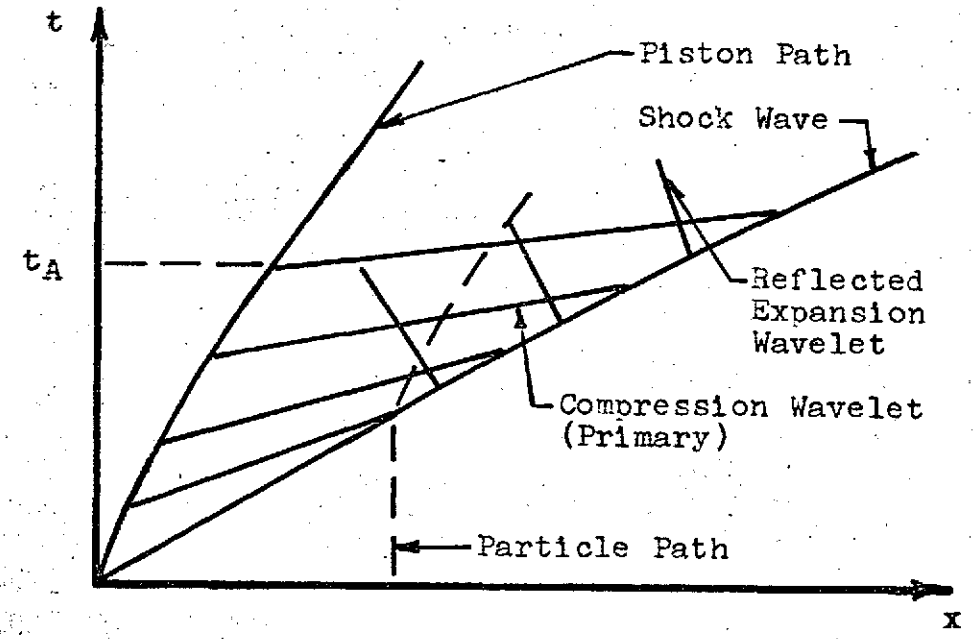

a

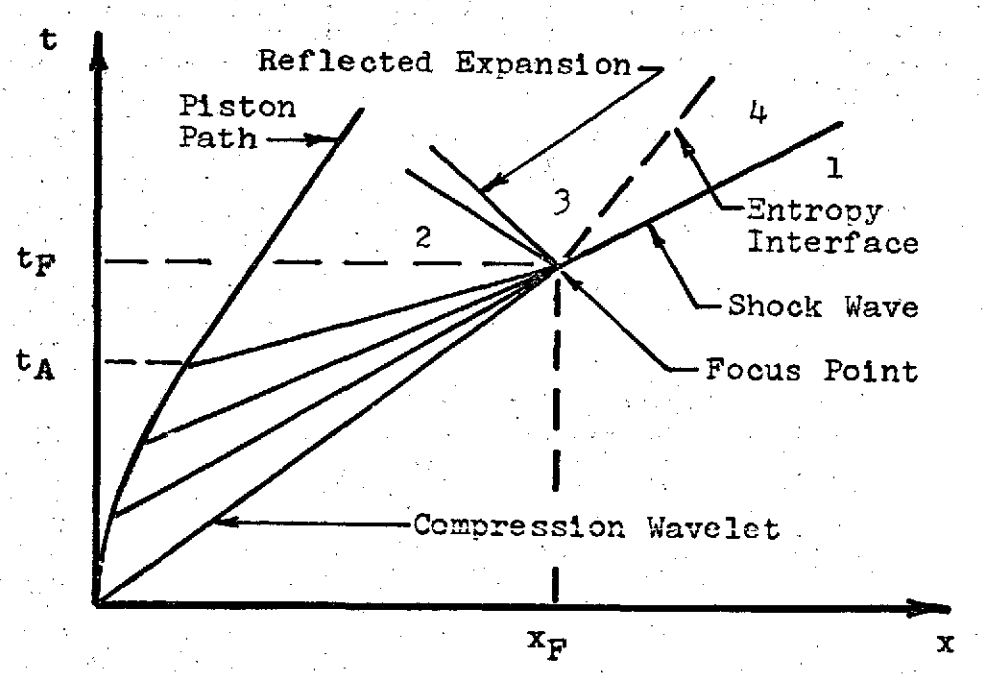

b

Fig. 1. Various Compression Wave Patterns in the Time-Distance Plane

a. Dispersed Wave

b. Focused Wave. Flow Regions for Fig. 2-4 are numbered.

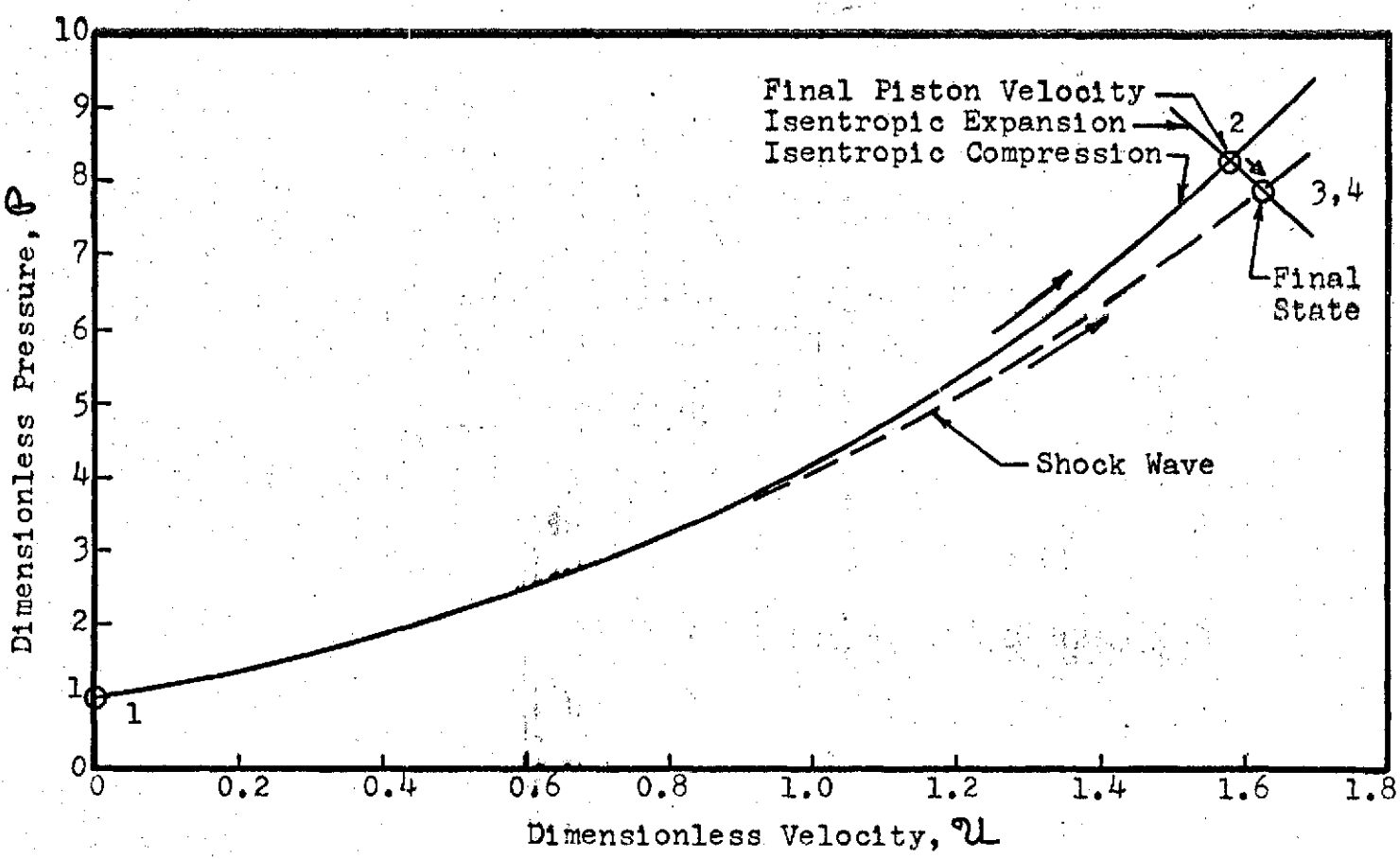

Fig. 2. Focused Compression Wave P, U Plane for Case I.

$u_1 = 0$, $p_o = p_1$, $a_o = a_1$, $\gamma = 1.667$, Flow Regions 1-4 Shown in Fig. 1b.

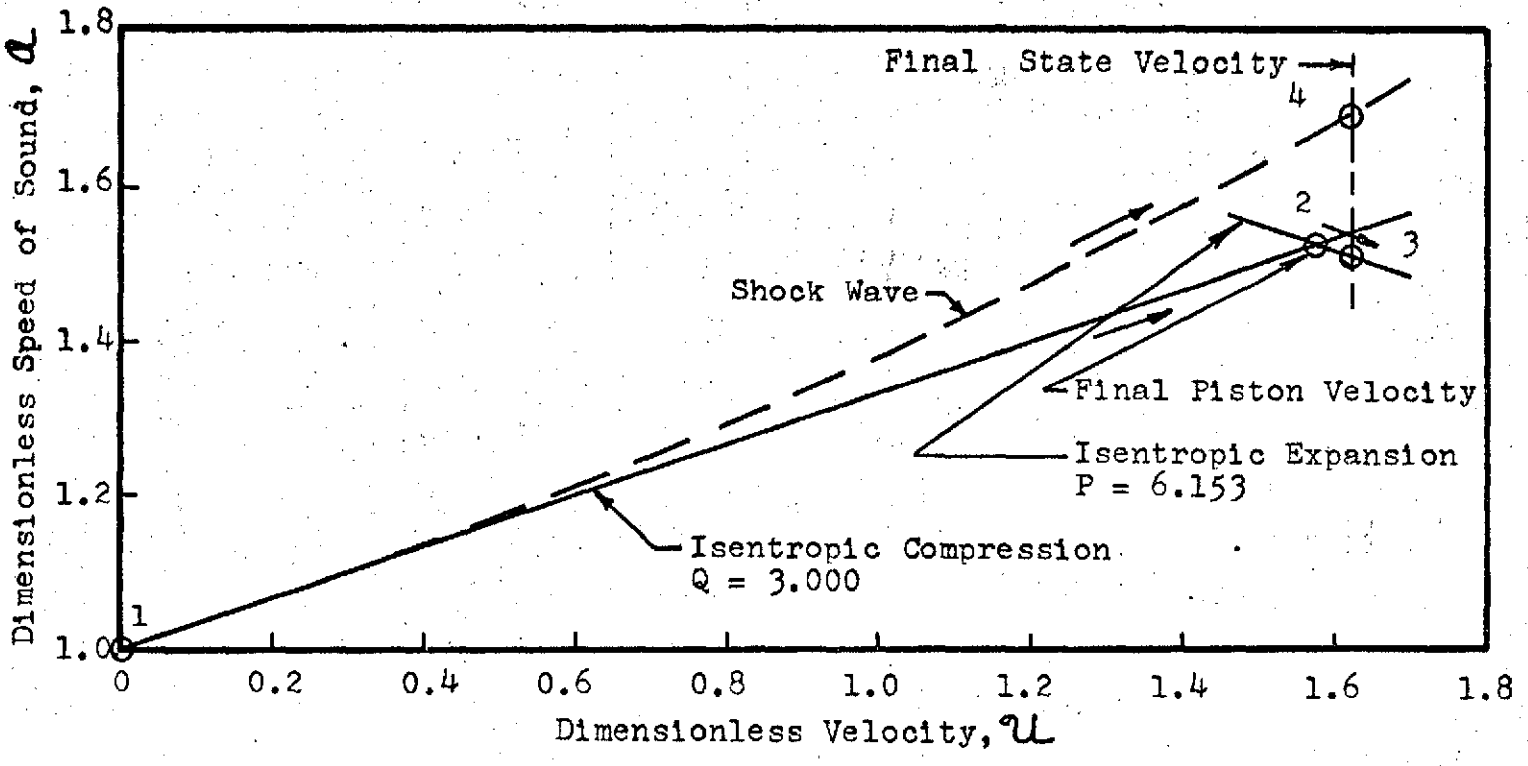

Fig. 3. Focused Compression Wave a, u Plane for Case I.

$u_1 = 0$, $a_o = a_1$, $\gamma = 1.667$, Flow Regions 1-4 Shown in Figure 1b.

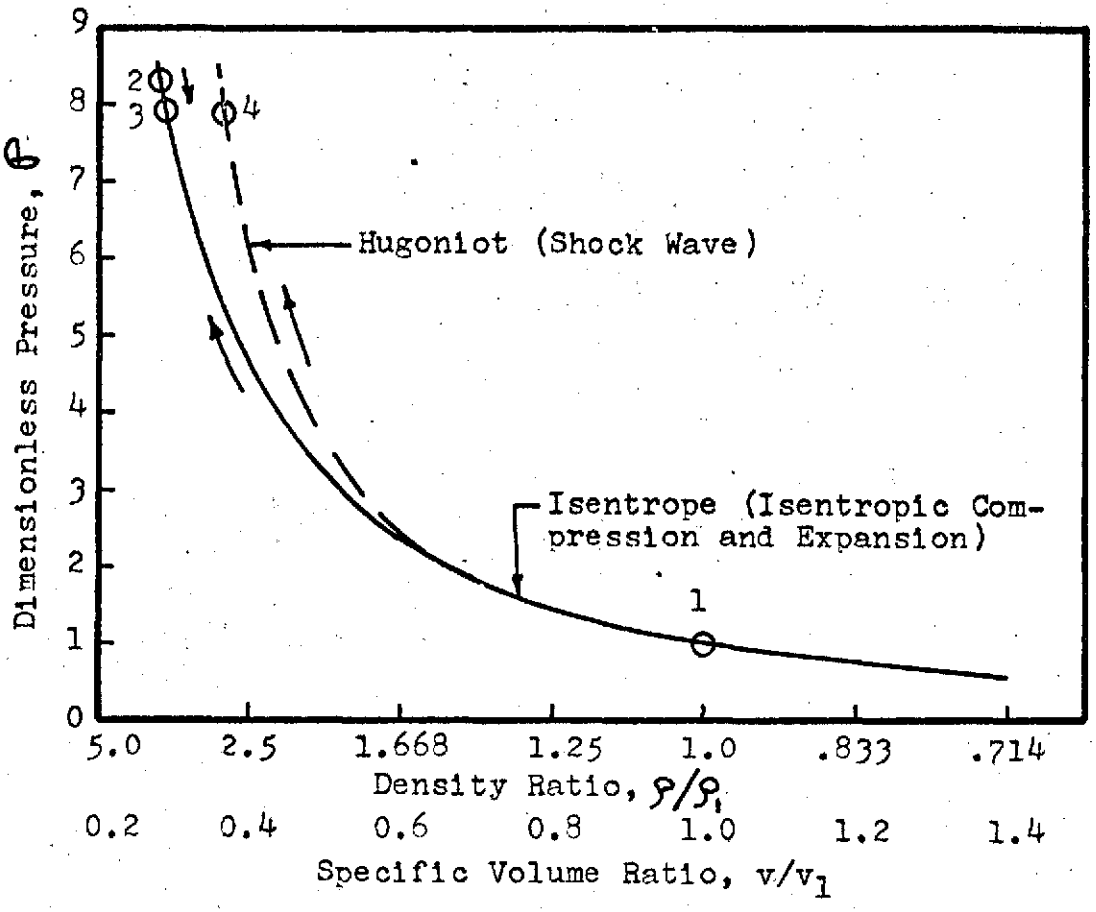

Fig. 4. Focused Compression Wave p,v Plane for Case I.

γ = 1.667, Flow Regions 1-4 Shown in Figure 1b.

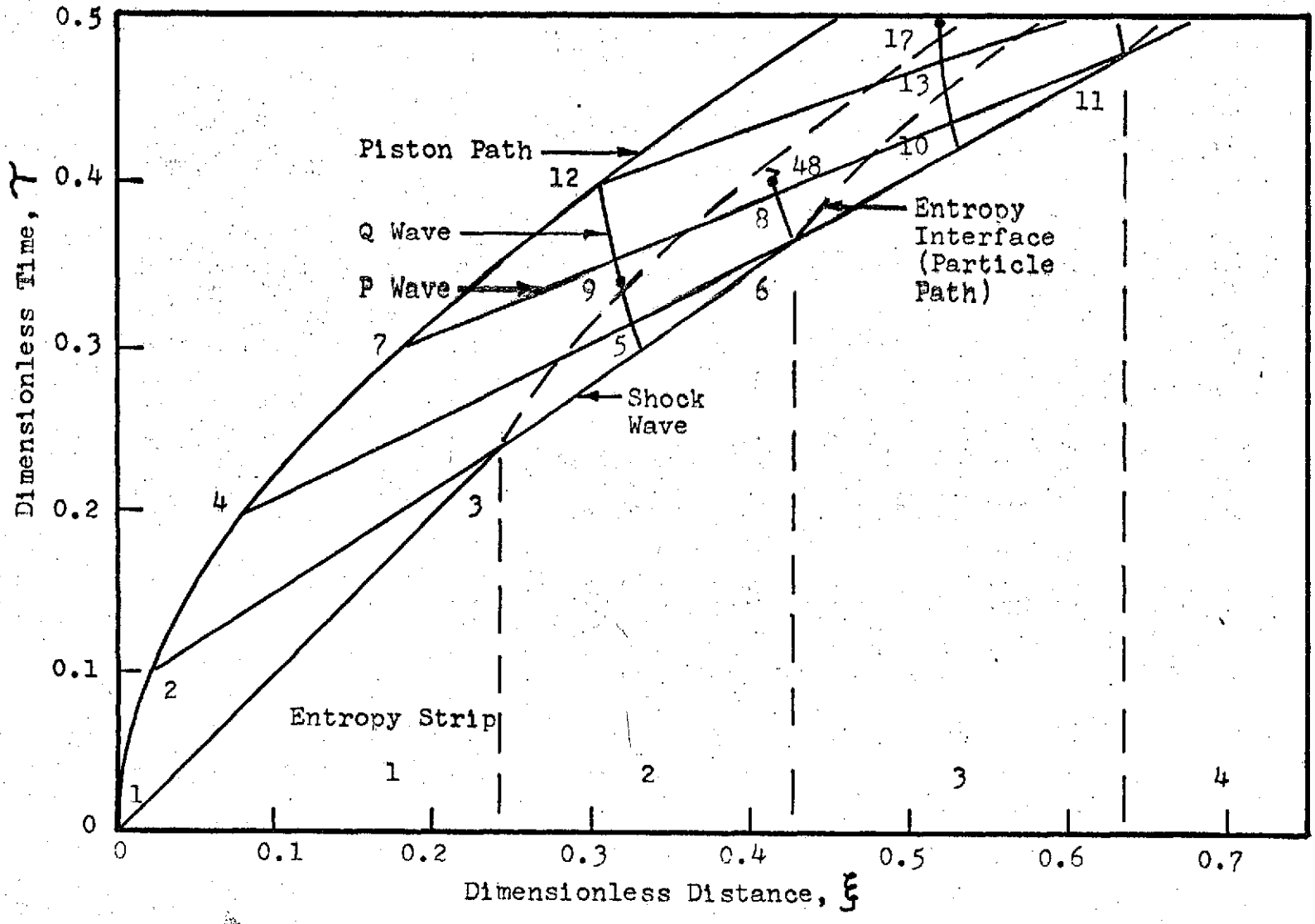

Fig. 5a. Wave Diagram Solution for Case II.
L_o = 24 ft, a_o = 1052 fps, t_o = 0.0228 sec = 22.8 msec.

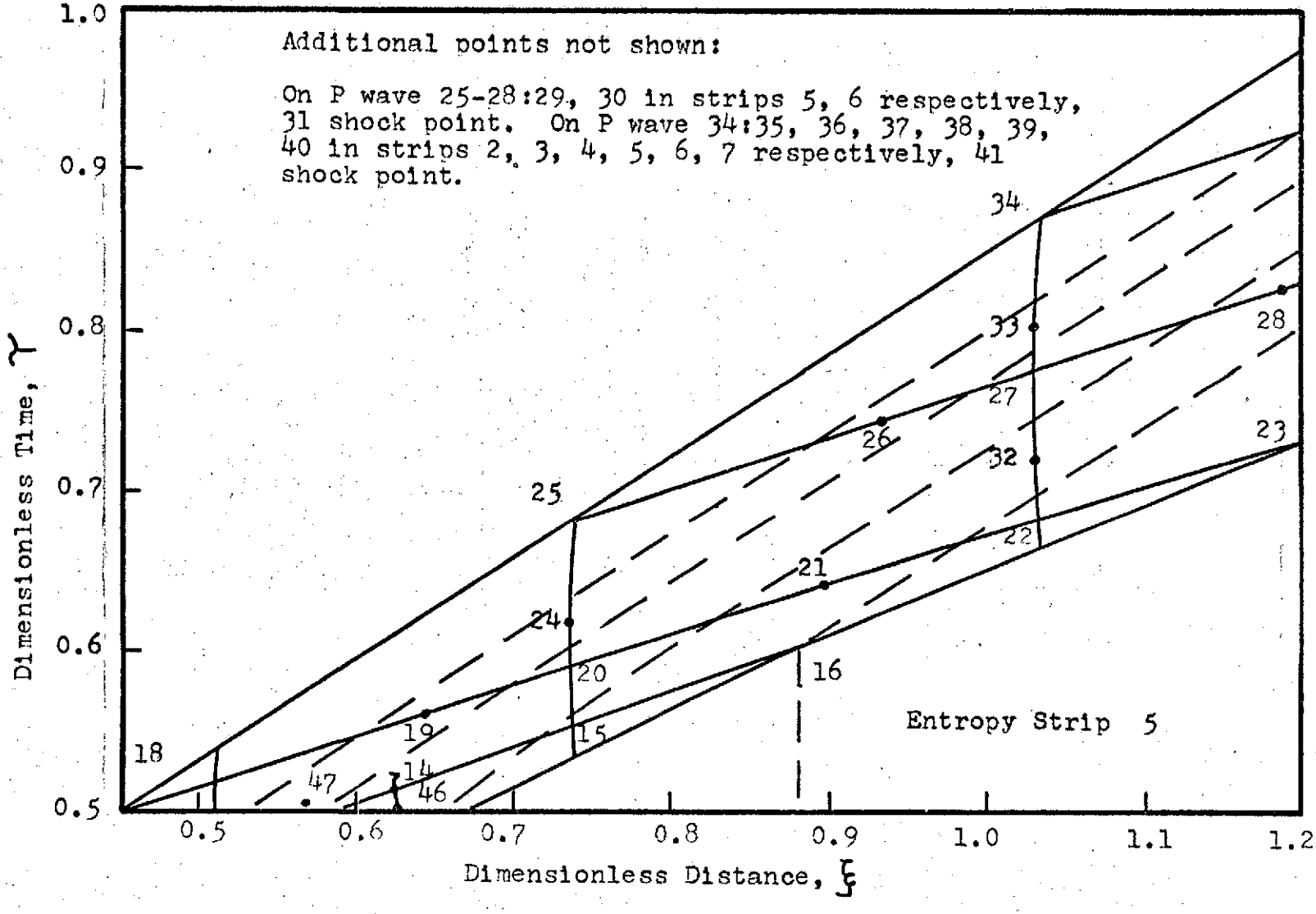

Fig. 56. Wave Diagram Solution for Case II.

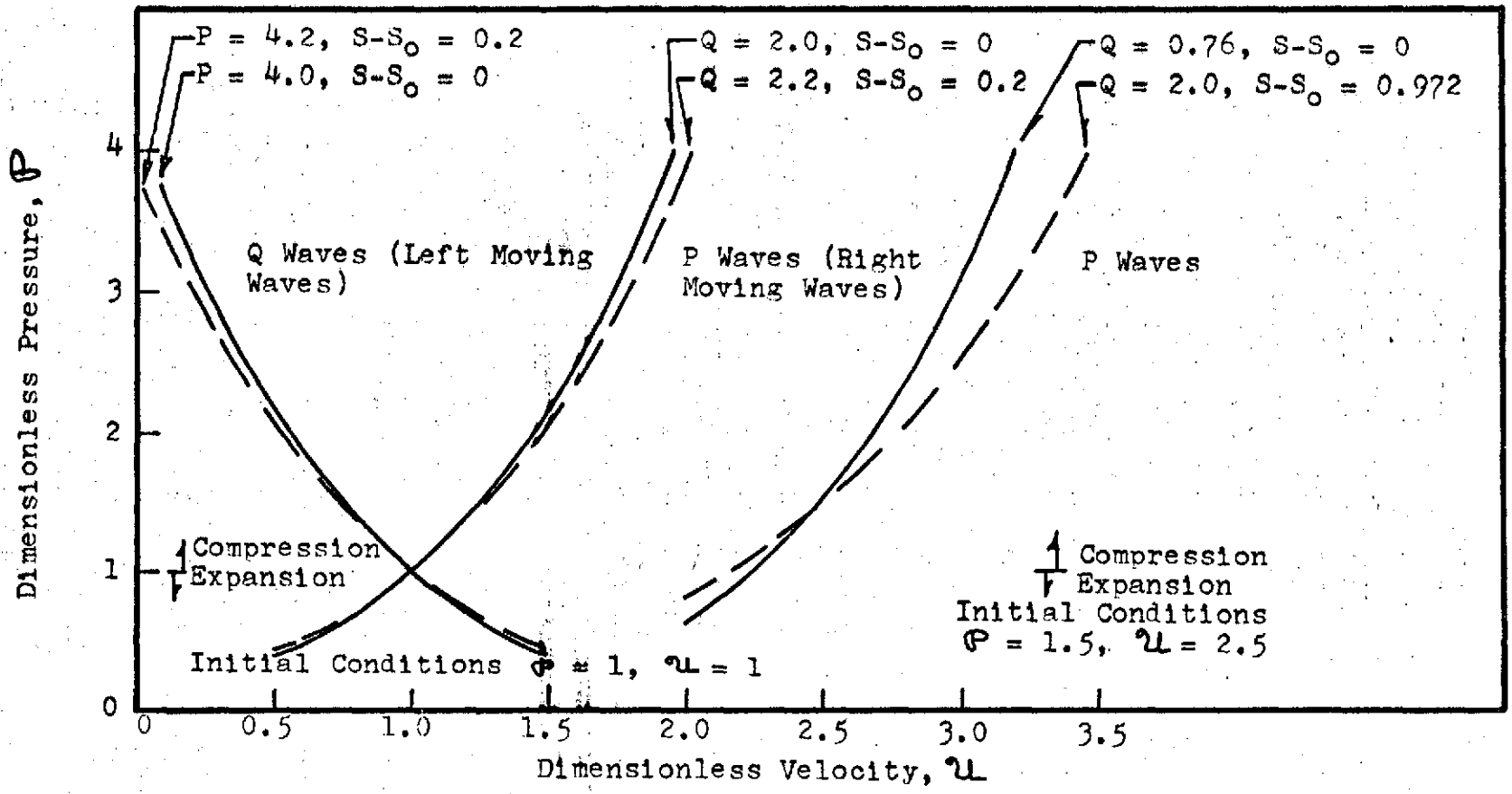

Fig. 6. $\mathcal{P}, \mathcal{U}$ Plane for Isentropic One-Dimensional Wave Motion. $\gamma = 1.667$.

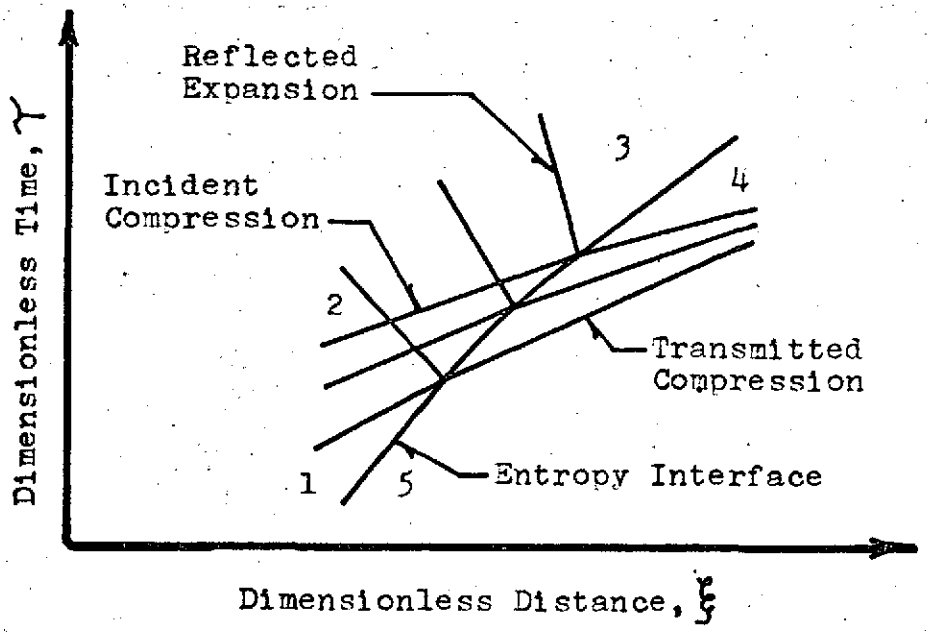

a

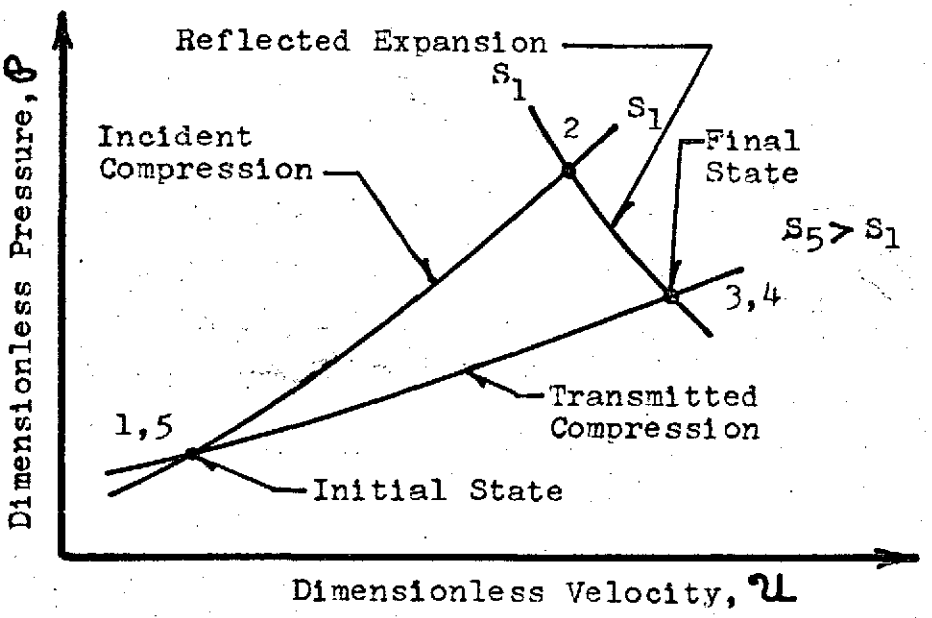

b

Fig. 7. Compression Wave Moving From Region of Low to High Entropy. Numbers Indicate Flow Regions.

a. τ, ξ Plane
b. P, u Plane

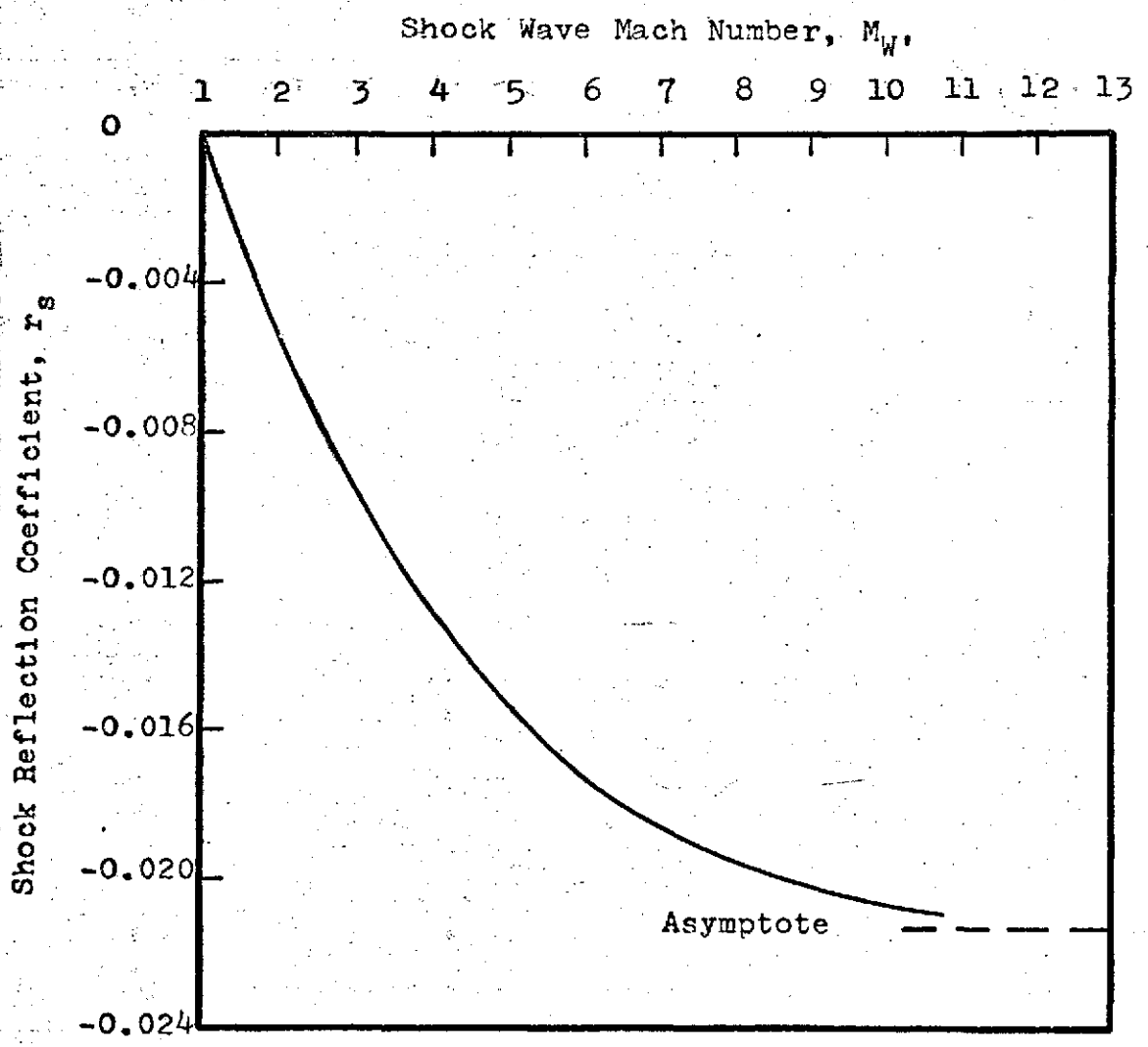

Fig. 8. Shock Reflection Coefficient as a Function of Mach Number. $\gamma = 1.667$.

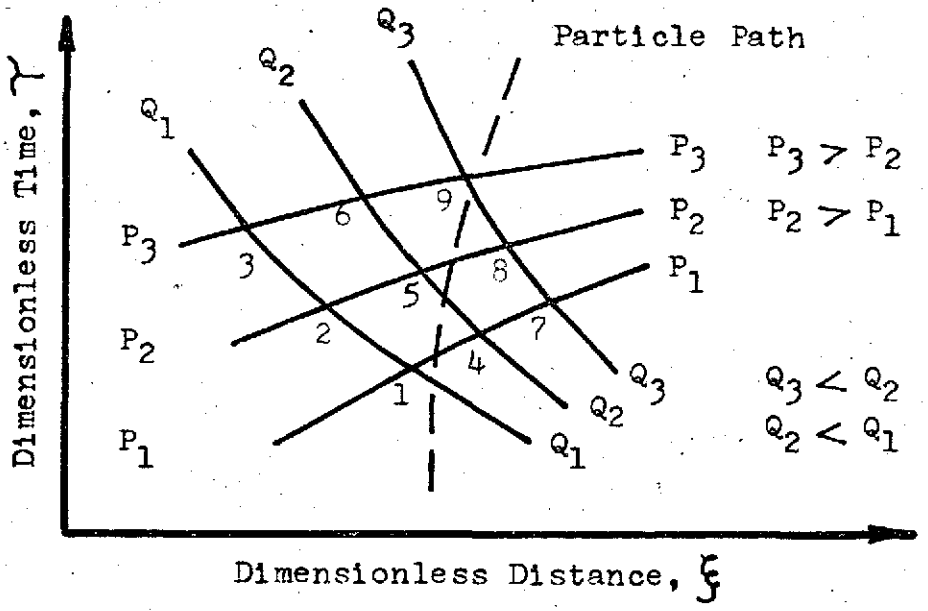

a

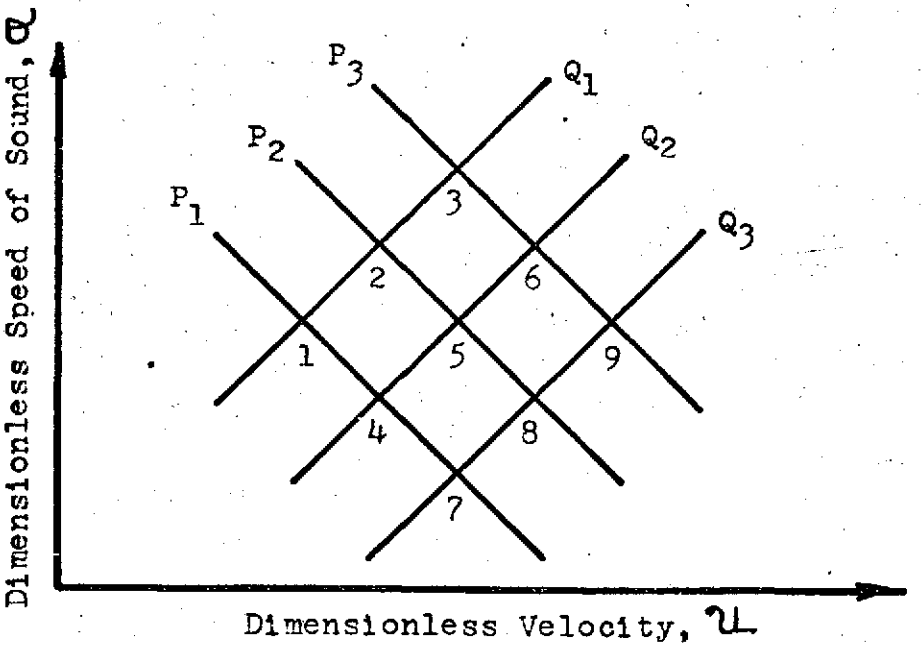

b

Fig. 9. Interaction of Isentropic Waves Moving in Opposite Directions.

a. ξ, τ Plane for Compression and Expansion Wave Interaction

b. a, u Plane for Compression and Expansion Wave Interaction

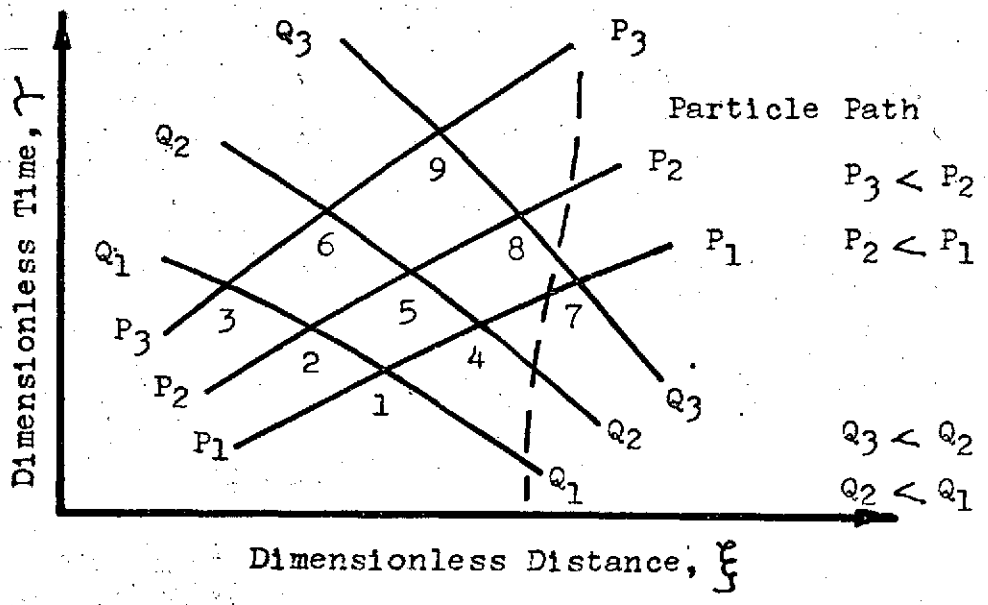

c

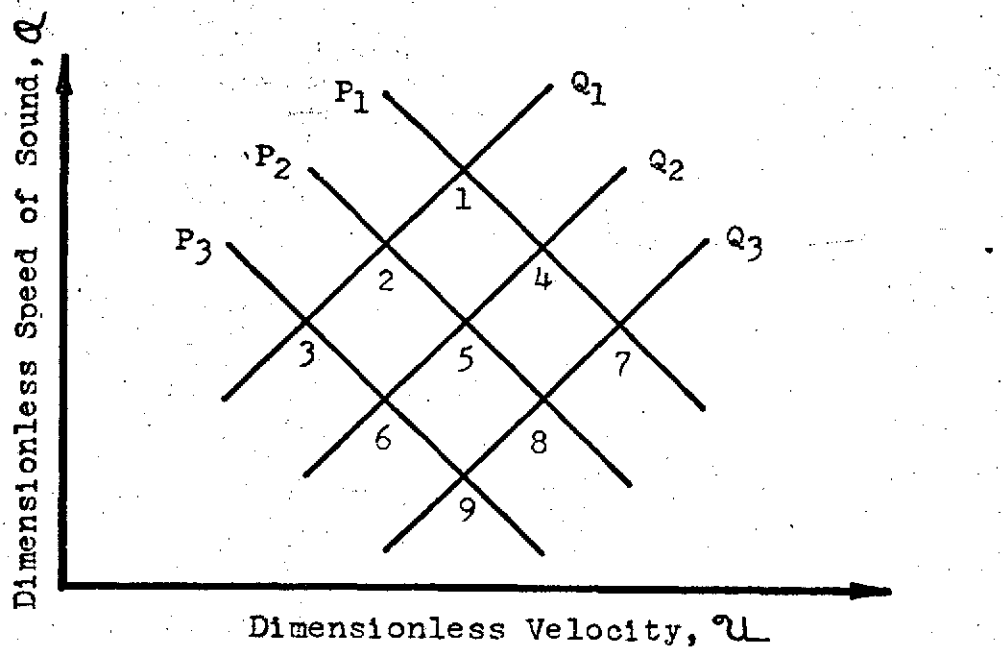

d

Fig. 9. Interaction of Isentropic Waves Moving in Opposite Directions.

c. ξ, τ Plane for Interaction of Two Expansion Waves

d. a, u Plane for Interaction of Two Expansion Waves

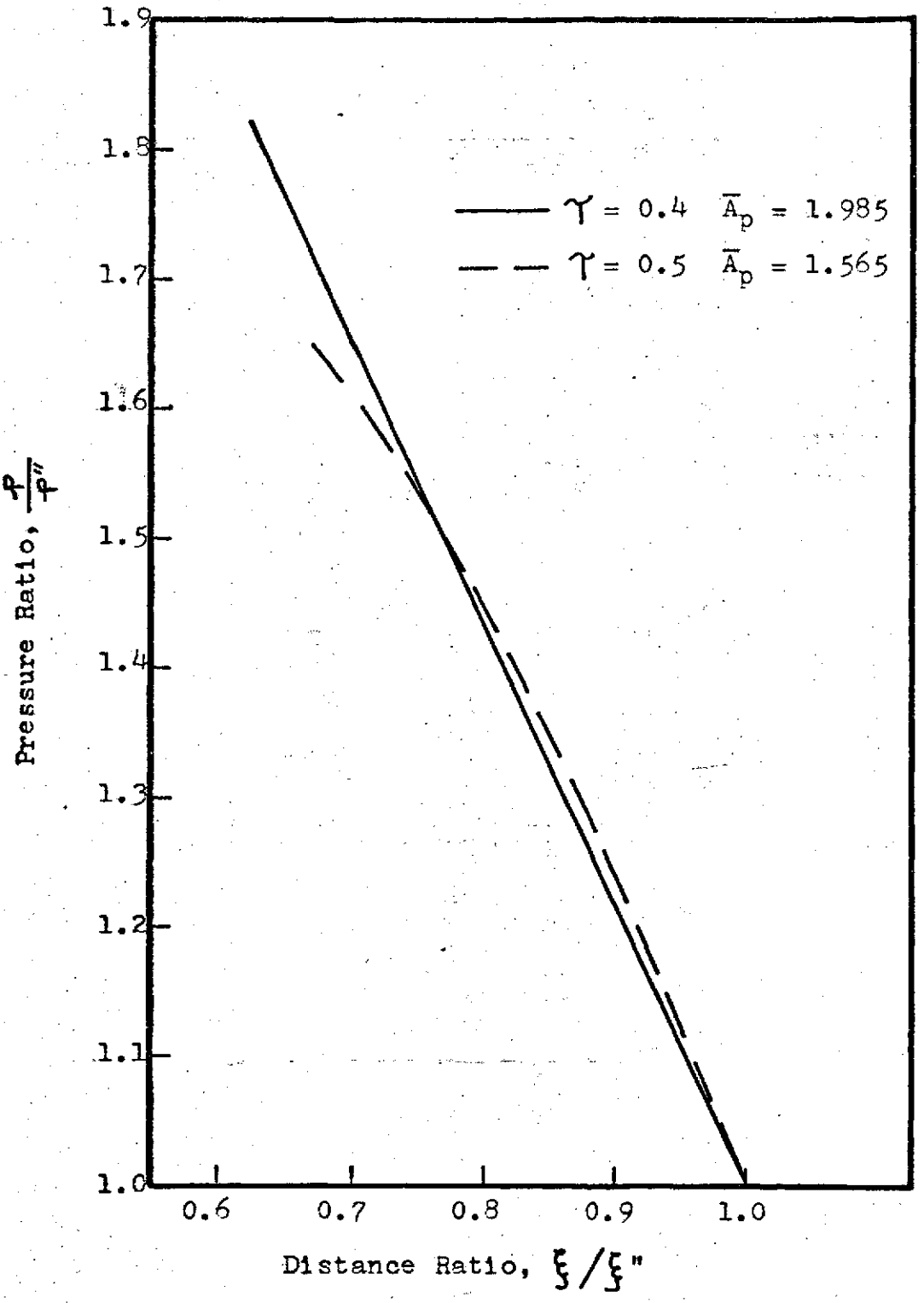

Fig. 10. Shock Layer Pressure Distributions During Piston Acceleration at Two Fixed Times for Case II. The Left End of Each Curve is at the Piston.

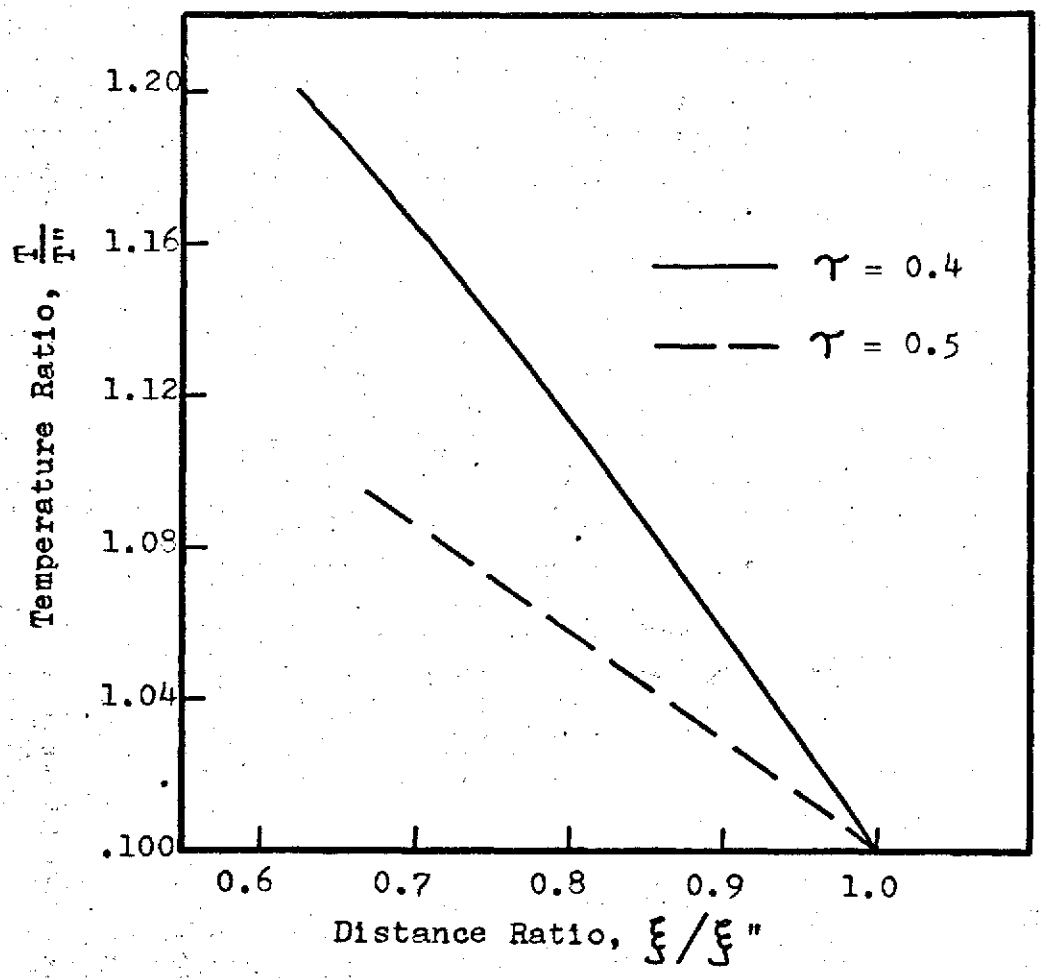

Fig. 11. Shock Layer Temperature Distributions During Piston Acceleration at Two Fixed Times for Case II. The Left End of Each Curve is at the Piston.

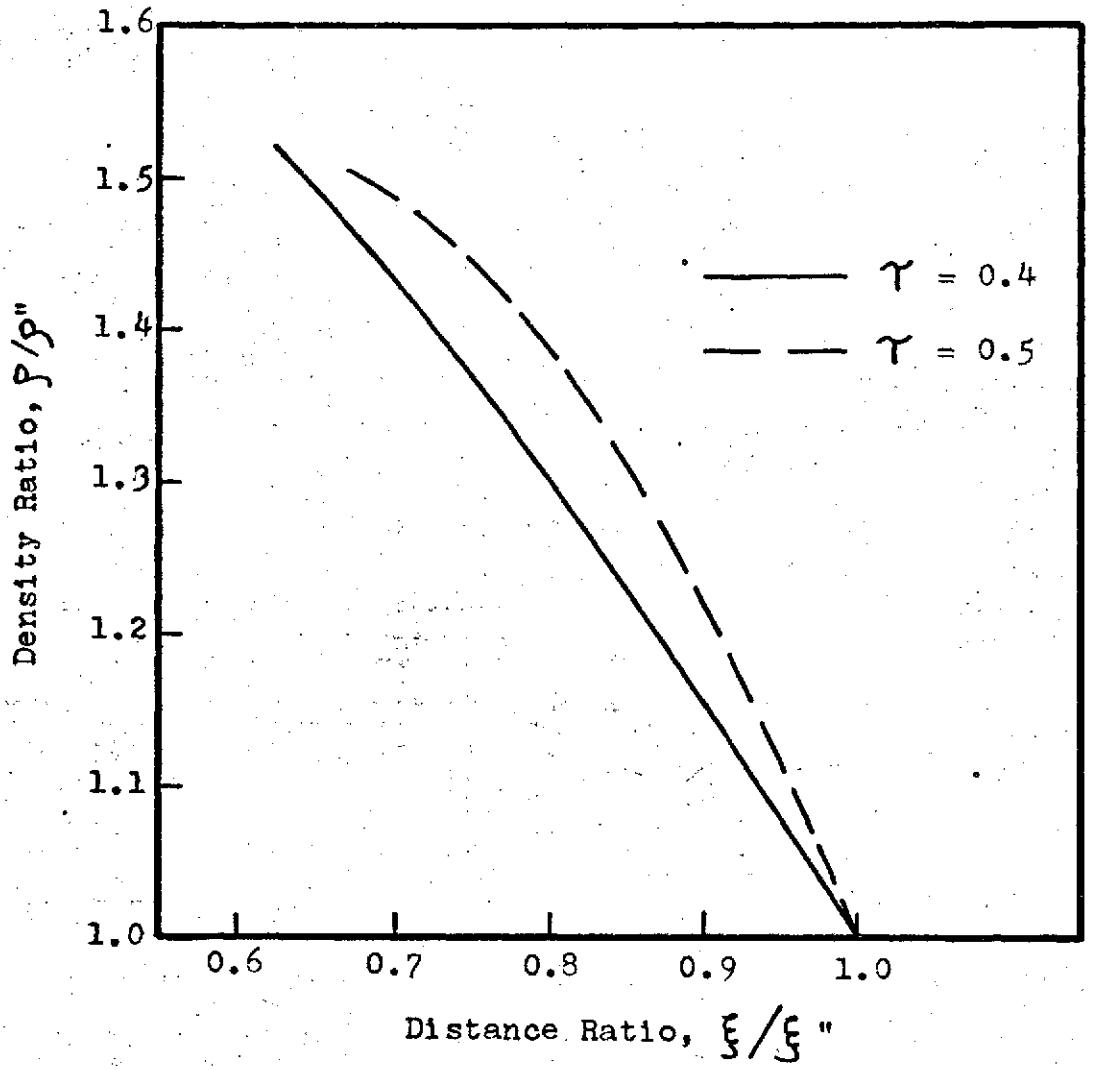

Fig. 12. Shock Layer Density Distributions During Piston Acceleration at Two Fixed Times for Case II. The Left End of Each Curve is at the Piston.

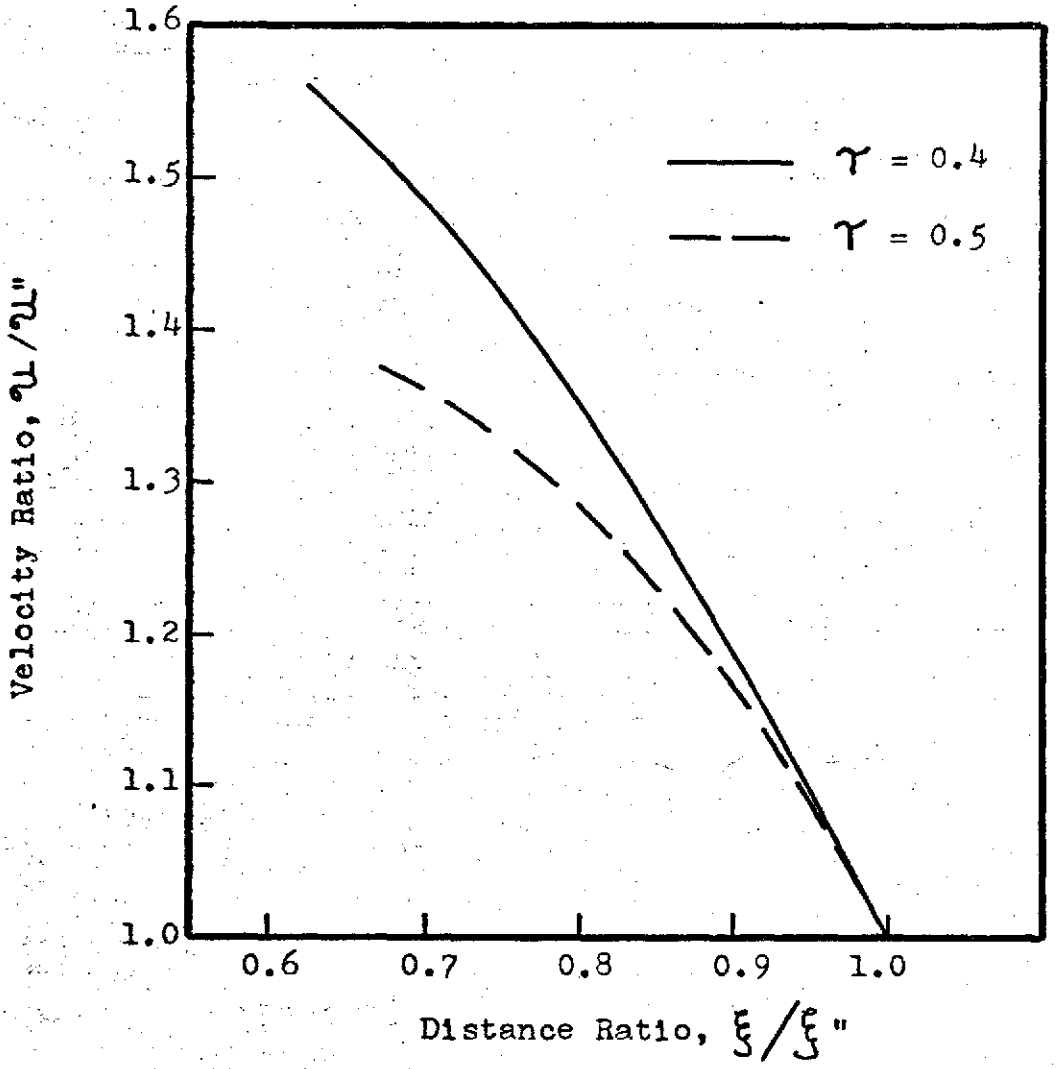

Fig. 13. Shock Layer Velocity Distributions During Piston Acceleration at Two Fixed Times for Case II. The Left End of Each Curve is at the Piston.

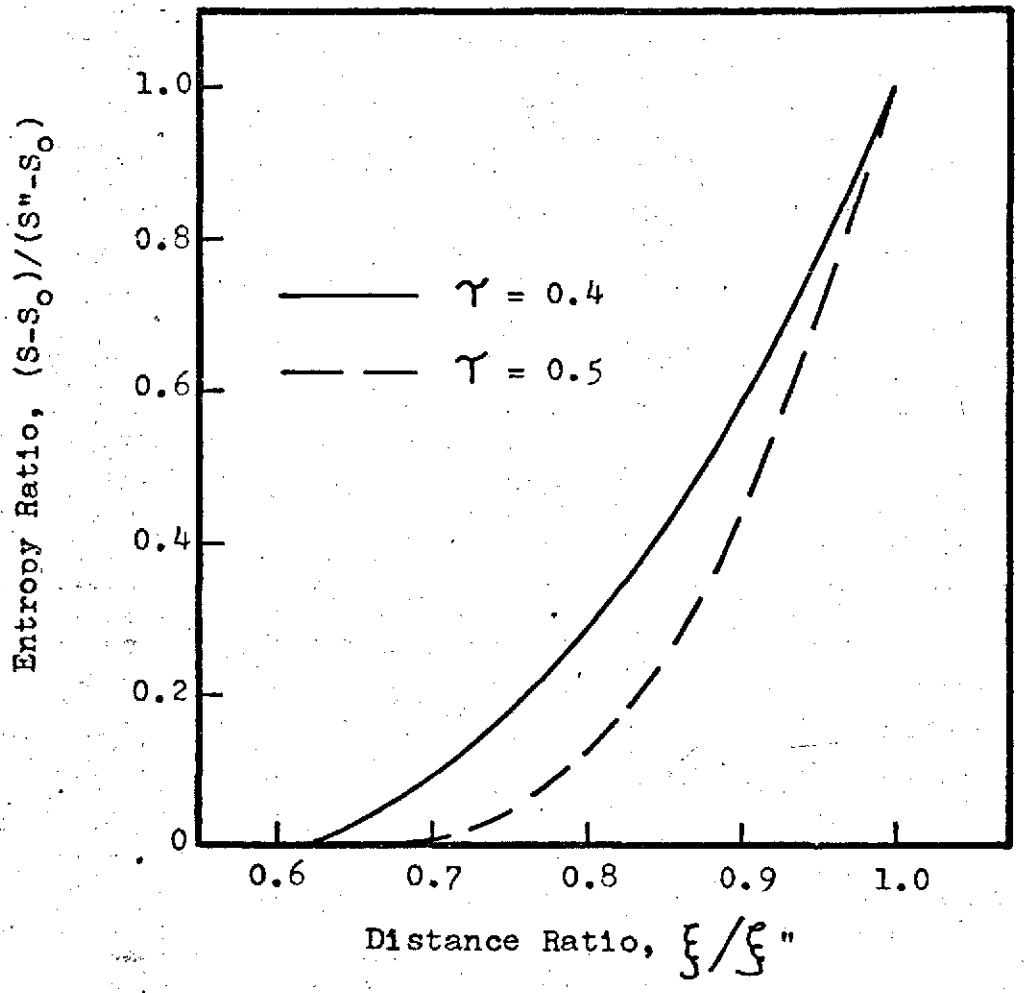

Fig. 14. Shock Layer Entropy Distributions During Piston Acceleration at Two Fixed Times For Case II. The Left End of Each Curve is at the Piston.

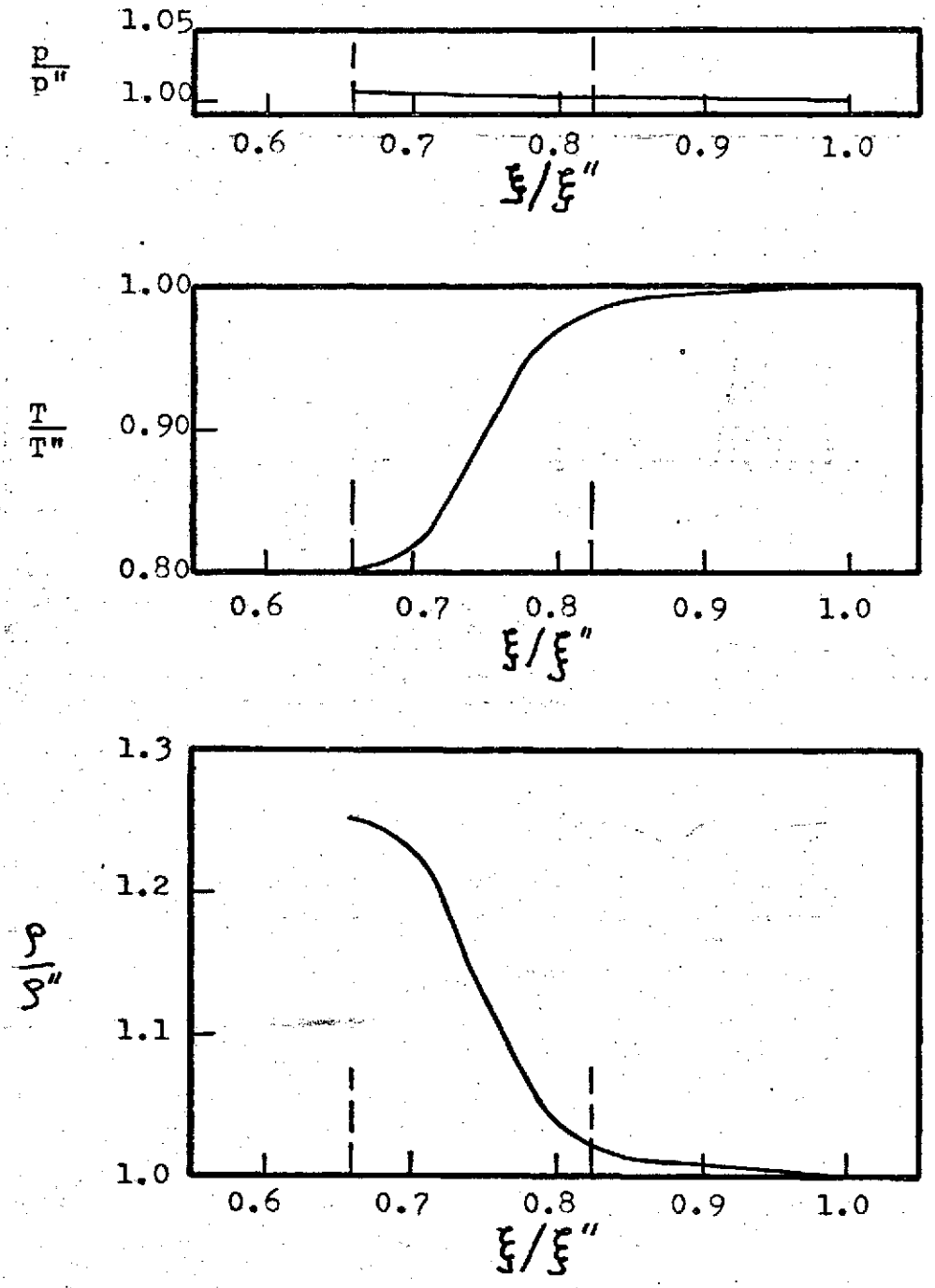

Fig. 15. Shock Layer Flow Variable Distributions After Piston Reaches Constant Velocity, at Fixed Time for Case II. The Left End of Each Curve is at the Piston. $\gamma = 1.22$, $(M_{W'})_f = 2.51$. Region Between Dashed Lines was Compressed by the Primary or Initial Compression Waves and the Variable Strength Shock.

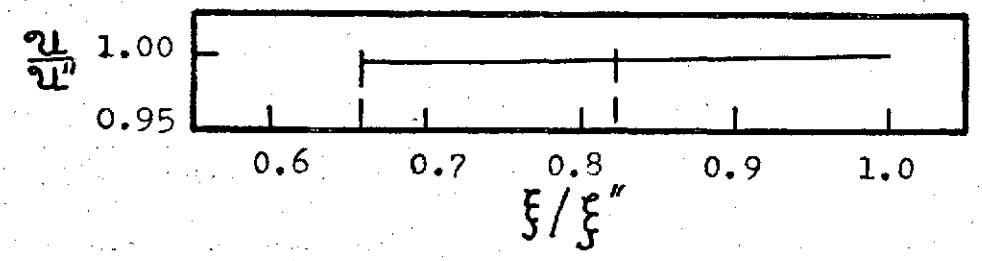

a

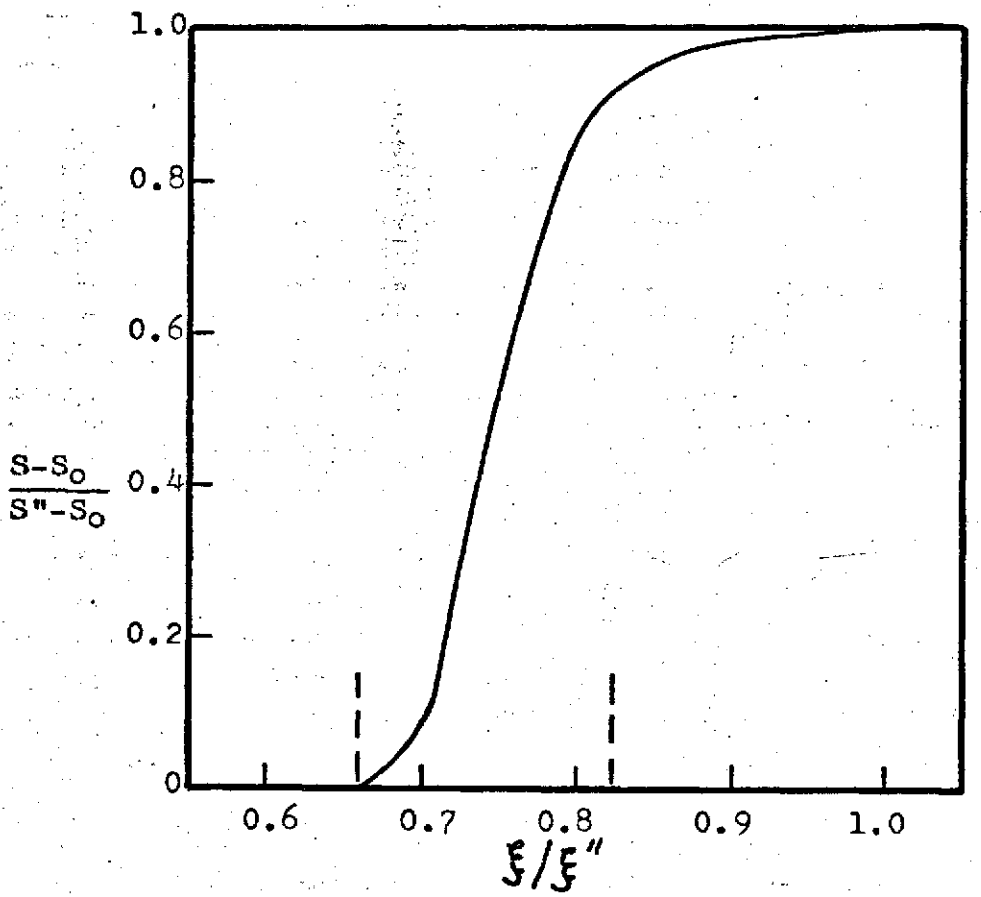

b

Fig. 16. Shock Layer Flow Variable Distributions After Piston Reaches Constant Velocity, at Fixed Time for Case II. The Left End of Each Curve is at the Piston. $\gamma = 1.22$, $(M_{W'})_f = 2.51$. Region Between Dashed Lines Was Compressed by the Primary or Initial Compression Waves and the Variable Strength Shock.

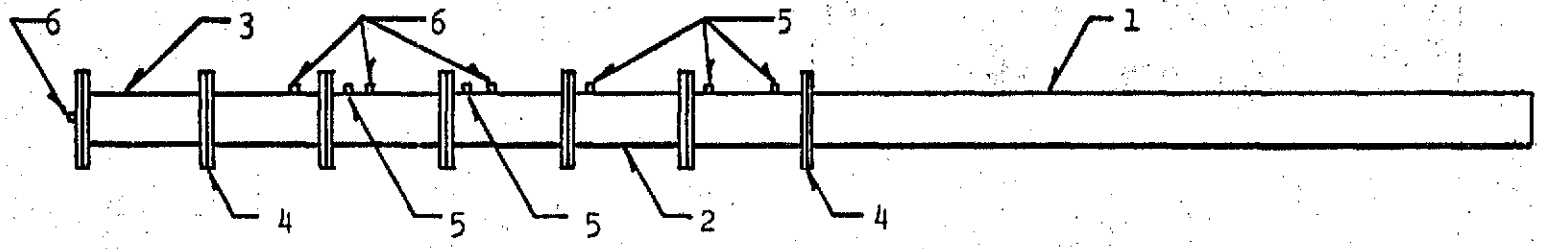

PC. No.	Name
1	Driver Tube
2	Driven Tube (5 Sections)
3	Brake Tube
4	Diaphragm
5	Magnetic Pickup
6	Pressure Transducer

Fig. 17. Piston Tube Arrangement and Instrumentation.

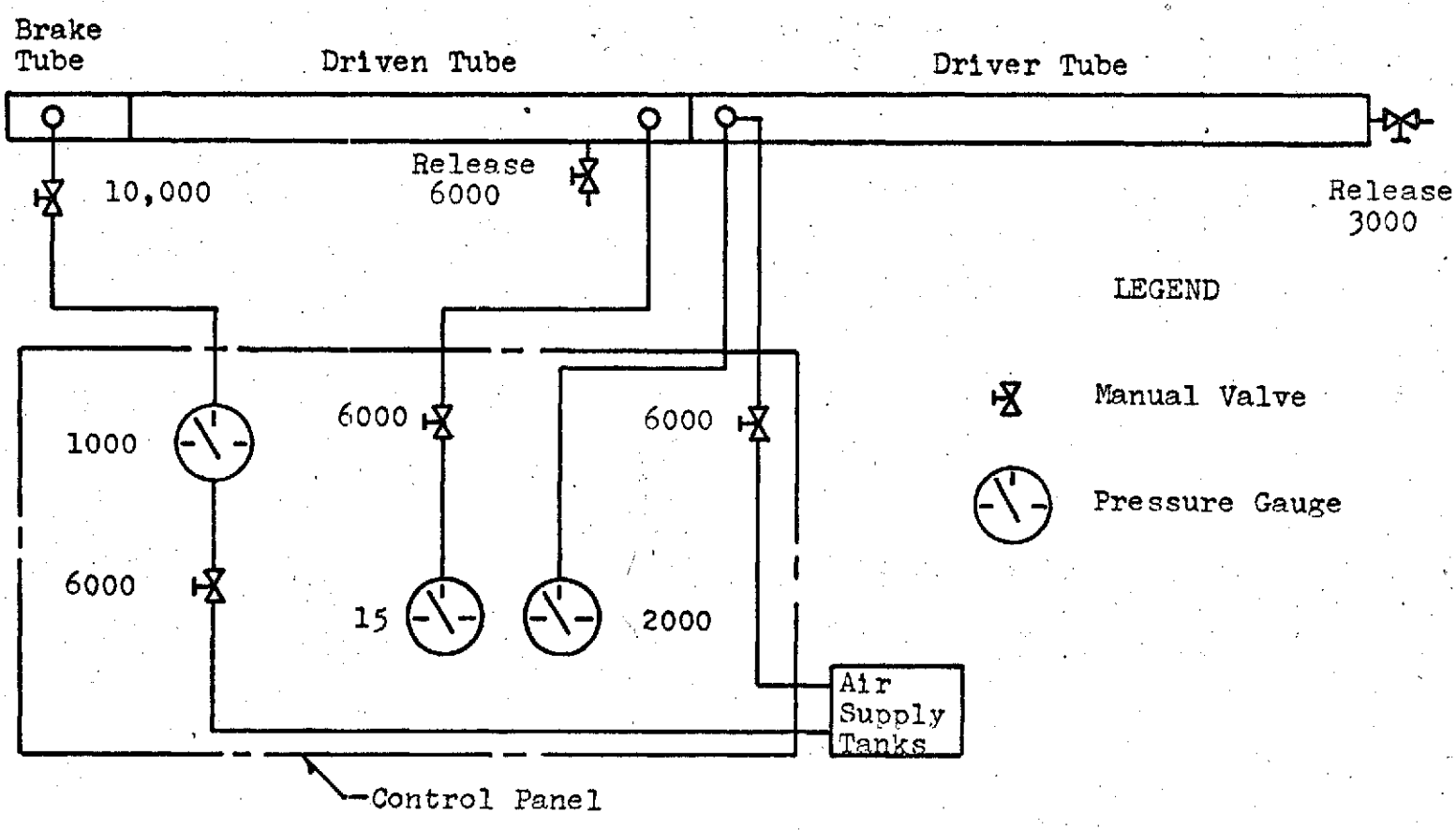

Fig. 18. Air Supply and Control System. Numbers Adjacent to Valves and Gauges Give Maximum Allowable Pressure in psi.

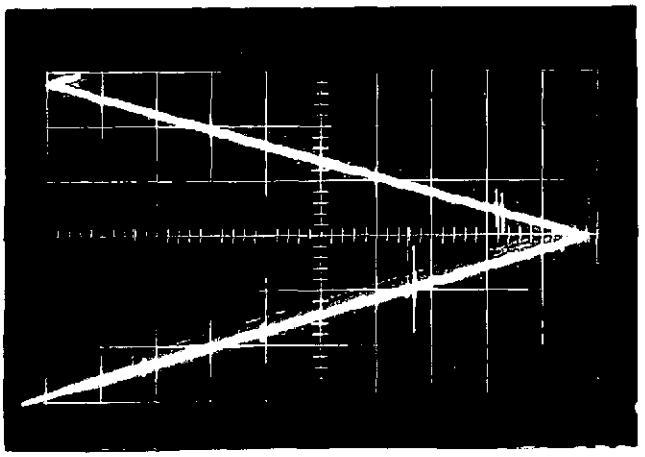

a. 1 msec/div horizontal sweep rate

1 v/div vertical gain

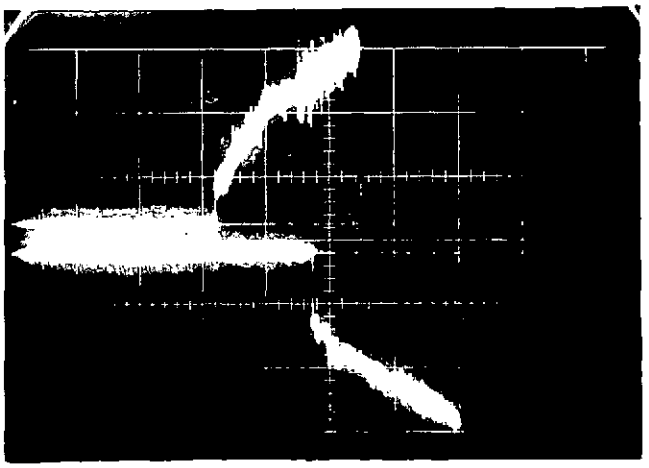

b. 2 msec/div horizontal sweep rate

2 v/div vertical gain

Fig. 19. Typical Magnetic Pickup and Pressure Transducer Traces

a. Magnetic Pickup Output, Case IV

b. First (top) and Third (bottom) Side Wall Pressure Transducer Output, Case III

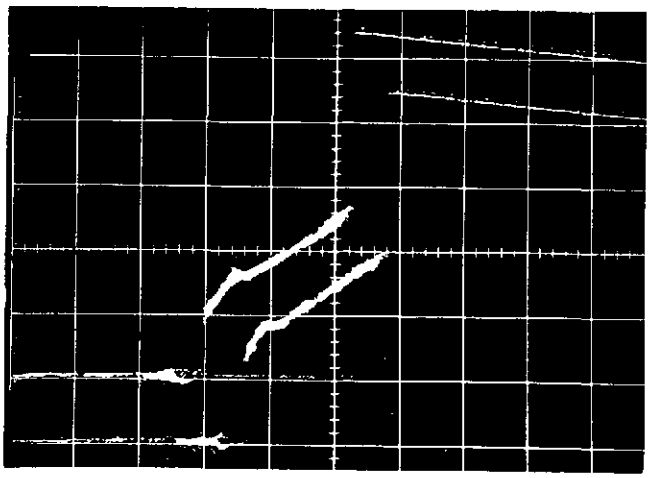

c. 2 msec/div horizontal sweep rate

2 v/div vertical gain

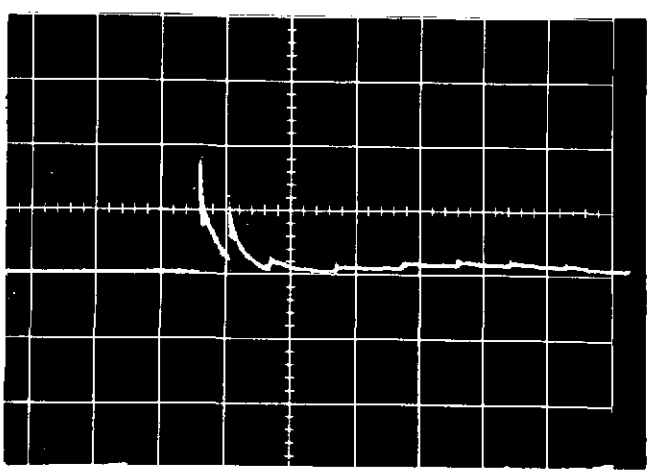

d. 5 msec/div horizontal sweep rate

2 v/div vertical gain

Fig. 19. Typical Magnetic Pickup and Pressure Transducer Traces

c. Second (top) and Third (bottom - not used) Side Wall Pressure Transducer Output, Case III

d. Brake Blind Flange Pressure Transducer Output. First Peak 9200 psi, Second Peak 6700 psi, Piston Mass 1 lb 1 ½ oz, $p_{DR,1}$ = 1735 psi

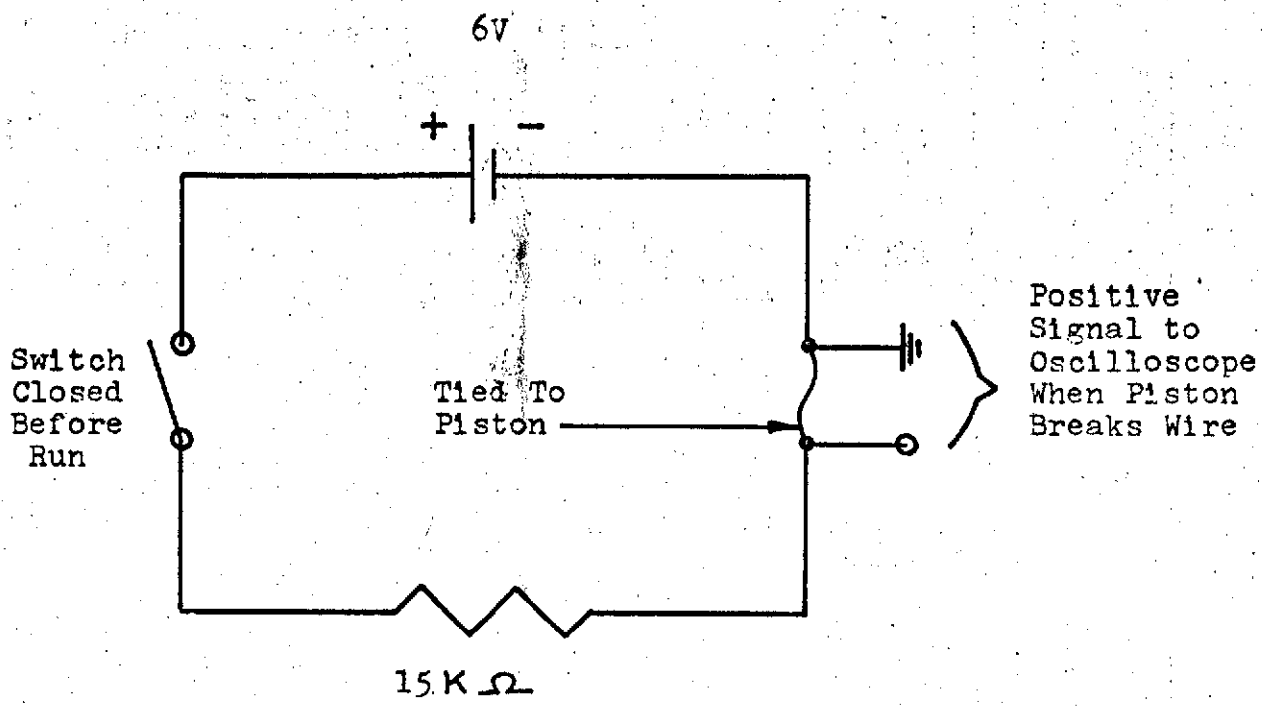

Fig. 20. Oscilloscope Trigger Circuit.

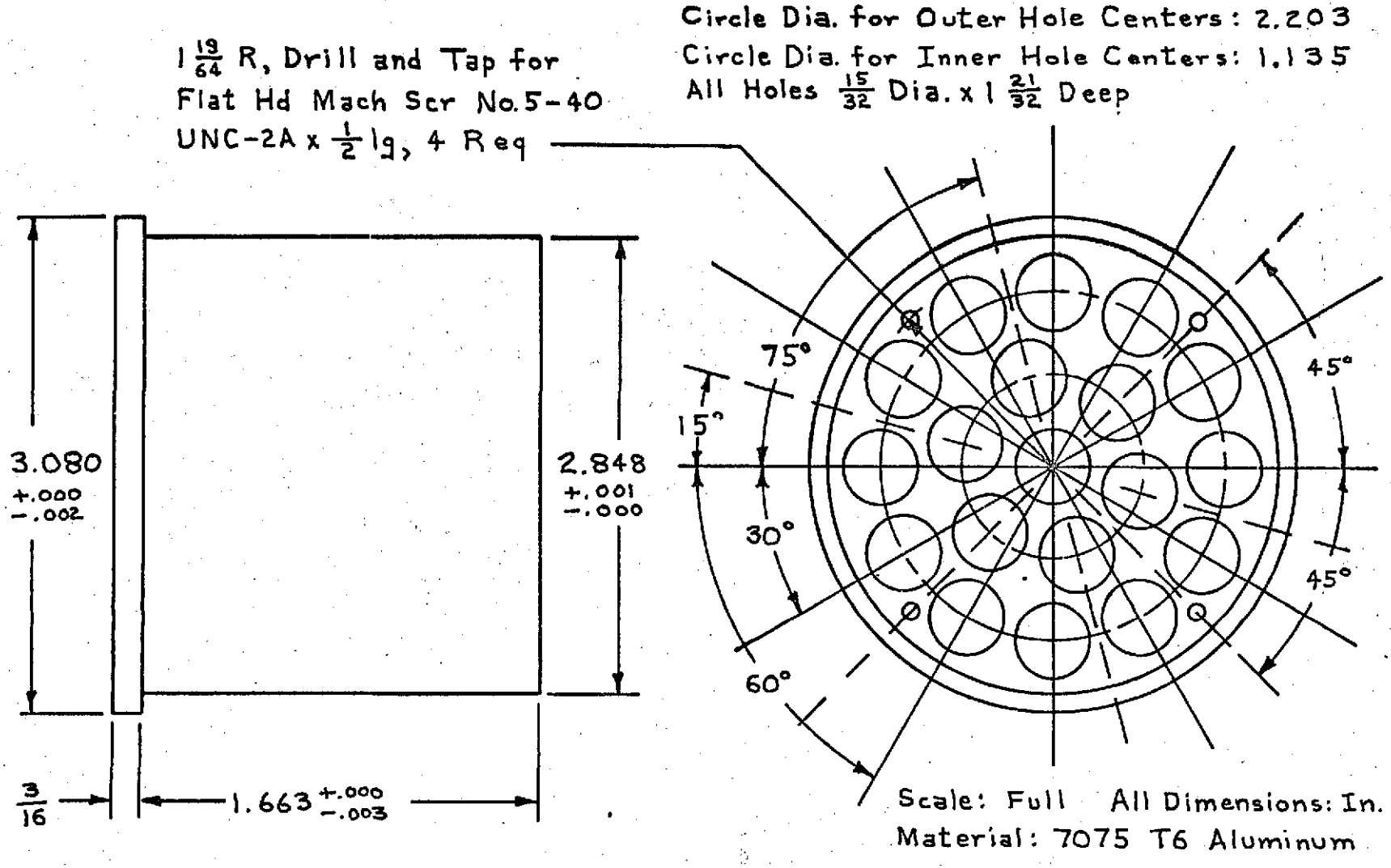

Fig. 21. Piston Body

Scale: Full All Dimensions: Inches
Material: Teflon

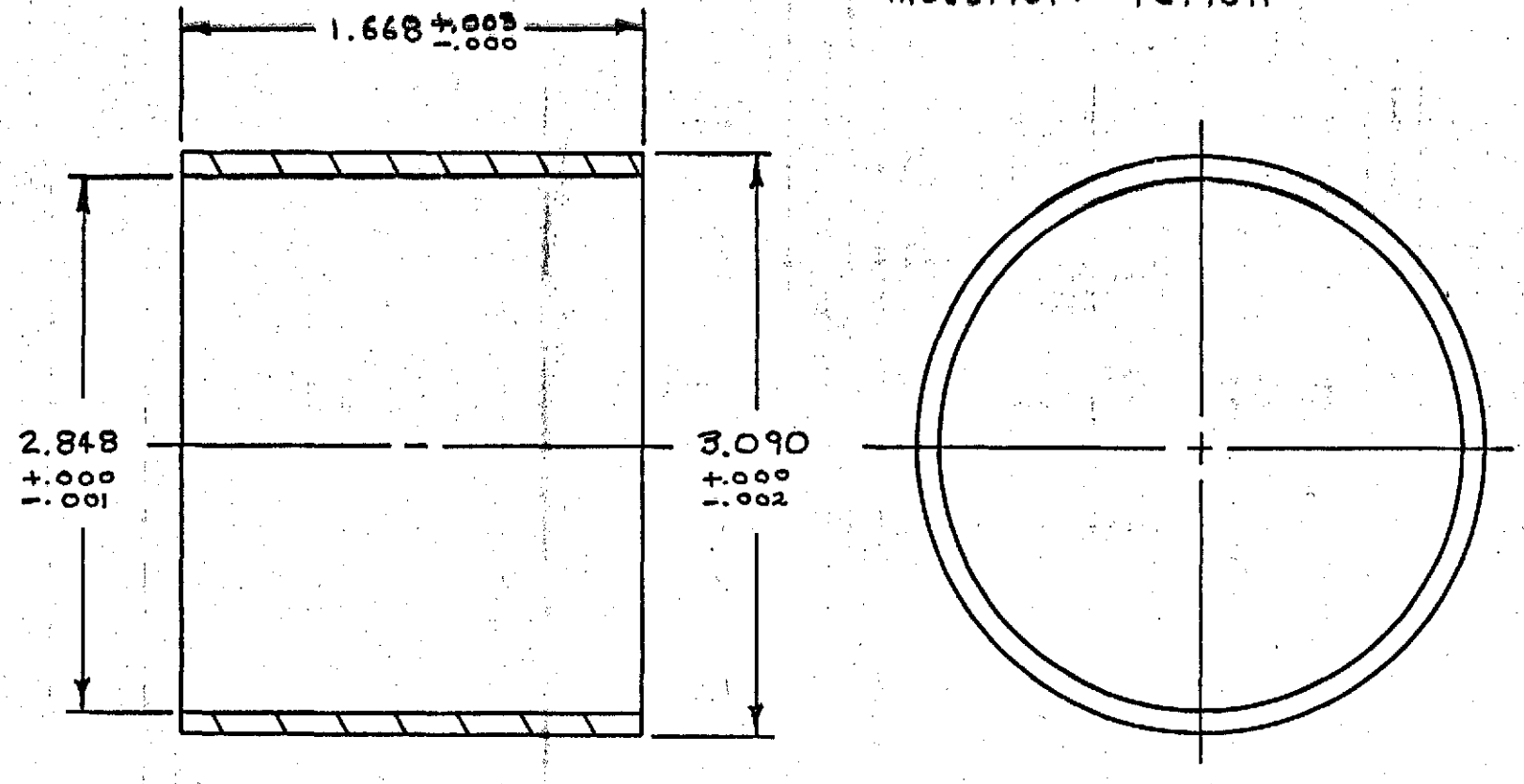

Fig. 22. Piston Sleeve

Scale: Full All Dimensions: Inches
Material: Aluminum

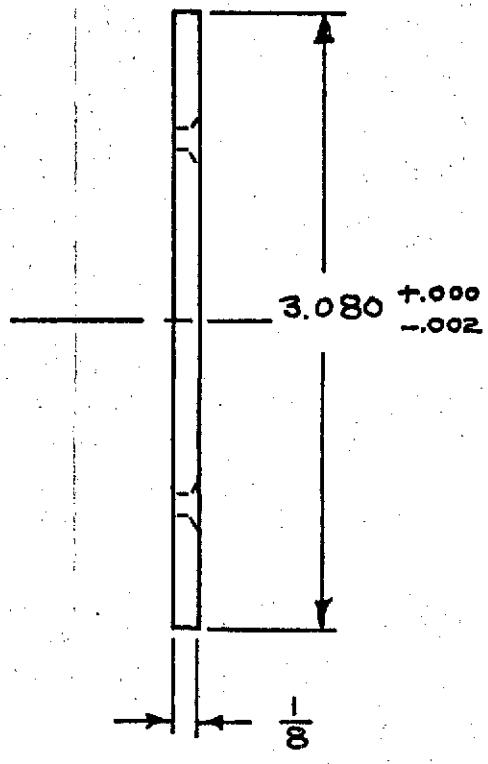

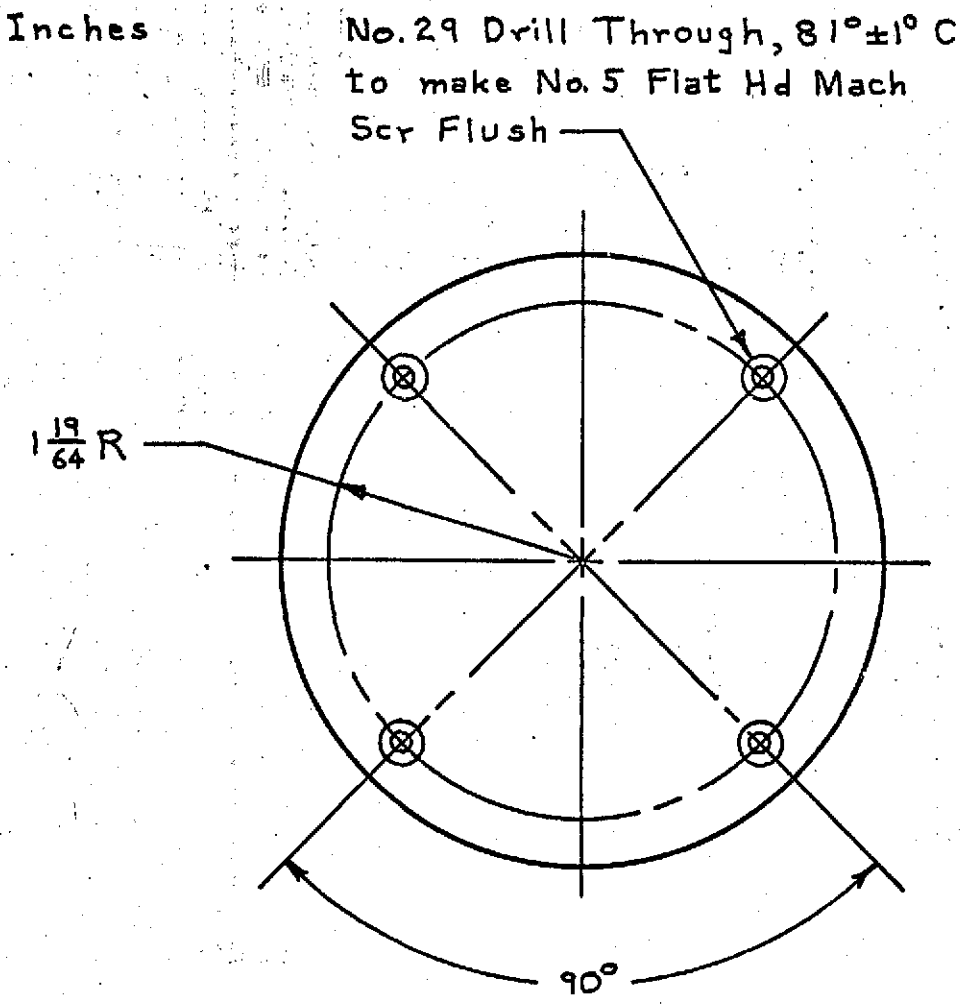

Fig. 23. Piston Face Plate

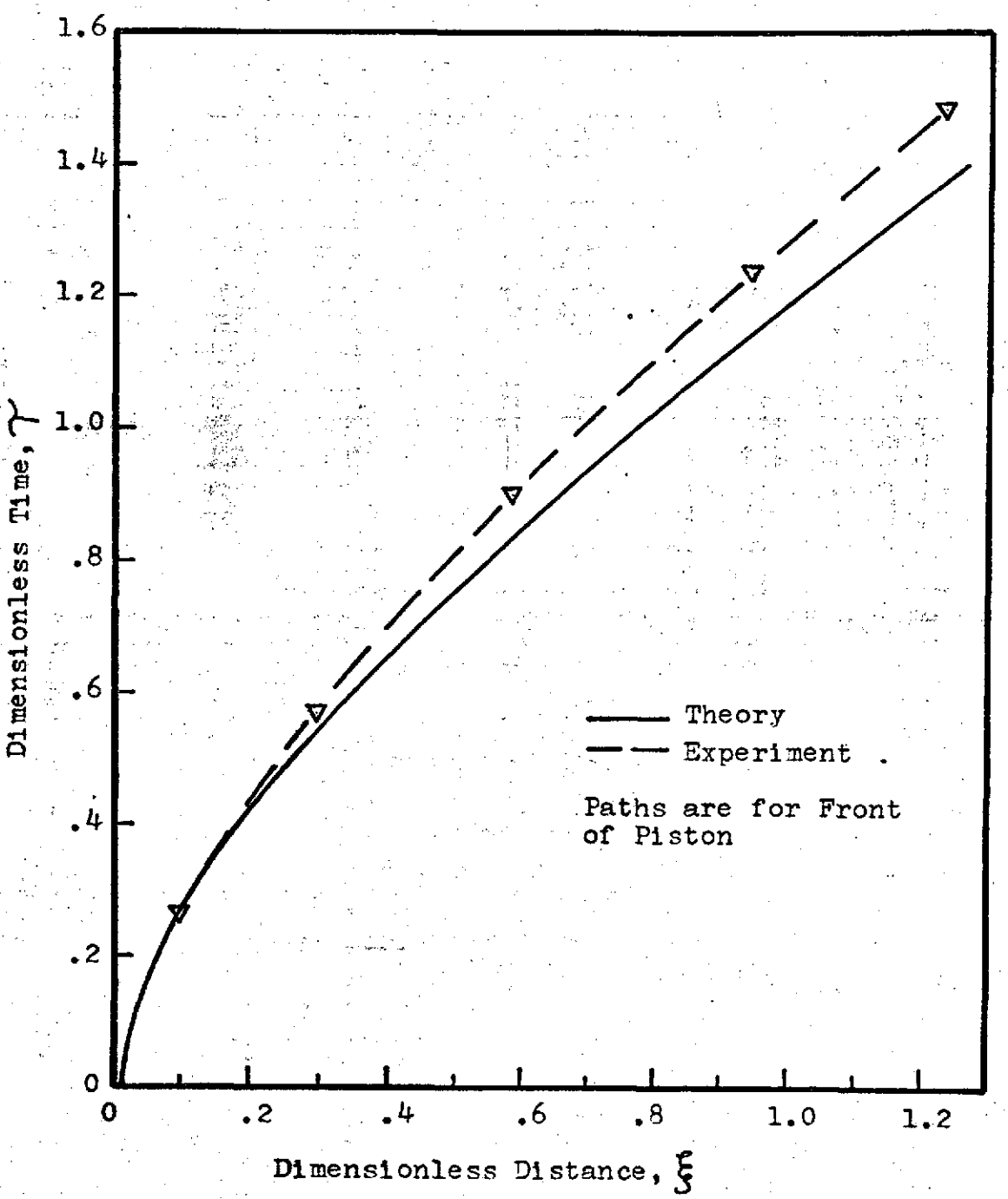

Fig. 24. Theoretical and Experimental Piston Paths for Case III.

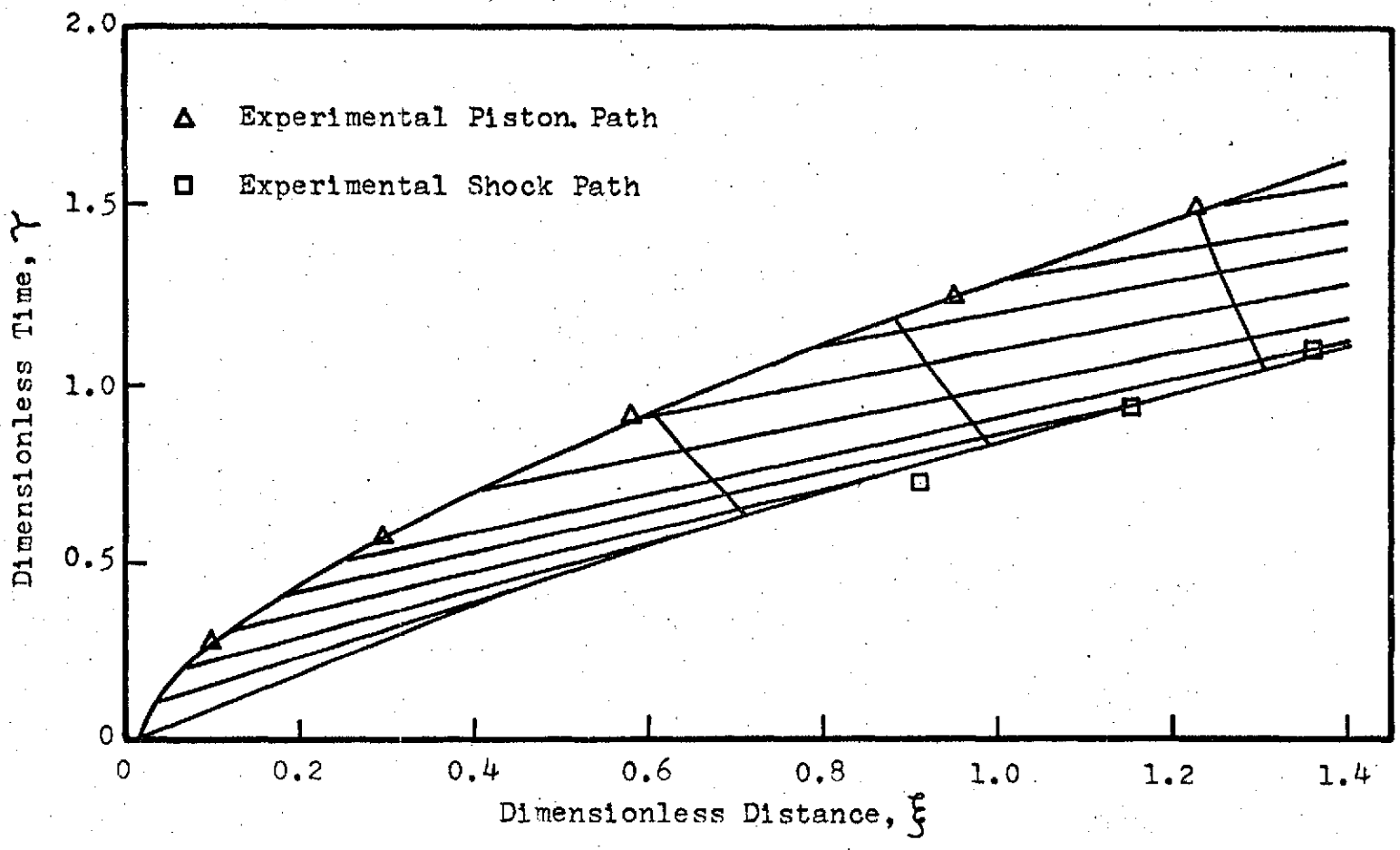

Fig. 25. Wave Diagram Solution for Case III and Comparison With Experimental Shock Path. $a_{DN,1} = a_o = 1130$ fps, $L_o = 10$ ft, $t_o = 8.85$ msec, $\gamma = 1.4$, $P_{DN,1} = 14.35$ psi, $T_{DN,1} = 73^oF$, $u_{DN,1} = 0$, $S_{DN,1} = S_o = 0$.

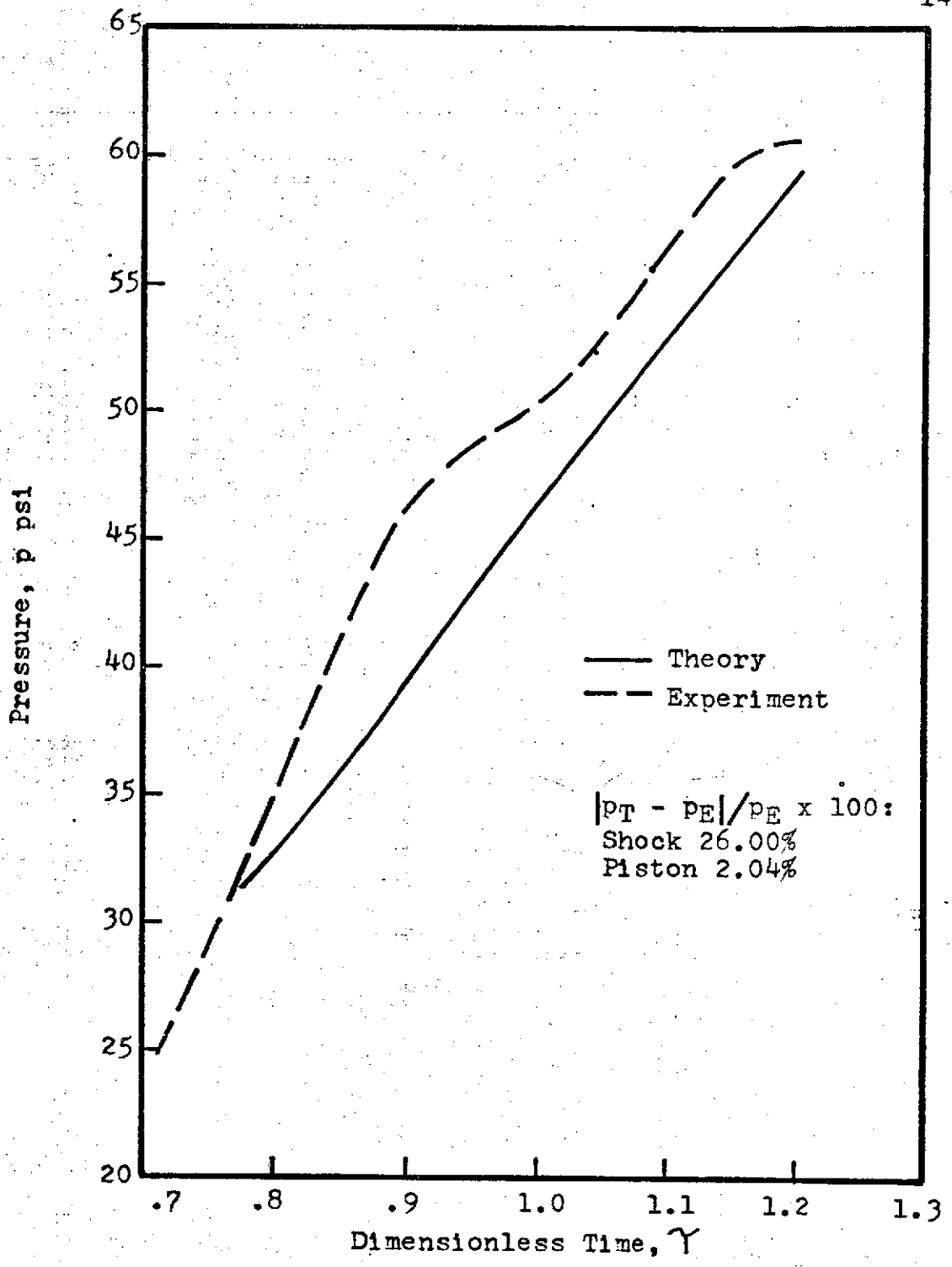

Fig. 26. Theoretical and Experimental Shock Layer Pressure Distributions at First Pressure Transducer for Case III. The Left End of Each Curve is Just Downstream of the Shock, The Right End is at the Front of the Piston.

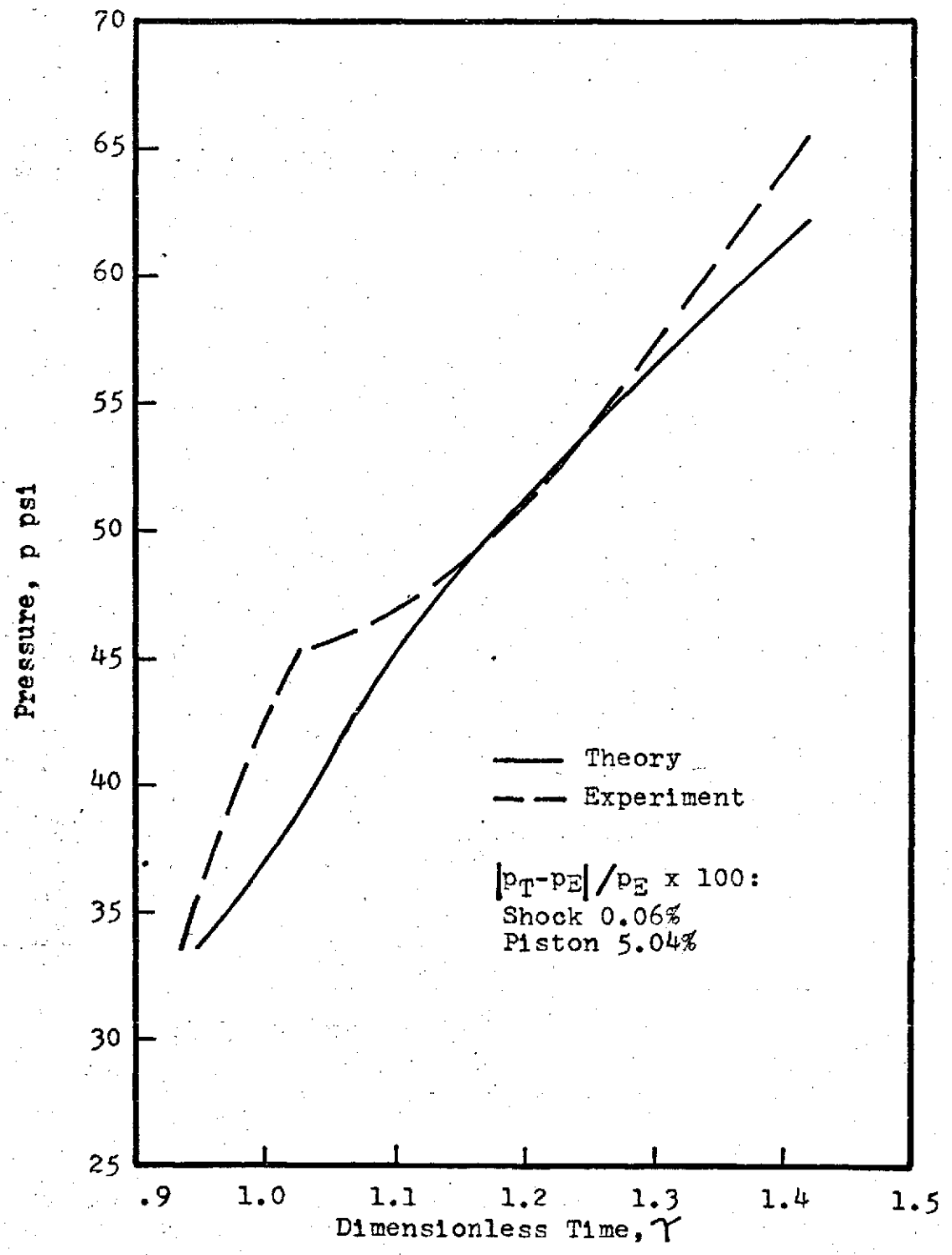

Fig. 27. Theoretical and Experimental Shock Layer Pressure Distributions at Second Pressure Transducer for Case III. The Left End of Each Curve is Just Downstream of the Shock, The Right End is at the Front of the Piston.

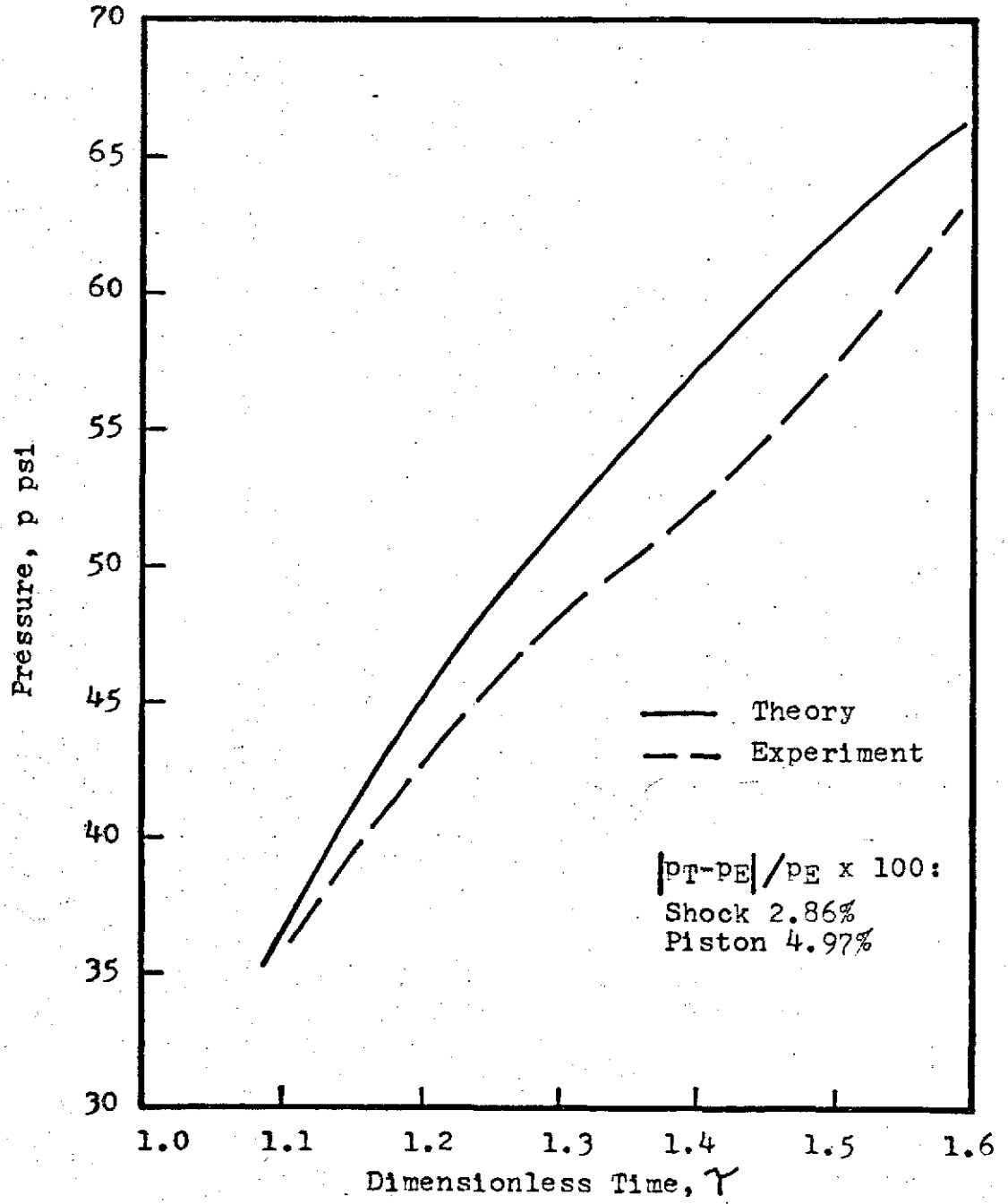

Fig. 28. Theoretical and Experimental Shock Layer Pressure Distributions at Third Pressure Transducer for Case III. The Left End of Each Curve is Just Downstream of the Shock, The Right End is at the Front of the Piston.

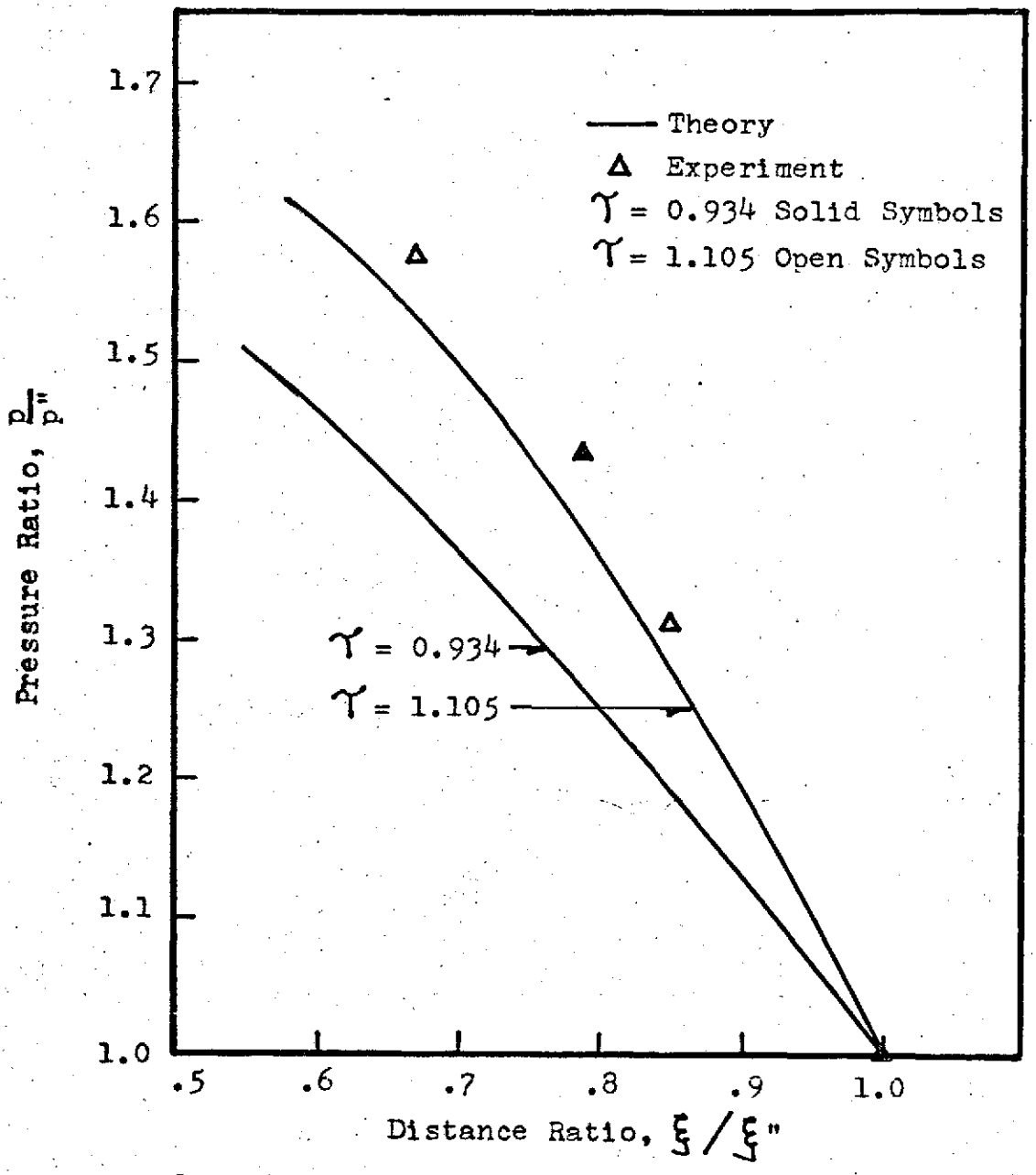

Fig. 29. Theoretical and Experimental Shock Layer Pressure Distributions at Two Fixed Times for Case III. The Left End of Each Theoretical Curve is at the Piston.

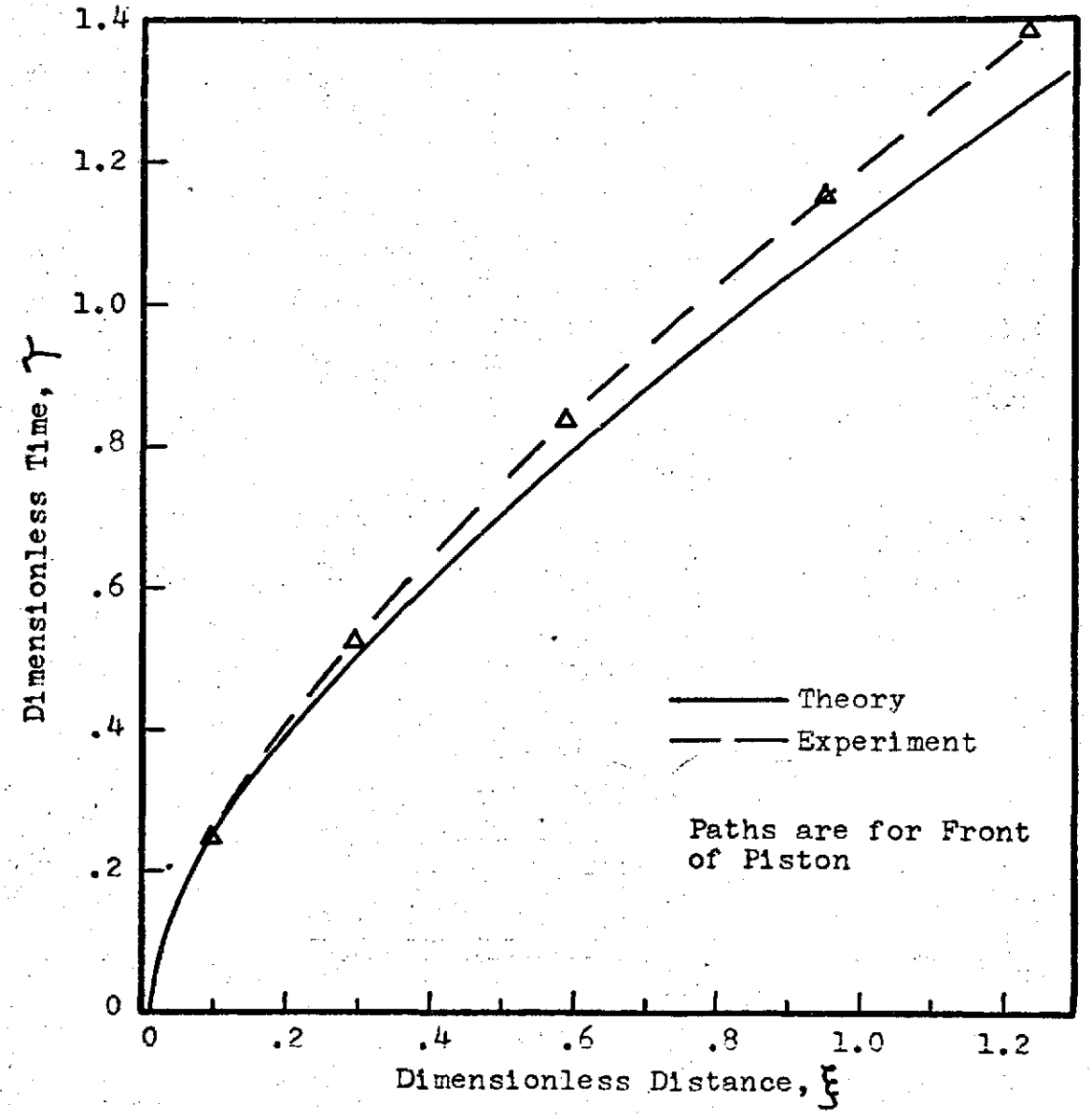

Fig. 30. Theoretical and Experimental Piston Paths for Case IV.

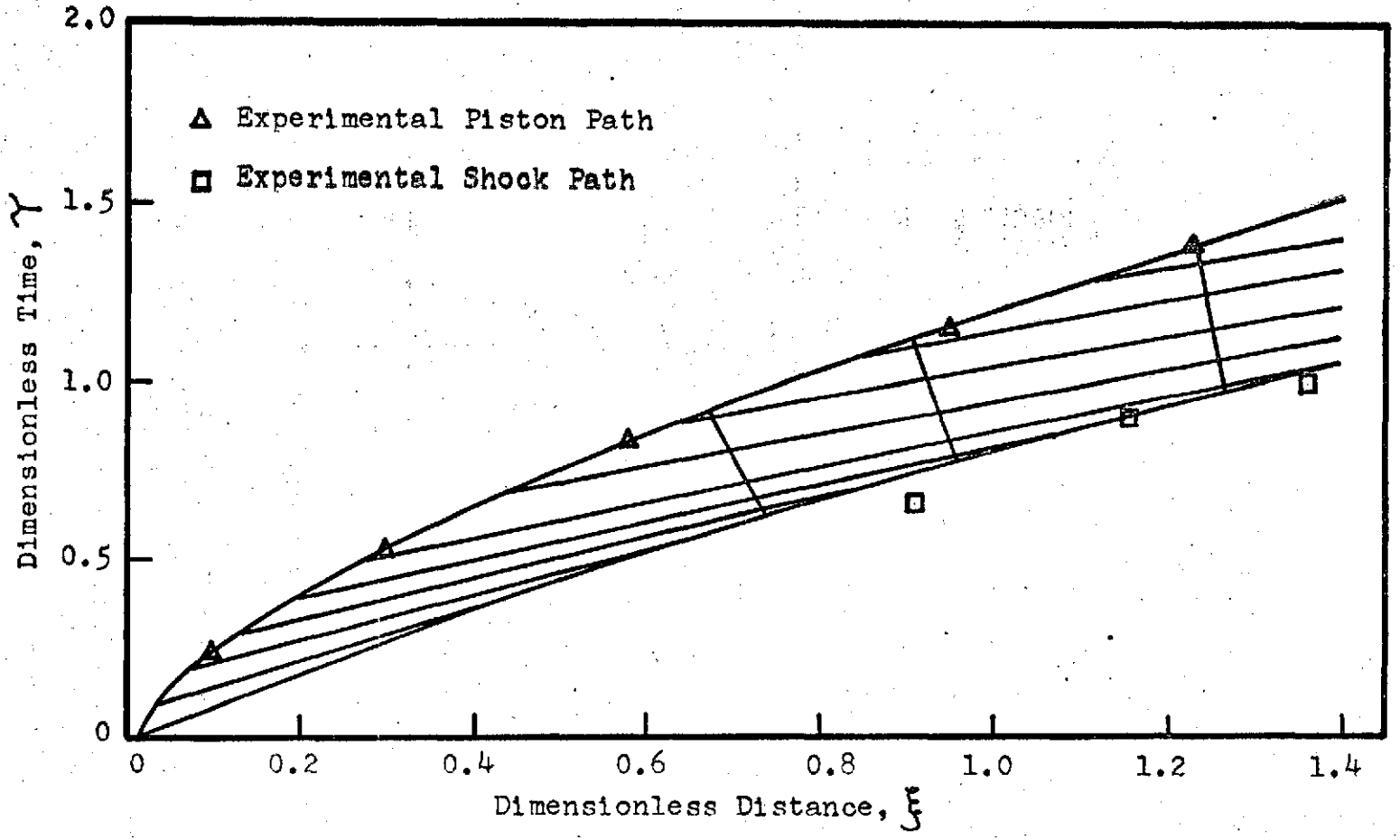

Fig. 31. Wave Diagram Solution for Case IV and Comparison With Experimental Shock Path. $a_{DN,i} = a_o = 1130$ fps, $L_o = 10$ ft, $t_o = 8.85$ msec, $\gamma = 1.4$, $P_{DN,i} = 14.13$ psi, $T_{DN,i} = 72^{\circ}F$, $u_{DN,i} = 0$, $S_{DN,i} = S_o = 0$.

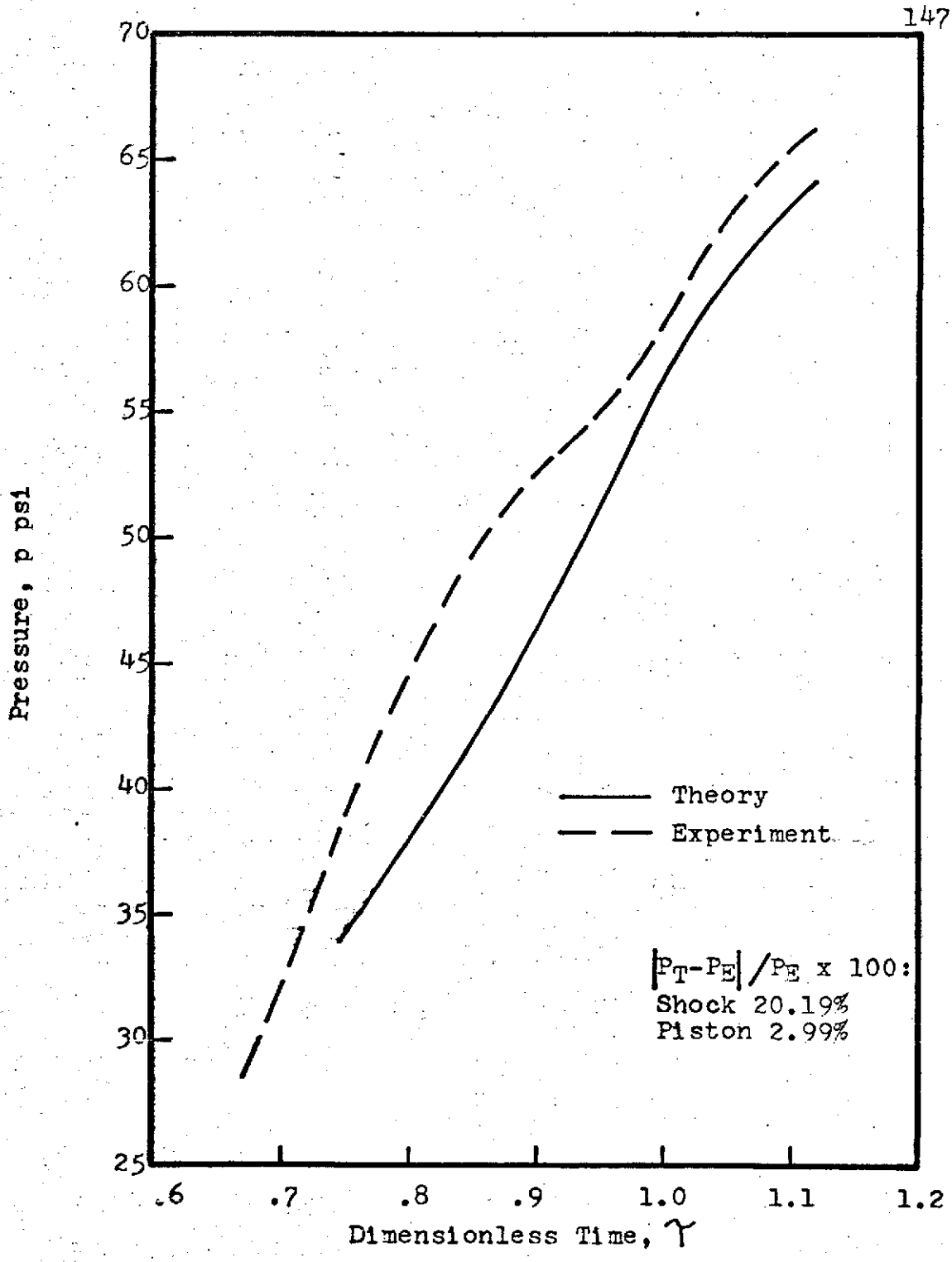

Fig. 32. Theoretical and Experimental Shock Layer Pressure Distributions at First Pressure Transducer for Case IV. The Left End of Each Curve is Just Downstream of the Shock, the Right End is at the Front of the Piston.

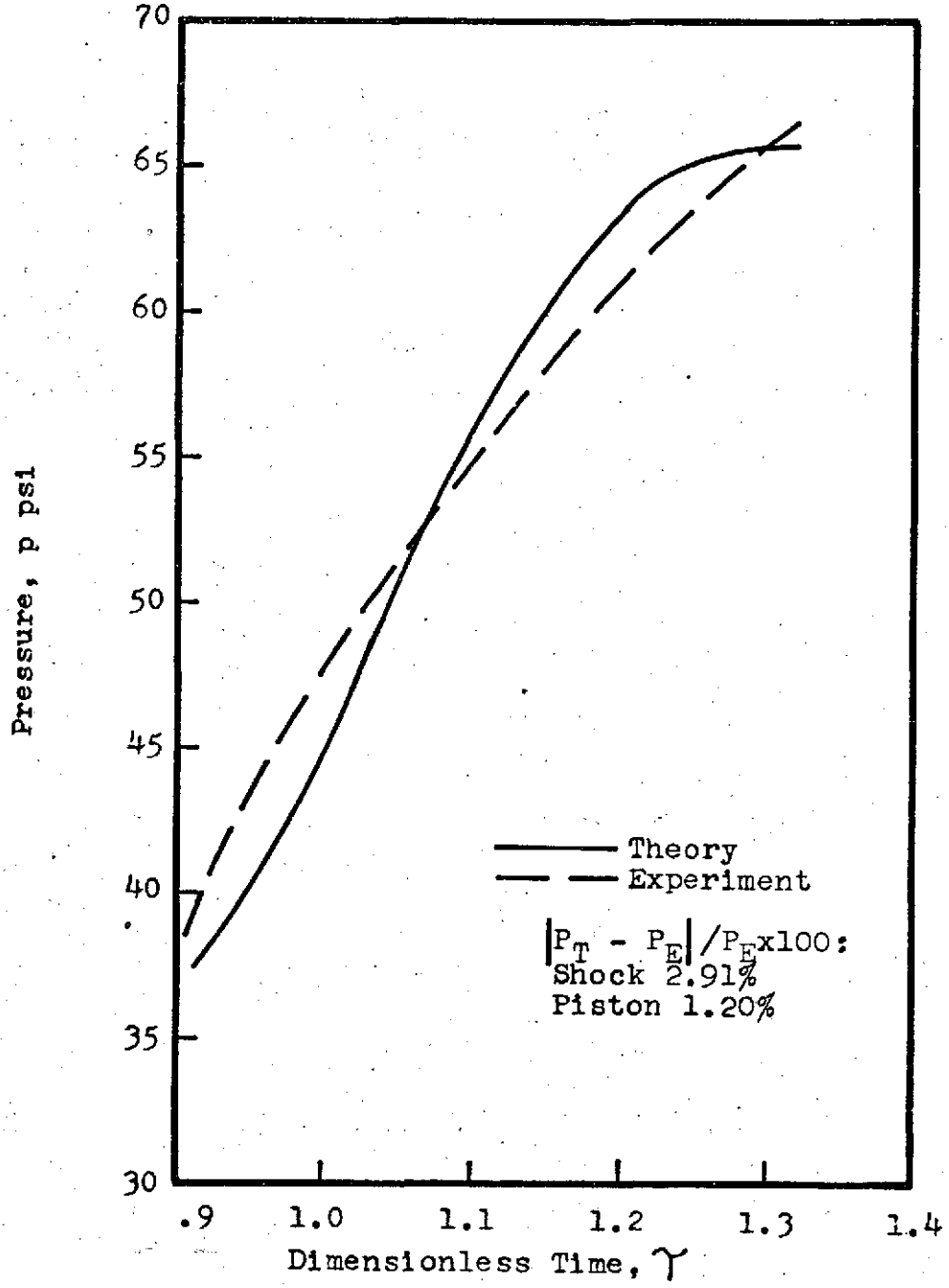

Fig. 33. Theoretical and Experimental Shock Layer Pressure Distributions at Second Pressure Transducer for Case IV. The Left End of Each Curve is Just Downstream of the Shock, The Right End is at the Front of the Piston.

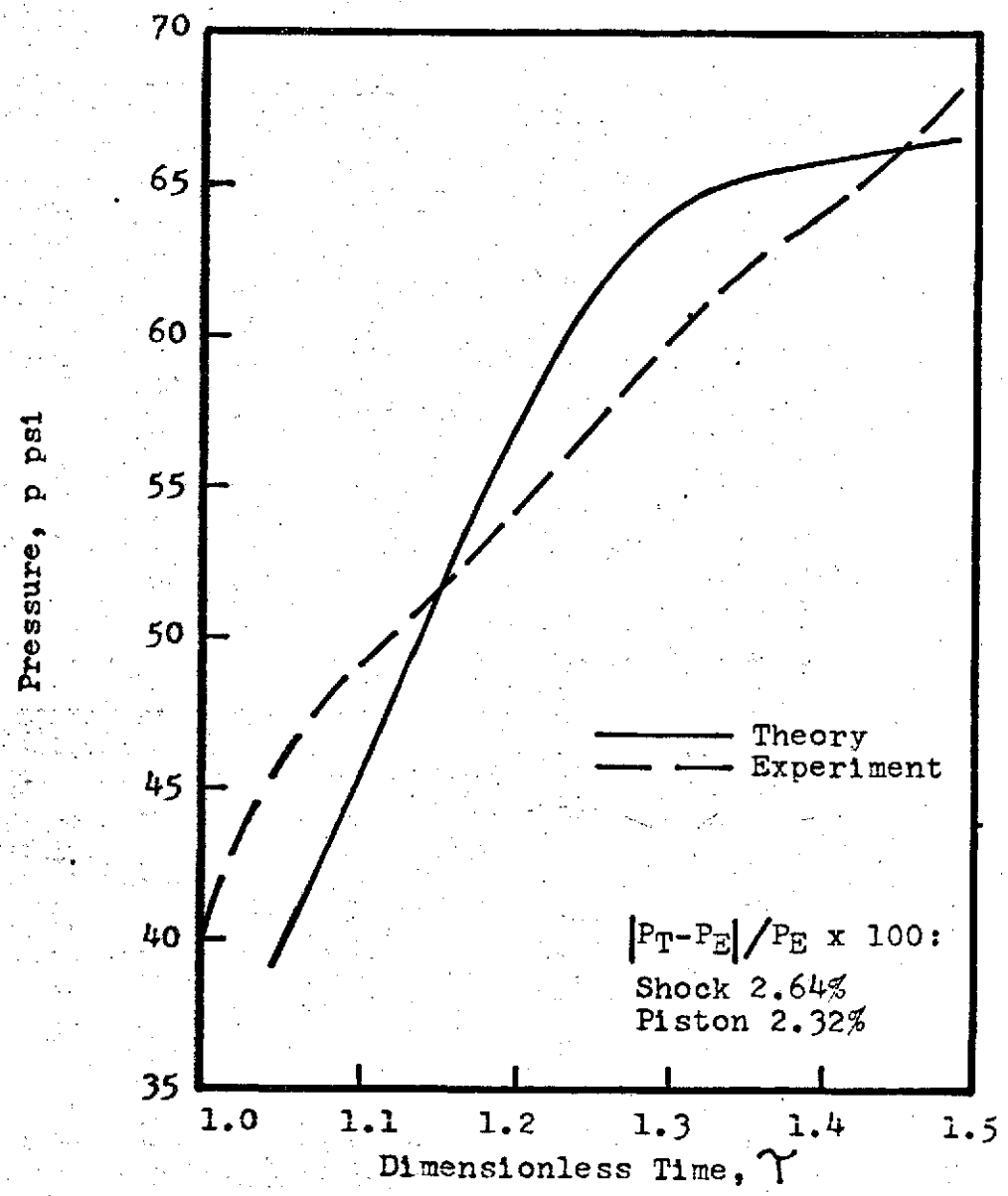

$\left(\frac{\rho''}{\rho'}\right)_{max} = \frac{40}{14.7} \approx 2.7$

Fig. 34. Theoretical and Experimental Shock Layer Pressure Distributions at Third Pressure Transducer for Case IV. The Left End of Each Curve is Just Downstream of the Shock, the Right End is at the Front of the Piston.

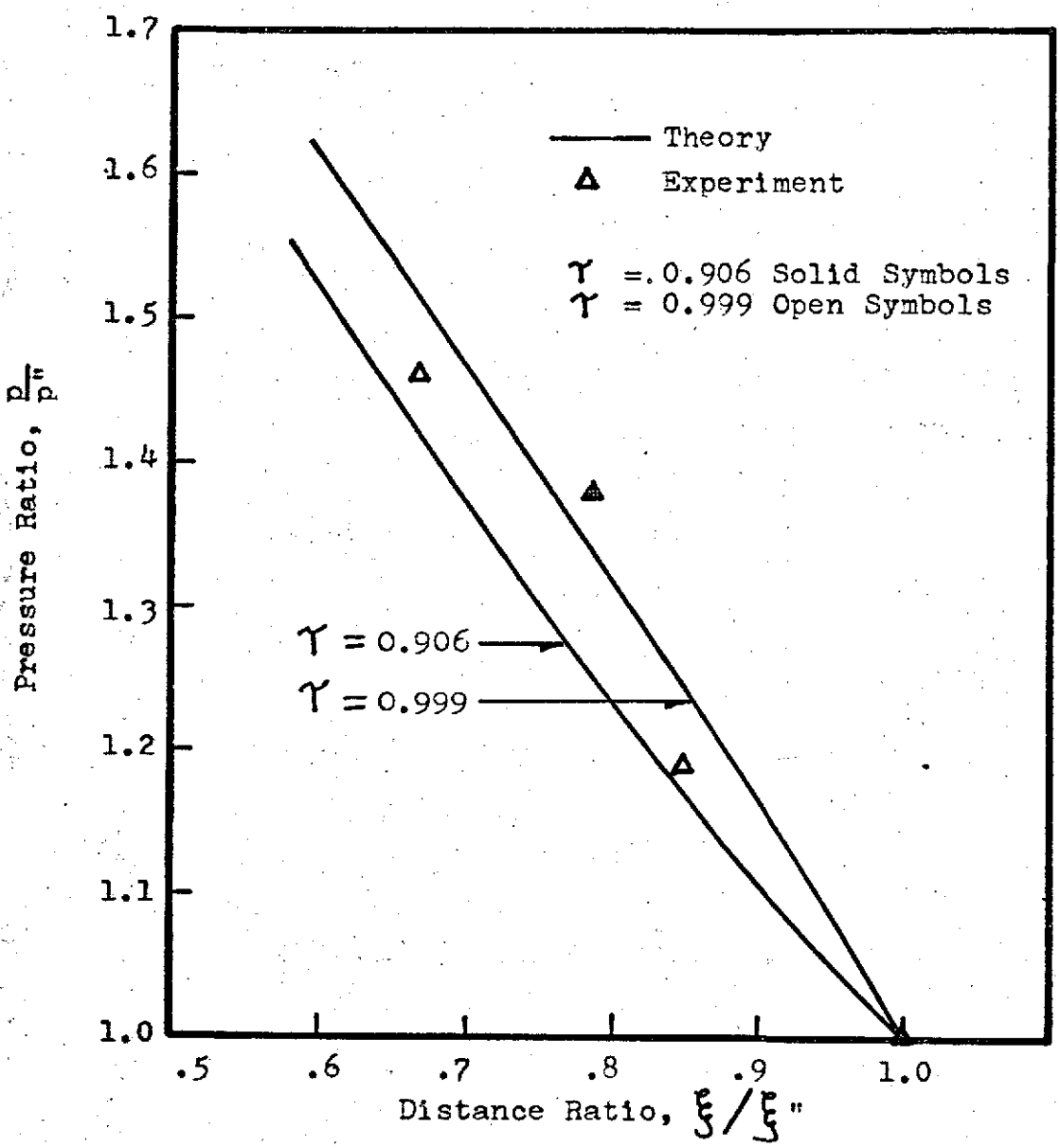

Fig. 35. Theoretical and Experimental Shock Layer Pressure Distributions at Two Fixed Times for Case IV. The Left End of Each Theoretical Curve is at the Piston.